Transport and Transfer of Total Dissolved Gases in the Lower Columbia River Hydropower System

by

Rajib Kamal

A thesis submitted in partial fulfillment of the requirements for the degree of

Doctor of Philosophy

in

WATER RESOURCES ENGINEERING

Department of Civil and Environmental Engineering
University of Alberta

ABSTRACT

Hydropower facilities can generate elevated or supersaturated total dissolved gases (TDGs) during spill operations that can impose environmental and ecological risk to downstream habitat, particularly to fishes causing gas bubble disease and mortality. Assessment of such impact and management of TDG can be challenging, particularly in river systems with multiple dams, as this requires investigation of complex physical processes related to gas transfer and dissolved gas generation in dam spillways as well as its transport, mixing and dissipation in riverine environment. This research aims on developing an analytical platform that can project system-wide total dissolved gas levels during spill events to evaluate the cumulative impact of multi-facility operations and assess relevant risk on fish and habitat ecosystem.

The current research has been carried out based on the comprehensive field study at the Lower Columbia River hydropower system in British Columbia, Canada. This transboundary river comprises the reach below Hugh L. Keenleyside Dam to Canada-US border and includes the confluences of Kootenay and Pend d'Oreille rivers regulated by the Brilliant Dam and Seven Mile and Waneta dams respectively. Several field work sessions were carried out in this system to measure total dissolved gas concentrations, water temperature and river hydraulics. In addition, facility-specific historical data as well as system-wide monitoring information were collected. This resulted in the collation of comprehensive system-wide field data which are extremely difficult to measure and rarely available in the literature.

TDG dissipation, a key process for transferring supersaturated dissolved gases out of the river system, was quantified directly based on field measurements during spill operations at the Hugh L. Keenleyside and Brilliant dams. To estimate the dissipation rate, an analytical approach based

on modified streamtube method was utilized incorporating transverse mixing between the spill and generation flow as well as tributary inflow. This presented a methodology to model TDG distribution in dam-regulated rivers with limited measurements. The dissipation rate was quantified at two hydraulically different reaches of the Columbia River. The effect of depth-velocity ratio on direct transfer, as well as the role of bubble-mediated transfer caused by liquid phase supersaturation was discussed.

The complex gas transfer processes and corresponding generation and degassing of TDG were investigated in the ski-jump spillways of the Seven Mile Dam located on the Pend d'Oreille River. A simplified mechanistic formulation, incorporating physical processes related to air entrainment, bubble characteristics and mass transfer across free surface and bubbles, was utilized to partition gas transfer in the spillway face, free jet and plunge pool and evaluate the contribution of each regions supported by extensive field measurements. Due to gas exchange dominated by bubble-mediated transfer, substantial degassing of high TDG water was observed during spill operations with the free jet being major contributor. Gas transfer efficiency was high when pre-aeration occurred on the spillway face. The plunge pool region was found to generate additional dissolved gases as well as degas TDGs depending on the spill rate, pool geometry and bubble-penetration depth. Similar approach was adopted to predict dissolved gas levels in other facilities of the system.

The mechanistic TDG generation models of individual facilities, the generalized mixing and dissipation relationships and the streamtube-method based transport model were integrated into an analytical platform to develop a two-dimensional TDG distribution model. To test its functionality, TDG monitoring data at the Columbia River system was evaluated for different case conditions. The system model provided spatial distribution of TDG for multi-facility spill operations, which is not only physically meaningful but provides rapid and accurate estimations for impact

assessment. A ranking process was developed to address cumulative TDG risk that was consistent with existing TDG management guidelines. This process involved estimation of risk scores considering severity of supersaturation level, depth compensation and exposure duration for a given spill event, and grouping the scores into four risk categories defined as: none, low, moderate and high. This resulted in a TDG risk assessment framework that anticipates potential risk in fish habitat for the combined operation of hydropower facilities in a complex river system. Results from this study can help inform water management decisions for regulatory compliance and environmental target achievement, thereby enabling sustainable hydropower generation.

PREFACE

The research conducted for this thesis forms part of a collaborative research project by Natural Sciences and Engineering Research Council of Canada (NSERC) and BC Hydro involving Carleton University, the University of Alberta, the University of Waterloo and the University of British Columbia. Professor D.Z. Zhu was the lead collaborator at the University of Alberta.

The field measurements described in Chapters 2, 3, and 4 of this thesis were planned by myself and executed by myself with assistance from colleagues. The data analysis and modeling discussed in this thesis are my original work with direction from my supervisor, Professor D. Z. Zhu.

Chapter 3 of this thesis has been published as Kamal, R., Zhu, D.Z., Leake, A. and Crossman, J. (2019). "Dissipation of Supersaturated Total Dissolved Gases in the Intermediate Mixing Zone of a Regulated River". *Journal of Environmental Engineering*, 145(2): 10.1061/(ASCE)EE.1943-7870.0001477. I was responsible for the data collection and analysis, and writing the manuscript. D. Z. Zhu was the supervisory author and was involved in the concept formation and manuscript composition and editing. A. Leake and J. Crossman facilitated data collection, contributed to manuscript edits and provided recommendations in the context of hydropower operation.

Chapter 4 of this thesis has been submitted as Kamal, R., Zhu, D.Z., Crossman, J. and Leake, A. (2019). "Modeling Total Dissolved Gas Transfer in a Ski-jump Spillway." *Journal of Hydraulic Engineering*, Manuscript ID HYENG-12160 (under review). I was responsible for the data collection and analysis, and writing the manuscript. D. Z. Zhu was the supervisory author and was involved in the concept formation and manuscript composition and editing. J. Crossman and A. Leake facilitated data collection, contributed to manuscript edits and provided recommendations in the context of hydropower operation.

To my mother,

and my family

ACKNOWLEDGMENTS

I would like to express my sincerest gratitude to my supervisor, Dr. David Z. Zhu, for his continuous encouragement and guidance throughout my doctoral program and providing me the opportunity to research, teach and learn. His cordial supervision and expertise guided me to expand my knowledge of environmental hydraulics and water resources engineering. I am very grateful to Dr. Nallamuthu Rajaratnam and Dr. Mark Loewen for their guidance as members of my supervisory committee, Dr. Fabian Bombardelli (University of California, Davis), Dr. Ian Buchanan and Dr. Wenming Zhang for serving on the PhD examining committee, and Dr. Evan Davies for chairing the exam. Their valuable suggestions on this thesis are much appreciated.

Thanks to Graeme Billay and Pengcheng Li, my research partners, for assisting me with field work. I would like to extend my gratitude to Alf Leake, James Crossman, and others at BC Hydro for facilitating field work operations and helping with logistics. Special thanks to Perry Fedun for his technical assistance with completing my field work and particularly for building the floating platforms for continuous measurement. I would also like to thank my friends and colleagues at the University of Alberta for the wonderful times we spent together.

This research was supported by the Natural Sciences and Engineering Research Council of Canada (NSERC) and BC Hydro, which is gratefully acknowledged. I would also like to acknowledge the University of Alberta for providing several scholarships during my graduate program, and funding from the Department of Civil and Environmental Engineering and Dr. David Zhu.

Last but not the least, I would like to thank my parents, friends and family for their continuous love, support and encouragement throughout this journey. A very special thanks to my wife Sharmina Nasreen and my daughter Safreen Kamal. This would not have been possible without their patience, sacrifices and understanding.

Above all, I am thankful to the Almighty Allah to make everything possible.

TABLE OF CONTENTS

LIST OF TABLES

LIST OF FIGURES

CHAPTER 1

General Introduction

1.1 Background

Globally, hydropower is the most widely used form of renewable energy. Due to growing recognition of climate change, interests are moving towards green energy sources and the demand for hydroelectric capacity is expected to increase in future. Despite being relatively clean in terms of environmental emissions, hydropower facilities alter regional water resources balance as well as the physical, chemical and biological features of an aquatic environment and habitat ecosystem (Richter and Thomas 2007; Anderson et al. 2015). Nowadays one of the major concerns in this aspect is the supersaturation of total dissolved gases (TDGs) produced downstream of spillways that can negatively impact aquatic life and fish population (Weitkamp 2008). Aquatic species like fish require dissolved oxygen (one component of total dissolved gas) to survive. However, spill operations in dams may result elevated dissolved gas content deteriorating water quality in habitat ecosystem compared to pre-construction conditions. Fish migrating through hydropower dams or residing in downstream rivers exposed to high levels of TDG can suffer gas bubble disease, which can lead to direct or indirect mortality (Ebel 1969; Weitkamp and Katz 1980). Currently, total dissolved gas levels upstream and downstream of dams is a major environmental issue critical for hydropower development, redevelopment and licensing applications.

In hydropower dam, flow is very complex in the tailrace and excess energy is produced by the turbulent flow (Castillo et al. 2017). During voluntary or involuntary spill releases, large volume of air in the form of bubbles can be entrained as the water passes along the structure and impacts the tailwater pool (Ervine and Falvey 1987; Wood 1991). These bubbles are carried into the deep pool by the momentum of plunging jet (Brattberg and Chanson 1998). The high pressure in the deep-water column increases solubility, transferring mass to the liquid and generating elevated levels of TDG downstream of the spillway (Geldert et al. 1998; Politano et al. 2007). Since water is already saturated with air, this increase in dissolved gas leads to a supersaturated condition with TDG levels exceeding 100 percent of atmospheric saturation. The gas transfer and corresponding generation of TDGs depends on the air content and bubble characteristics, depth, velocity and

turbulence in the stilling basin (Geldert et al. 1998), and is strongly related to operational conditions like duration, rate and volume of spill, forebay and tailrace water elevations etc. (USACE 1996; Hibbs and Gulliver 1997). Furthermore, geometric configuration like chute profile, stilling basin design, flip-buckets or flow deflectors also affect the dissolved gas levels (USACE 2001; Lu et al. 2019). Efforts have been made to predict TDG using operational models (Anderson et al. 2000; Bruce 2016); physical process based mechanistic approaches (Geldert et al. 1998; Urban et al. 2008) or numerical models (Orlins and Gulliver 2000; Weber et al. 2004; Politano et al. 2007). Due to complicated air-water two-phase flow and involvement of many local factors, the generation of dissolved gases is specific to each facility and requires detailed investigation and field measurement for individual cases.

Upon supersaturation, the excess gas must escape from the solution through desorption in order to re-establish equilibrium (Jones et al. 1999). In a quiescent liquid, this can be a rather slow process which involves diffusion through the free surface and formation of gas bubbles that rise through the liquid and burst at the surface (Enríquez et al. 2013). As the supersaturated water moves out of the tailrace channel, the net mass transfer reverses resulting in TDG dissipation (Urban et al. 2008). With maximum concentration in the stilling basin, supersaturated dissolved gases, primarily nitrogen and oxygen, tend to re-establish atmospheric equilibration through dissipation at the free surface (i.e. gas exchange through atmosphere-water interface) and mixing with adjacent waters. The dissipation is the key process for degassing supersaturated TDG out of the river system. In rivers or reservoirs, elevated or even supersaturated gas levels may persist far from the source due to slower rate of dissipation (Feng et al. 2014). The surface transfer of TDG was considered by incorporating bulk hydrodynamics of flow (Geldert et al. 1998; Orlins and Gulliver 2000), dissolved oxygen transfer estimates (Politano et al. 2009), or utilizing mechanistic approach based on small-eddy model (Weber et al. 2004; Urban et al. 2008). However, these studies were limited in the tailrace bubbly region. Empirical relationships available to estimate this rate (Li et al. 2013; Feng et al. 2014) can result in prediction errors when applied to other river systems. For quantitative prediction of TDG in downstream, the mixing and dissipation rates should be accounted based on field measurements.

When TDG exceed saturation level, the ambient pressure including the barometric pressure and the hydrostatic pressure exerted by water to fish is less than the total gas pressure within the water

(Colt 1984). Then the blood and tissues of the fish become supersaturated relative to the atmospheric pressure according to Henry's law and bubbles may form beneath the skin, tails, fins and eyes. This is usually known as gas bubble trauma (GBT). Acute GBT can result in fish mortality through tissue damage, cardiac blockage, hemorrhaging, and increase risk of predation due to reduced mobility (Fidler and Miller 1997). The tolerance of supersaturated TDG and risk of GBT varies by fish species and life stage, dissolved gas levels, compensation depth, exposure duration, past exposure etc. (Weitkamp 2008). Mortality was observed beyond total gas pressure of 120% (Weitkamp and Katz 1980). Recognizing this threat to fish, a water quality criterion of 110% TDG has been established in Canada and the United States (USEPA 1986; CCME 1999). Managing dissolved gas levels in aquatic environments downstream of hydropower dams is of great ecological importance and illustrates the need for the current study.

Hydropower facilities are often built in a cascade manner. The operation of one dam impacts the next and the cumulative effect of group of dams impacts the system as a whole (Ma et al. 2018). Most previous studies focused on TDG prediction in the tailrace without considering changes along the spillway face and the free jet before plunging in the pool (Lu et al. 2019). The physical processes involving air entrainment and bubble distribution in the spillway face and free jet is different than the plunge pool (Chanson 1996; Wilhelms and Gulliver 2005; Pfister and Hager 2012), and the corresponding gas transfer in these individual regions can affect the overall TDG concentration in the downstream. This is particularly important for cascading system where background TDG (i.e. forebay concentration) can be highly supersaturated and requires independent consideration of gas transfer at different regions of a spillway. While transporting downstream, TDG change in the riverine environment is coupled with the hydraulic processes of dissipation and mixing. Uncertainties surrounding impacts to the aquatic environment at varying distances downstream from the source of TDG generation necessitates the need for direct quantification of dissipation. The mixing of spilled water with powerhouse flow and secondary sources also affects TDG levels by diluting dissolved gas pressures (USACE 2001). As environmental regulations and approval requirements are becoming more stringent (Weitkamp 2008), system-wide assessment approach is needed to evaluate TDG risk on fish. Understanding the generation, distribution and dissipation of TDG and its fate in a complex river system is therefore crucial from hydro-environmental-ecological perspective as well as in regulatory context for habitat protection.

1.2 Motivation

Canada, world's one of the largest producers of hydroelectricity, generates 60% of electricity from hydropower sources which impact 19% of the country's watersheds (Lee et al. 2012). The province of British Columbia has several large watersheds with hydropower facilities already developed, ongoing construction (e.g. Site C Project) or under consideration. Majority of these facilities are operated by BC Hydro, the primary hydroelectric utility in the province, along with Columbia Power Corporation and FortisBC. The hydroelectric installations in the Columbia Region provide almost half of BC Hydro's total generating capacity. The Columbia River Basin extends from the headwaters of the British Columbian Rocky Mountains into the United States and is of significant ecological and economic concern to both countries. In 1964, the Columbia River Treaty was ratified in an attempt to increase the potential for hydropower generation and flood protection in the region (Sandford et al. 2014).

Over the past decade, there have been increased concerns regarding the possible effects of high TDG on fisheries resources in rivers within British Columbia. The Columbia River below Hugh L. Keenleyside Dam (one of the Treaty Dams) has been identified as having some of the highest TDG levels in the province (Bruce 2016). The operations at this dam are partly regulated by the treaty and introduce constraints to minimize TDG generation. The river is also the outlet of Kootenay and Pend d'Oreille rivers regulated by the Brilliant Dam and the Seven Mile and Waneta dams respectively. The reaches downstream of these dams inhabit a variety of fish species, including white sturgeon, mountain whitefish, rainbow trout, kokanee etc. (RL& L Environmental Services 2002). Spill operations in these facilities and their cumulative contributions in the river system can exceed Provincial and Federal water quality guideline of 110% TDG level (BCMOE 1997; CCME 1999) during spring freshet and summer that can negatively impact fish populations. Assessment of such impact can be very complex and require reliable estimation of TDG in individual facilities and downstream environment.

Recently, system-wide optimization of hydropower generation through coordinated approach has gained attention as an effective means for TDG Management (BC Hydro 2014; Witt et al. 2017). Such approach can be very complex and becomes more complicated when multiple facilities are involved in series on a single river system, in parallel on multiple river systems, or both. Given the complexity of the TDG generation process, gas transfer in individual facilities needs to be modeled

for downstream impact assessment. As the TDG level changes with the downstream distance, its dissipation rate needs to be quantified and incorporated into transport and mixing model. In order to properly assess the impact of TDGs on fish and mitigate relevant risk, system-wide TDG mapping with changing spill and generation discharges needs to be developed based on detailed numerical study. Such investigation, particularly in multi-facility system, can be very complicated due to various physical processes associated with air-water, two-phase flow. Hydropower operators, such as BC Hydro, are in urgent need of a reliable tool to predict TDG levels across the system and identify potential risk-zones in the habitat ecosystem. This motivates our study to conduct a system-wide investigation on the transport, transfer and fate of total dissolved gases in a complex hydropower system.

1.3 Literature Review

Dissolved gas supersaturation occurs when the partial pressures of atmospheric gases (oxygen, nitrogen and trace gases such as argon and carbon dioxide) in water exceed their respective partial pressures in the atmosphere. It can result from a wide variety of natural and manmade causes, such as at falls and hydraulic structures, warm water discharges from cooling facilities, solar heating of water bodies, air ingestion into pumping systems, natural and artificial oxygenation, etc. (Weitkamp and Katz 1980), among which hydroelectric and impoundment dams are known to cause high levels of total dissolved gases (TDGs).

In dam spillways, the generation of total dissolved gases involves various physical processes related to air entrainment, mass transfer between entrained bubbles and ambient water, bubble quantity and its size and distribution, mass transfer across the free surface etc. In free-surface flows, air entrainment occurs if turbulence is sufficient enough to overcome surface tension and buoyancy (Ervine et al. 1980; Volkart 1980). Flow through spillway can be considered as inclined supported plunging jet (Sene 1988; Chanson 1996). On relatively long and steep chutes with small discharges, air can be entrained on the spillway face if the turbulent boundary layer expands to coincide with the free surface at a location called inception point (Keller and Rastogi 1975), beyond which the air content (usually denoted as gas void ratio) gradually increases. From the reanalysis of Straub and Anderson (1958) and Killen's (1968) data, Wilhelms and Gulliver (2005) showed that the mean concentration of entrained air gradually increases as a function of chute

slope and depth at the inception point. In the fully developed flow region, the mean air content is independent of the discharge and is a function of the slope only (Wood 1991; Chanson 1996). However, air entrainment may not take place in small dams or with high discharges due to lack of distance for boundary layer development (Meireles et al. 2012). The more obvious mode of air entrainment occurs at the tailrace when the jet plunges into stilling basin, drawing significant amount of air with it due to surface disturbances, formation of air boundary layer or free aeration at impact (Ervine 1998).

Air can also be entrained in the free jet issued from flip-bucket or flow deflectors of a spillway (Pfister and Hager 2012). This high-velocity jet experiences surface instabilities initiated by the turbulence from chute flow and jet take-off, and the shear forces of surrounding air (Rajaratnam 1976; Heller et al. 2005). This leads to 'self-aeration' along the jet surface, which spreads the initial compact flow while reducing the core water thickness (Chanson 1996). If the trajectory is long enough, the jet breaks up and becomes fully aerated. This break-up length affects the air concentration distribution along the jet, which is linked to the initial jet thickness (Ervine and Falvey 1987; Pfister et al. 2014). When the aerated jet impinges on the plunge pool, the total resistance and buoyancy forces of the bubbles spreads the jet wider with shorter penetration depth compared to momentum driven pure water jet (van de Sande and Smith 1975).

The entrained bubbles in aerated flows significantly increase the surface area available for gas transfer. The specific interfacial area is an important parameter as it describes the air-water contact area that allows gas to dissolve through. Gulliver et al. (1990) found a 500-fold increment in surface area in a 30 degree spillway flow contributed by the entrained air. There are two groups of methods to determine interfacial area (Bin 1993). The first group, based on physical characteristics, utilizes bubble size and gas void ratio to estimate the interfacial area (Azbel 1981). This familiar form has been widely used in hydraulic structures (Gulliver et al. 1990; Chanson 1996). The second group involves experimental determination of the specific area (e.g. Ohkawa et al. 1987). The bubble size in self-aerated flow is governed by the turbulent shear forces in the flow which breaks larger bubbles into smaller sizes until it is balanced by surface tension forces (Hinze 1955). A number of studies utilized the familiar model based on critical Weber number by defining energy dissipation rate in a system (Sevik and Park 1973; Killen 1982; Gulliver et al. 1990; Bin 1993; Chanson 1996).

Gas-transfer in turbulent flow is usually characterized by a first-order process where the rate is dependent on the difference between the local gas concentration and surrounding. Typically, bubble-mediated mass-transfer is the predominant means of TDG generation in dam tailrace and the most difficult parameter to estimate such transfer is the liquid film coefficient (denoted by k_L). Calderbank and Moo-Young (1961) obtained correlations for k_L in gas-liquid dispersed phase using measured values of transfer rate and interfacial area. Their correlations for small and large bubbles were theoretically derived later by Kawase and Moo-Young (1992) based on the approach for natural convection mass transfer. These relationships were used by Chanson (1995) and Toombes and Chanson (2005) to quantify interfacial transfer in self-aerated flows. However, k_L obtained from these models is independent of bubble size and flow situation and only relates temperature dependent physical properties. Based on dimensional analysis, Akita and Yoshida (1974) presented an empirical equation relating physical parameters and bubble size. Bubble-mediated transfer considering gas solubility was derived by Cirpka et al. (1993) and Asher et al. (1997). For numerical modeling of large-scale bubble plumes, Buscaglia et al. (2002) presented a formulation for oxygen and nitrogen dissolution.

Azbel (1981) incorporated slip velocity of a bubble in turbulent flow field into Levich's (1962) expression for air-water mass flux from a spherical bubble and developed a theoretical relation for liquid film coefficient in bubble swarm. Gulliver et al. (1990) investigated temperature effects on bubble-mediated transfer based on this approach. Takemura and Yabe (1998) numerically estimated dissolution of gas bubbles by solving the Navier-Stokes equations and the convection-diffusion equation. These theoretical methods have been widely used to account bubble mass-transfer for dissolved gas generation downstream of hydropower dams (Geldert et al. 1998; Orlins and Gulliver 2000; Weber et al. 2004; Urban et al. 2008; Politano et al. 2007, 2009). Because of the scaling up for prototype condition and the great complexity of turbulence and bubble characteristics, these equations are often applied with numerical coefficient to correct for uncertainties.

Since any hydraulic structure that entrains air may theoretically raise dissolved gas levels, a number of empirical and semi-empirical equations have been developed. Gulliver et al. (1998) reviewed 12 equations for different type of structures to predict dissolved oxygen, most of which were found to have limited generality. The authors stated that field observation is the best mean to

determine gas transfer characteristics. Early attempts to predict TDG in spillways were based on correlation of TDG with various parameters using data-mining and curve-fitting techniques. The U.S. Army Corps of Engineers used four empirical equations in the CRiSP Model as a part of the Dissolved Gas Abatement Study (Anderson et al. 2000; USACE 2001). Similar approach was used by Bruce (2016) for the hydropower facilities in the Canadian part of the Columbia River. These empirical correlations were limited to the geometry and operational condition range used to obtain the model parameters.

The mechanistic approaches for TDG prediction were influenced by the early works of Roesner and Norton (1971) and Johnson and King (1975) which estimated bulk gas transfer coefficient relating turbulence level and hydraulic performance of the stilling basin respectively. Later studies focused on control-volume or one-dimensional models accounting for mass transfer. Hibbs and Gulliver (1997) introduced the concept of equilibrium saturation concentration and proposed a model for gas transfer efficiency. Geldert et al. (1998) improved the model of Roesner and Norton (1971) by considering the mass transfer at the bubble-liquid interface and free surface, and accounting the stilling basin and river depths to include the effect of hydrostatic pressure on bubbles. USACE implemented similar physically based models (known as the Gasspill 1 and 2) as back up to the other empirical equations in their CRiSP Model (Anderson et al. 2000). Further improvement was made by Urban et al. (2008) who implemented the jet entrainment and de-entrainment in the stilling basin to account gas-void ratio variation, bubble coalescence and break-up phenomena along with the mass transfer processes. These models require calibration of some equation coefficients which are specific for each case. Recently, Lu et al. (2019) developed a TDG predictive model considering the bubble residence time in stilling basin based on laboratory experiment and field observations.

With the advancement of computational efforts, numerical modeling of TDG was attempted considering various physical processes. Based on the data from a reduced scale model of Wanapum Dam, Orlins and Gulliver (2000) developed a two-dimensional, laterally averaged mass transport relationship that incorporated both convection and turbulent diffusion along with bubble and surface transfer. Weber et al. (2004) improved the model by predicting the hydrodynamics and extending the model to three-dimensions. Computational fluid dynamics (CFD) models have also been used to model the TDG (Politano et al. 2007, 2009; Ma et al. 2016). Politano et al. (2007)

predicted the TDG concentrations below a spillway with a modified k-ε model, bubble-mediated transfer equation involving the gas volume fraction and bubble size and a bubble number density transport equation to predict the bubble size variations. The limitation of this approach was discussed in Politano et al. (2009). These models assumed the initial bubble size and void ratio are known and were used as calibration parameters. Wang et al. (2018) simulated the spillway jet regimes and distribution of TDG based on similar approach.

Literature indicates that a degree of empiricism is present within all predictive methods, whether a mechanistic control-volume, one-dimensional approach or multi-dimensional numerical model is employed. All of them have some empirical aspect that requires knowledge of the individual structure in question and field data, which limits their potential to be applied more generally. Furthermore, most of the studies predicted TDG in the plunge pool and tailrace region assuming negligible change in the spillway face and free jet. In a cascading hydropower system, supersaturation may occur in the upstream of a dam and the plunge pool transfer could be affected by the incoming high TDG water associated with the changes in spillway face and free jet (Lu et al. 2019). Wilhelms and Gulliver (2005) investigated dissolved oxygen transfer in spillway face which resulted from bubble-mediated exchange from entrained air. Such transfer is of greater importance for the jet since more bubbles are exposed to high level of turbulence (Davies and Ting 1967; Xue et al. 2019). The literature lacks a general description of how gas transfer in these individual regions impacts downstream TDG levels.

The dissipation of TDG is usually conceived as the physical process involving gas exchange at the free surface similar to reaeration. So far, very few studies have been devoted to the prediction of TDG dissipation rate in downstream rivers and reservoirs. Chinese rivers downstream of hydroelectric dams indicated that the dissipation coefficients varied by two orders of magnitude (0.012 to 0.65 h^{-1}) depending on flow rate (Li. et al. 2013). Some efforts have been made to relate TDG dissipation rate with flow rate (Li. et al. 2013) and by including the effect of water depth, friction velocity, hydraulic radius and Froude number (Feng et al. 2014). However, these formulations are largely empirical in nature and cannot be applied in other river systems. Li et al. (2015) showed that the TDG dissipation rate depended on the Schmidt number, the aspect ratio of the channel and the shear Reynolds number.

The gas exchange at the free surface (dissipation or reaeration) is but one example within a wider class of interfacial mass transfer processes. Theoretically for low-solubility gases such as nitrogen and oxygen, the dissipation across the air-water interface is constrained by turbulence in the surface boundary layer similar to the stream reaeration process (Moog and Jirka, 1999). In reaeration studies, the film-penetration theory and surface renewal model are widely used as conceptual treatments. These were later related to turbulence by considering the presence of a wide range of eddy sizes, ranging between flow domain (integral scale) to smallest sizes (Kolmogorov scale). These two extreme estimates are known as the large-eddy (Fortescue and Pearson 1967) and small-eddy (Lamont and Scott 1970) models respectively. A number of experimental works supported the small-eddy model (Moog and Jirka 1999), while some others suggested the influence of large-scale motions in interfacial transport (Gulliver and Halverson 1989). Due to the need of scaling up and difficulty in direct field measurements, numerous empirical and semi-empirical methods have been developed to estimate the stream reaeration coefficient with a wide array of predictor variables (Gualtieri et al. 2002). Some of the well-known models were developed as a function of depth and velocity (O'Connor and Dobbins 1958; Churchill et al. 1962; Owens et al. 1964; Bennett and Rathbun 1972); with channel slope as an additional variable (Tsivoglou and Wallace 1972; Smoot 1988); or dimensionally correct form of equations (Thackston and Krenkel 1969; Lau et al. 1972; Gualtieri et al. 2002). These equations are site-specific and can result in large prediction errors of 40-50% in conditions outside the type of streams for which they were formulated (Bowie et al. 1985; Melching and Flores 1999; Palumbo and Brown 2014).

To estimate TDG dissipation, the US Army Corps of Engineers employed the form of surface renewal theory based on O'Connor and Dobbins' (1958) model (USACE 2001). Early studies considered the interfacial transfer by incorporating bulk hydrodynamics of flow (Geldert et al. 1998). Orlins and Gulliver (2000) assumed a TDG mass transfer coefficient that is proportional to the square of the vertical surface velocity to account for turbulence. Weber et al. (2004) and Urban et al. (2008) adopted the small-eddy model recommended by Moog and Jirka (1999) to relate surface gas transfer with Schmidt number and turbulence dissipation rate. In modeling the bubbly environment at a dam tailrace, Politano et al. (2009) used a free-surface TDG mass transfer coefficient based on reaeration coefficient calculated for a bubble plume by DeMoyer et al. (2003). However, these studies were limited in the tailrace region where bubble dissolution is the dominant

process. The gas transfer at the free surface was also neglected in some studies (Politano et al. 2017; Wang et al. 2018).

The error due to approximation or neglecting TDG dissipation may not be significant near a dam spillway, where bubble-water mass transfer processes dominate the evolution of supersaturated TDG (Urban et al. 2008). However such assumption may not be valid further downstream of a dam, where gas entrainment is minimal and TDG degasification depends on the turbulent transport processes in river. Orlins and Gulliver (2000) specifically suggested that the gas exchange of supersaturated TDG with the atmosphere downstream in the river require further investigation. From experimental study, Li et al. (2013) found that rate of TDG dissipation in supersaturated water was quantitatively different than the reaeration in unsaturated condition. When gas transfer is accompanied by bubble formation, it is no longer a reverse process of reaeration (Hikita and Konishi 1984; Woolf and Thorpe 1991). Hence, there is still scope to evaluate and, if possible, refine the current reaeration theories in order to understand the TDG dissipation process better. Quantification of TDG requires an appropriate model for TDG dissipation through the air-water interface as a function of hydraulic conditions.

Besides dissipation, TDG concentrations can change due to mixing while transporting in the downstream river. The interaction between powerhouse flows and the highly supersaturated spill releases in the turbulent stilling basin can result in dilution and reduction of total gas pressure (USACE 2001). Additional mixing and dilution can result by flows from secondary sources, such as tributary inflows. In rivers, contaminants are well mixed over the depth long before they are well mixed across the channel and hence transverse mixing is considered the dominant mechanism for spreading across the river. Although many studies have been reported in this area (as summarized by Fischer et al. 1979; Elhadi et al. 1984; and Rutherford 1994), uncertainty still remains in the accurate prediction of mixing coefficient (Dow et al. 2009; Zhang and Zhu 2011). The dimensionless transverse mixing coefficients can vary from 0.3-0.6 for regular channels, 0.6-0.9 for gently meandering channels and 1-3 for sharp curved channels (Fischer et al. 1979; Rutherford 1994). Rutherford (1994) summarized that transverse mixing increased with discharge while the dimensionless coefficient remained constant. Researches on some aspects related to transverse mixing are still quite limited, such as the effect of secondary flow and mixing in river confluence (Chen et al. 2017). Several methods have been reported to calculate transverse mixing

such as the classical method of moment (Fischer et al. 1979), generalized method of moment (Holly et al. 1972), the streamtube model (Yotsukura and Sayre 1976), and the cumulative discharge concept (Rutherford 1994). However, all of these methods have different limitations to apply. Some recent attempts have been made to improve the estimation of transverse mixing (Dow et al. 2009; Zhang and Zhu 2011; Pilechi et al. 2016; Chen et al. 2017).

Study on the cumulative effect of TDG supersaturation due to multi-facility operations and its overall risk on fish is very limited in the literature. Witt et al. (2017) presented a simplified model to assess tailrace TDG in a multi-reservoir system without considering the dissipation process in downstream environment. The model was used to optimize spill operations meeting state water-quality standards. Ma et al. (2018) utilized numerical models to simulate TDG distribution in reservoir and river as a result of cascade operations. This study considered the magnitude and duration to evaluate potential TDG risk. In general, the guideline of 110% saturation is often conservative, potentially resulting in costly mitigation when none is required. A comprehensive review by Fidler and Miller (1997) and Weitkamp (2008) revealed that lethal signs of GBT vary with fish species as well as the level of excess dissolved gas pressure, and can be affected by length of exposure, swimming depth of fish, past exposure to high TDG etc. Physiological investigation on rainbow trout from Fidler (1988) and Shrimpton et al. (1990) suggested three distinct dissolved gas thresholds of 103, 110 and 115 percent of saturation for certain signs of GBT during TDG exposure. TDG levels exceeding 120% are considered harmful to fish beyond which mortality was observed (Weitkamp and Katz 1980). Access to water below hydrostatic compensation depth, at which barometric plus the hydrostatic pressure is equal to the total gas pressure, can reduce TDG risk. The hydrostatic compensation of each meter of fresh water is approximately 10% of ambient TDG supersaturation (Colt 1984). Bubble formation will not occur when fish are at or below this depth (Antcliffe et al. 2002). The movement of dissolved gas from ambient water to fish tissues also depends on the duration of exposure. Longer exposure at high degree of supersaturation poses greater risk to mortality (BC Hydro 2014). A more practical assessment of TDG risk is possible when dissolved gas level thresholds are combined with the compensatory effect of depth and exposure duration. Detailed assessment is therefore needed to evaluate the effect of these impacting factors and identify their role in specific river reaches exposed to TDG risk.

1.4 Research Objectives

Operation of hydroelectric system to meet power demand while ensuring water-quality constraints can be challenging, particularly in complex river systems involving multiple dams. Management of TDG in such system requires a coordinated approach and decision-support tools to assess TDG risk during spill operations which involves complex physical processes related to dissolved gas generation, and its transport, mixing and dissipation. The aim of this research is to provide an integrated framework that can project system-wide total dissolved gas levels for different spill incidents and consequently anticipate relevant risk in the habitat ecosystem.

Toward this overall aim, the thesis is organized around the following specific objectives:

1. To estimate the dissipation rate of total dissolved gases in regulated rivers subjected to supersaturation. The dissipation rate is quantified from field measurements considering the mixing effects of generation flow and tributary inflow. Predictive capabilities of available surface reaeration models and gas transfer theories to estimate the dissipation rate is evaluated.

2. To investigate the transfer and corresponding generation and degassing of total dissolved gases in dam spillways, with focus towards evaluating the contribution in individual regions like spillway face, free jet and plunge pool. A mechanistic approach considering important physical processes is utilized to predict dissolved gas levels at hydropower facilities supported by prototype field measurements.

3. To develop a total dissolved gas distribution model and risk assessment framework in complex river system involving multiple facilities for real-time application. An integrated analytical platform combining generation, transport and dissipation models is utilized to examine spill-total dissolved gas responses by means of both mechanistic and whole-system approaches. A risk ranking process is developed to identify the degree and extent of potential risk zones in fish habitat.

This study will improve our understanding on gas transfer in individual regions of a dam spillway as well as dissolved gas dissipation in downstream riverine environment. The outcome of this research is the practical estimation and accurate parameterization of total dissolved gas generation and dissipation. It will contribute to the scientific knowledge by improving methodologies and

introducing generalized predictive tools. The integrated framework presented here can be used as a tool to quickly evaluate hydropower operational conditions that can pose negative ecological consequences. This tool can be generalized for application to other systems and can be expanded to account different water quality parameters that can harm the receiving environment. Results from this study can help inform the system managers for environmental regulations compliance and meet their own social and environmental targets, thereby enabling them to operate in a sustainable manner.

1.5 Thesis Organization

This thesis is organized in two formats. Chapter 2 is presented as a thesis chapter format, and Chapters 3, 4 and 5 are written in paper format with each focusing on a specific aspect of total dissolved gas supersaturation in a hydropower system.

In Chapter 2, a comprehensive overview of the field works conducted for this research is presented. This includes detailed description of measurement procedure, instrumentation and laboratory testing, monitoring logistics and data analyses. The uncertainties in total dissolved gas measurements obtained from the field are also quantified.

In Chapter 3, the dissipation of total dissolved gases in regulated rivers is studied based on field measurements. The objective is to quantify the rate of dissipation and evaluate whether it can be predicted by surface reaeration theories. To analyze dissipation, a modified streamtube method is utilized incorporating transverse mixing between the spill and generation flow as well as tributary inflow.

In Chapter 4, investigation is carried out on the transfer of total dissolved gases in a prototype ski-jump spillway receiving supersaturated water from upstream facilities. Gas transfer in individual regions of the ski-jump design, i.e. spillway face, free jet and plunge pool is evaluated through field measurements and physical process based mechanistic modeling. Practical relationships are also proposed for prototype application.

In Chapter 5, the development of an integrated framework is discussed that considers the cumulative impact of multi-facility operations on total dissolved gas supersaturation and its risk

on fish in a complex river system. The framework includes a multi-stage approach incorporating total dissolved gas modeling in spillways and downstream rivers, spatial mapping and risk assessment. For this, a risk ranking process is developed considering several impacting factors.

Finally, the summary and conclusions of this research and recommendations for future work are presented in Chapter 6.

CHAPTER 2

Field Work and Uncertainty Estimates of Total Dissolved Gas Measurements

2.1 Introduction

Total dissolved gas (TDG) refers to the amount of gases, typically the air constituents comprising nitrogen, oxygen and trace gases like carbon dioxide and argon, dissolved in water. This is usually expressed in the units of pressure (e.g. mmHg) or percent saturation relative to ambient barometric pressure (Pickett 2006). When partial pressures of the dissolved gases in water exceed their respective partial pressures in the atmosphere, water becomes supersaturated with TDG levels exceeding 100 percent of the atmospheric saturation. The physical processes that cause and affect TDG supersaturation in hydropower system are difficult to replicate in laboratory studies and require detailed field investigation. The quantification of TDG supersaturation involves measurement of total gas pressure (TGP) in water. Sampling TGP has wider range of applications in fisheries management, oceanography, limnology and groundwater studies (D'Aoust and Clark 1980; Anderson and Johnson 1992; Manning et al. 2003), and has gained increasing importance in hydropower facilities and regulated river-reservoir systems (USACE 2001; Weitkamp 2008). Measurements in hydropower facilities are often difficult as the operational conditions change frequently to meet power demand, water use requirements, environmental regulations and facility-specific constraints.

To monitor TDG supersaturation in the Columbia River hydropower system (Figure 2.1), three separate field work sessions were carried out during spill operations at the Hugh L. Keenleyside, Brilliant, Seven Mile and Waneta dams. For measuring total dissolved gases, two data collection methods were adopted – continuous monitoring and spot measurements. Continuous monitoring captures the variation of TDG with time and its response to change in operational scenarios. Spot measurements are more preferable method to obtain spatial variation of TDG across and along a river. These data were collected following extensive laboratory preparation and calibration, detailed measurement logistics and careful monitoring practice. For accurate description of TDG supersaturation in the hydropower facilities, detailed analyses on total gas pressure, barometric

pressure and temperature were carried out. The uncertainties in the field measurements were also quantified. These are described in detail in the following sections.

2.2 Field Work Overview

The first field work session was conducted from July 25-30, 2016 during spill operation at the Hugh L. Keenleyside Dam. This survey covered about 20 km stretch of the Columbia River downstream of the dam including the Kootenay River confluence. The field work was carried out for four scenarios (1A-1D) consisting of different combinations of low-level outlet gates operations. Over the course of the field work period, the generation flow remained consistent while the spills through the individual units were varied to produce different TDG levels (Table 2.1). These scenarios were operated for 22-26 hours and detailed measurements were carried out in seven transects located at 0.56, 0.98, 2.03, 4.39, 6.70, 11.30 and 19.68 km downstream of HLK. Additional measurements were taken in the forebay and tailrace of the dam as well as on the Kootenay River. During this session, velocity measurements were also carried out using Acoustic Doppler Current Profiler (ADCP) which will be discussed in Chapter 3.

The second field work session focused on the Brilliant Dam and Brilliant Expansion facilities on the Kootenay River. The field work was conducted over two days from June 7-8, 2017 to determine the change in TDG for two spill scenarios (2A and 2B). These scenarios consisted of different spillway bays operations discharging similar amount of water. For these cases, the generation discharge from the dam and the expansion project was held constant. The survey included the 2.8 km reach of the Kootenay River between the dam and its confluence with the Columbia River and was extended up to 13.5 km downstream of the confluence. Detailed measurements were taken in the dam forebay, across two transects on the Kootenay River and four transects on the Columbia River. The third field work session covered the Seven Mile Dam, the Waneta Dam and Waneta Expansion facilities on the Pend d'Oreille River and included the short downstream reach of the Columbia River before the international border. TDG was measured for two operational scenarios (3A and 3B) during the survey period from June 19-20, 2017. At the Seven Mile Dam, maximum flow was passed through the generation units for the first scenario. The second scenario consisted operation of bays at high spill rate. Measurements were carried out in the forebay and tailrace of

each dam, as well as at a location between the two dams and upstream of the Pend d'Oreille-Columbia River confluence.

2.2.1 Instrumentation for Dissolved Gas Measurements

Total dissolved gas pressure (TGP) probes specialized for field measurements are commercially available from various manufacturers. These probes use membrane diffusion technique equivalent to APHA Standard Method 2810 (APHA et al. 1998). For the present study, measurements were taken using the PT4 Smart TGP probe and the Lumi4 DO-TGP probe manufactured by Pentair Aquatic Eco-Systems Inc., Apopka, Florida. These probes measure total dissolved gas pressure directly and convert it to percent saturation relative to atmospheric or barometric pressure.

The TGP probe incorporates a pressure transducer, conditioning electronics, a gas-permeable membrane cartridge, and a fixed length of cable for connection to an external data-logging unit (Figure 2.2). The membrane cartridge consists of small-diameter, thin-walled silicon tubing and is connected to the transducer's pressure-sensing element. The silicon tubing is gas permeable but water impermeable, and creates a void volume that simply contains air prior to submersion in water. When the probe is submerged, dissolved gases are exchanged between the ambient water and the probe's void volume until equilibrium condition is reached. Consequently the pressure transducer measures the total dissolved gas pressure by converting the internal void volume pressure to an electrical signal (PentairAES 2014). The tracker of the PT4 Smart TGP and the Lumi4 DO-TGP probes also contains a sensor to measure barometric pressure (BP). Another temperature measuring sensor is attached to the main body of the probe. For the Lumi4 probe, an additional optical sensor is included to measure dissolved oxygen (DO). This allows determining the percentage of TGP attributed to nitrogen and other gases.

The PT4 Smart TGP and the Lumi4 DO-TGP probes are capable of recording TGP and BP up to 1550 mmHg, which corresponds to about 200% saturation under standard atmospheric pressure (PentairAES 2014). These probes measure total dissolved gas pressure and barometric pressure with an accuracy of ±2 mmHg resulting in an overall resolution of TDG of about 0.1% for temperature operating range of 0-50 ºC. Both types of probes also measure water temperature with an accuracy of 0.2 ºC. The dissolved oxygen measurement range of Lumi4 probe is 0-25 mg/L at 20 ºC and the corresponding accuracy is ±0.2 mg/L.

2.2.2 Laboratory Testing and Calibration

A total of six PT4 Smart TGP probes and a Lumi4 DO-TGP probe were used during the field measurements. Prior to field deployment, these probes were tested in the laboratory to ensure proper calibration and to confirm that they agreed with each other. The probes were also tested against a dissolved oxygen (DO) sensor (Model LDO101, HACH, USA) as a way to confirm the adequacy of the probes' readings.

The testing of the TDG equipment involved calibration of the internal tracker barometer and pressure sensor of the probe as per manufacturer's instructions. This is known as 'one-point calibration' (PentairAES 2014). For this, the TGP membrane cartridge was removed to expose the pressure sensor to ambient atmospheric pressure. The local barometric pressure was collected from the University of Alberta Earth and Atmospheric Sciences (EAS) weather station (www.ualberta.ca/earth-sciences/facilities/weather). While in the open air, pressure reading of the internal barometer was compared and corrected to match the ambient barometric pressure. Then the probe sensor was calibrated to current conditions ensuring TDG measurement of 100% saturation in open air. The instrument manuals also included results from a 'two-point calibration', which was not recommended unless large errors in readings are observed. The Lumi4 DO-TGP probe's DO reading was also calibrated as per manual instruction. To calibrate the DO sensor, a bottle partially filled with water was sealed and shook for 30 seconds to completely saturate the air within and then allowed to equilibrate for 30 minutes. The probe was then rinsed with deionized water and dried, placed inside the bottle and calibrated for concentration of DO in 100% water-saturated environment (HACH 2013). The temperature sensor of each probe was calibrated in water with a thermometer.

Once the calibrations were complete, a small tank was filled with boiled water which was under saturated and was then cooled to allow the probes to be lowered into the tank. Undersaturating the water was simpler than trying to generate a supersaturated condition. All the probes were placed at the same time and measurements were taken every five minutes (Figure 2.3a). Initially, there was a large difference between the concentrations and percent saturation among the probes. An air diffuser was placed into the tank to increase the rate of aeration. The difference in TDG saturation between the Lumi4 and TGP probes became 1% within 25 minutes and varied from 0.1-1.0% for the remainder of the test. The difference in DO concentrations between the Lumi4 and LDO probes

reduced more quickly with the addition of the diffuser. After one hour and five minutes, the aeration rate was increased. At this point the difference between the various measurements of the probes was minimal. However, the percent saturation of TDG was slightly lower than the DO readings at the beginning. The aeration rate was further increased at two-hour and 35-minutes mark, after which the probes remained consistent with each other. Once the probes were stabilized, the TDG and DO readings between different probes agreed very well during the entire test (Figure 2.3b). The greatest difference for TDG measurements was 1.0% between Lumi4 and TGP smart probes. The maximum DO concentration difference between Lumi4 and LDO probes was 0.1 mg/L (1.4% saturation) with the later being a slightly higher. After the experiment, the probes were placed in a water tank and left to collect data for a 24-hour period. The readings were compared to the different probes which agreed very well with each other. These tests gave confidence about the adequacy of measurements between the probes.

In the field, the local barometric pressure was used to one-point calibrate each probe before it was installed or used into the river for TDG monitoring. The barometric pressure was obtained from local weather stations (https://climate.weather.gc.ca) at Castlegar and Trail, BC. This was used to confirm all probes were indicating same measurements and to normalize the readings to the current barometric pressure. The consistency in TGP, BP and temperature readings between the probes was also checked. Prior to deployment for continuous monitoring, the time and date of all units were synchronized, and the data logging intervals were set. Each unit was then tested to confirm successful data logging. The TDG probes used for spot measurements were also calibrated each day before collecting data.

2.2.3 Continuous Monitoring

For continuous monitoring, probes are usually installed from the bank. But often this method results inaccurate TDG readings due to presence of dead water zones near the banks or other local features. Therefore custom-built floating platforms were prepared at the University of Alberta prior to the field work. These floating platforms were made of PVC pipes to hold the TDG meter in a water-tight enclosure (Figure 2.4a). This enclosure also housed a battery power supply for the meter and was secured with a padlock. A long PVC pipe was attached to the underside of the platform for the TDG probe to slide into and be protected from possible debris. This PVC pipe had

holes drilled into it to allow water to freely move around the TDG probe. The platform was attached to a 30-lb river anchor (Figure 2.4b). The anchor was attached to the platform via chain, anchor line and rope. The procedure for deployment of floating platforms and installation of TDG probes varied depending on the local river condition and bank slope (Figure 2.5). To avoid locations of large depth and high velocity water, platforms were mostly deployed along the side channels. Navigation was also a factor since the Columbia River is used frequently by recreational boaters and fishermen. Placing the floating platforms far from the bank would increase the risk of collision with other people sharing the water.

For continuous monitoring during the spill events at the HLK Dam (session 1), five stations were set up near the left bank at 0.98 km; along the right banks at 4.39, 11.30 and 19.68 km of the Columbia River; and upstream on the Kootenay River. In addition, another station was installed (courtesy: James Bruce, Creekside Aquatic Sciences) along the southern berm of the tailrace. At 0.98 km, the side channel was shallow enough to carry the floating platform and anchor into the water and install the station. The rest of the platforms were deployed from the boat with the anchor, chain and rope fastened prior to loading. The anchor was lowered into the water until it hit the bottom, and then the platform (with plenty of slack) was lowered gently from the side of the boat. The TDG monitoring case, chord, and probe were also fastened to the platform before being lowered into the water. Sufficient length of chain and rope was provided to allow the platform to drift downstream with the current and allow for an appropriate angle to aid in securing the anchor to the bed (Figure 2.5a). The velocity was very high at 11.30 and 19.68 km, and the floating platforms were tied to cinder blocks and trees on the bank to protect it from quicker moving water (Figure 2.5b). In all cases, the platforms were deployed at 3–5 m away from the banks. The monitoring station at the tailrace was set by attaching the probes along the banks of the man-made dike which was very steep with rocky boulders. In this case, a PVC pipe was lowered into the river and extended above the water to be tied to a boulder. The TDG probe was lowered into the PVC pipe and the chord was attached to the monitor housed in a locked case further up the bank (Figure 2.5c). The deployment tasks during this session required about 2 days of work prior to the spill.

A total of four monitoring stations were deployed during the field work at the Brilliant Dam for continuous measurement of TDG. Using floating platforms, two stations were set at the left banks of Kootenay River located at 1.2 and 2.6 km downstream of the dam. However, the flow was

highly turbulent at the tailrace and inconsistent readings were found for the deployed platform at 1.2 km. TDG was also measured continuously at the left banks of 12.49 and 17.62 km of the Columbia River (approximately 4.8 and 9.9 km downstream of Brilliant Dam). For these cases, the floating platforms were installed in a similar manner as shown in Figure 2.5b. During the third field work session, two stationary platforms were deployed in the forebay and tailrace (about 1.7 km downstream) of Seven Mile Dam. Instead of anchoring, the forebay station was launched by attaching it to the log booms. The tailrace station was anchored near the left bank and was also tied to a stationary object on the bank. Near the Waneta Dam, another monitoring station was installed at the forebay. Bubbles can form and adhere to the silicon membrane when the probes are placed in shallow, quiescent water, and may lead to inaccurate readings (Pickett 2006; D'Aoust 2007). Therefore in all monitoring platforms, TDG probes were set below compensation depth (2 – 5 m depth) to avoid bubble formation in probe membranes.

2.2.4 Spot Measurements

Taking spot measurements of TDG from boat at one point in time within the river was another method of data acquisition during the field works. This was done by moving the boat across a section and taking measurements at different points along that transect. In this case, the probe was lowered over the side of the boat and submerged below the water surface. The probe was attached to a heavy weight tied to a rope. The TDG readings were recorded from the data-logging tracker kept on board. To maintain a stationary position and avoid drifting, the boat was anchored at the measurement point during data collection.

For different spill scenarios at the HLK Dam, spot measurements were carried out in the seven downstream transects. Due to time limitation and other constraints, it was not possible to take measurements at 0.56 and 0.98 km for scenario 1A and at 11.30 and 19.68 km for scenario 1D. Additional measurements were also taken along a transect in the forebay and at a point close to the spillway gates in the tailrace. In the second field work session (spill at the Brilliant Dam), spot measurements were taken across two transects on the Kootenay River and four transects on the Columbia River as well as at a location in the forebay. For scenario 2A, TDG was measured at 1.2 and 2.6 km downstream of the dam on the Kootenay River. Scenario 2B was operated for a longer period of about 8 hours and additional downstream measurements were carried out at 10.10, 12.49,

17.62 and 24.19 km of the Columbia River. The third session included spot measurement across six transects around the Seven Mile and Waneta facilities. For scenario 3A, measurements were carried out in the forebay, tailrace (1.7 km downstream) and at a transect 5.7 km downstream of the Seven Mile Dam. Further measurements were also conducted at the forebay and tailrace of Waneta Dam and upstream of the Pend d'Oreille-Columbia River confluence. For scenario 3B, measurements were taken at four transects from forebay-to-forebay of the dams. For both scenarios, TDG variation with depth was also measured at the Seven Mile Dam forebay.

The spot measurements were usually taken at 4–7 points of each transect during the field works. It took 10 to 20 minutes to collect TDG data at each location resulting in about one to two hours per transect. The probe was kept submerged between points along the same transect to decrease the response time for each measurement. Maintaining its submersion increased the likelihood of obtaining stable readings within a reasonable duration. For most of the cases, readings were taken using two different probes to ensure reliable measurements. During each of the spot measurements, the water depths were also recorded from the boat. The locations of these measurements were logged using a handheld GPS (GPSMAP 78, Garmin, Canada).

2.3 Data Analysis

The TDG concentrations can be a function of pressure, water temperature, solubility and gas composition (Colt 1984), and are influenced by operational conditions of the hydropower facilities. During the period of field work sessions, attempts were made to keep the gate operations consistent, so that steady state conditions could be achieved for the desired scenarios. However, seasonal and daily changes in temperature and barometric pressure can result in TDG fluctuations (USACE 2001). For given temperature and pressure conditions, TDG can be represented as either a concentration or pressure units and is usually expressed as the percentage ratio of total gas pressure and barometric pressure.

Typically, mixing across the depth is much quicker than transverse mixing, and is expected to be well-mixed within a short distance. As a rule of thumb, the length for complete vertical mixing can be taken as 50 times the depth (Rutherford 1994), which corresponds to approximately half a kilometer distance for the study area. Moreover, the highly turbulent conditions associated with

spill operations can enhance the mixing. Therefore, well-mixed conditions were expected in the downstream measurement transects of the river.

2.3.1 Total Gas Pressure

The total gas pressure (TGP) in water is composed of the sum of the partial pressures of atmospheric gases dissolved in the water. The primary gases making up TDG pressure in water are oxygen, nitrogen, argon and carbon dioxide. This TGP was measured directly in the field with an accuracy of ±2 mmHg (PentairAES 2014). During the field work sessions, measurements through the continuous monitoring stations (Figure 2.6) showed that TGP varied depending on the location and was influenced by the spill operations for different scenarios. Because of the consistent gate operation for each of the individual scenarios (i.e. similar condition), stabilized concentrations were observed at the tailrace or near dam locations. Such condition operated over longer duration allowed carrying out spot measurements at the dam tailraces and downstream river.

For each spot measurement, sufficient time was allowed so that the probes can acquire stable TGP readings. These stable TGP readings along with measured barometric pressure were used to calculate the TDG percentage in water (Figure 2.7). During the field work at the HLK Dam, the maximum TGP was 892 mmHg at 0.56 km downstream for scenario 1C which corresponded to a TDG concentration of 122.1%. In the second and third field sessions, the maximum TGP at the Brilliant Dam tailrace was 916 mmHg for scenario 2A, while it was 891 and 851 mmHg at Seven Mile and Waneta dam tailraces respectively for scenario 3A. For these measurements, readings were taken using two different probes to ensure proper data collection and verify quality of data. The TGP readings were consistent between these probes with a maximum variation of 6 mmHg, which corresponded to 0.8% change in TDG.

2.3.2 Barometric Pressure

The total pressure in the water column at any location is composed of the barometric pressure (BP) and the hydrostatic pressure. From Figure 2.6 it can be seen that the TDG could fluctuate with time due to variation of barometric pressure, although the TGP remained same for some cases. The barometric pressure generally varies with local weather patterns and elevation of the water surface and can fluctuate day-to-day or within a day. Over the monitoring period at the HLK dam (session

1), the temporal variation in BP at the continuous monitoring stations was as high as 18 mmHg (Figure 2.6a). The variation in elevation also caused the average barometric pressure to vary throughout the study area. Frequency distribution of the barometric pressures indicated that the most frequent BP at 4.39 km downstream location was 727 mmHg which was on average 5 mmHg less than the observed BP at 19.68 km. The BP also varied along the spot measurements in the downstream transects (e.g. Figure 2.7a). The maximum BP fluctuation in these transects was 2 mmHg with a standard deviation of 0.7 mmHg. The barometric pressure at the continuous stations during the second field-work session ranged from 716-724 mmHg (Figure 2.6b). Mean BP (from spot measurement) at the tailrace of Brilliant Dam (1.2 km d/s) was 715.6±0.2 mmHg for scenario 2B (Figure 2.7b), while it increased to 719.7±0.6 mmHg at 24.19 km. During the field work at the Seven Mile and Waneta dams, the BP varied from 713-726 mmHg as recorded by the continuous stations (Figure 2.6c). Due to the difference in elevation, the average barometric pressure in the forebay and tailrace of Seven Mile Dam was 719.5 and 722.0 mmHg respectively for scenario 3A. It was 726.5 mmHg at the tailrace of Waneta Dam (Figure 2.7d) which was on average 4 mmHg higher than the observed BP at the forebay.

2.3.3 Temperature

The solubility of dissolved gases decreases with temperature (Colt 1984). If water is heated keeping the amount of dissolved gas unchanged, the pressure and the corresponding percent saturation of TDG will increase. From the field measurements at the HLK dam tailrace (Figure 2.7a), it was observed that initially the left bank flows were relatively cooler (15.6 – 16.8 ºC) compared to the right bank corresponding to spill releases (16.9 – 17.9 ºC). Such variation indicated that comparatively cooler water was released through the powerhouse which was expected considering withdrawal from the upstream deep and cold reservoir. The lateral temperature gradient reduced in the downstream as observed during transect measurements. For spill operations at the Brilliant Dam, similar temperatures (about 10 ºC) were observed across the section at 1.2 km downstream for both scenarios (Figure 2.7b). Similarly, temperature variations at the Seven Mile Dam tailrace (1.7 km d/s) were relatively small (Figure 2.7c). The average temperature for scenarios 3A and 3B was 14.5 and 14.9 ºC respectively, with a maximum variation of 0.5 ºC. There was a significant temperature gradient at the downstream of Waneta Dam due to

the effect of Columbia River inflow, with temperature of 14.5 ºC near the left bank and 11.3 ºC near the right bank (Figure 2.7d).

2.3.4 Instrument Response Time

Accurate measurements of TDG depend on the attainment of stable total gas pressure (TGP) readings which are often limited by the instrument response time to obtain precise measurement (D'Aoust 2007). The TDG probes used for the present study utilizes gas diffusion technique to measure the TGP, therefore a finite time must be allowed for equilibration before any measurement can be made. The diffusion of dissolved gases from water to the void volume of the probe occurs through the boundary layer in water-silicone tubing wall. Assuming the boundary layer is thin, the probe's equilibration time will depend on the time required for O_2 and N_2 to diffuse through the tubing wall (Anderson and Johnson 1992). This transient equilibration time for a gas can be derived from Fick's law and can be a function of $V\delta/AD$, where V = void volume; δ = tubing wall thickness; A = tubing surface area; and D = diffusivity of gas in silicone. The diffusivity of N_2 in silicone is lower than O_2. Therefore equilibration of N_2 usually controls the probe's response time (Manning et al. 2003).

According to the manufacturer, the response time for dissolved gas pressure measurement is about 5 minutes within which the TGP smart probe achieves 90% equilibration and the Lumi4 DO-TGP probe achieve 95% equilibration (PentairAES, 2014). Complete equilibration times for commercially available probes were reported ranging from 3 to 20 minutes (Anderson and Johnson 1992; Manning et al. 2003; Pickett 2006). However, this can vary with flow condition, temperature and depth. The response time of the probes used in this study were evaluated for spot measurements carried out during different field-work sessions. As shown in Figure 2.8, TGP readings become stable with time after submersion in water. The response times for TGP equilibration in the forebay of different dams were 8 to 14 minutes. It was shorter in the dam tailraces which varied from 6 to 8.5 minutes. Similar equilibration times were also observed for downstream river measurements. High-velocity water below dams and in the river resulted in greater diffusion between the ambient water and the probe's void volume, and thereby faster response times. The response time also depends on the void volume of the probe. Smaller void volume results in quicker equilibration time.

2.3.5 Measurement Uncertainty

Uncertainty in TDG measurement may arise due to instrument accuracy, inadequate sampling or measurement errors. Therefore analyses were carried out to quantify all significant measurement uncertainties for the data obtained from field measurements. The TDG concentration (C) is obtained from the measurements of total gas pressure (G) in water and the barometric pressure (P). To account for the uncertainty in C, a measure of the total uncertainty (U_C) should be considered for each of these measurements. The total uncertainty of any measurement consists of precision uncertainty and bias uncertainty (Tavoularis 2005). Precision uncertainty is random and can be obtained from repeated measurements, while bias error is consistent and can be identical for each measurement. Based on first-order, second-moment technique (Abernethy et al. 1985), the total uncertainty in TDG measurement can be quantified as:

$$U_C = \sqrt{W_C^2 + B_C^2} \qquad (2.1)$$

where W_C and B_C are the precision and bias uncertainties in percent saturation respectively. TDG obtained from spot measurements were derived from stable total gas pressure readings and average barometric pressures. Due to time constraint, it was not possible to repeat these measurements and hence the precision uncertainties cannot be found for these cases. Measurements through the continuous monitoring stations allowed the estimation of precision uncertainties for different conditions (Table 2.2). From the fluctuation in percent saturation over time (which includes natural variation as well) observed during continuous TDG measurements, W_C was ≤ 0.5% for a given scenario. On the other hand, a maximum variation of 1.0% was observed for repeated measurements while testing in the laboratory.

The bias error in TDG measurement can be associated with the probe, meter and calibration errors. The accuracy of both total dissolved gas pressure and barometric pressure measurement is ± 2.0 mmHg (PentairAES, 2014). The bias uncertainty of the instrument, $B_{C(Instrument)}$, was estimated from the following:

$$B_{C(Instrument)}^2 = \left(\frac{\partial C}{\partial G} B_G\right)^2 + \left(\frac{\partial C}{\partial P} B_P\right)^2 = \left(\frac{1}{\mathrm{P}} \mathrm{B_G}\right)^2 + \left(\frac{-\mathrm{G}}{\mathrm{P^2}} \mathrm{B_P}\right)^2 \qquad (2.2)$$

where B_G and B_p are the bias uncertainties in total dissolved gas pressure and barometric pressure respectively. The corresponding instrument error varied from 0.40-0.45% for the field data

obtained during spot measurements. From laboratory testing, the maximum calibration error was found as 1.0%. Uncertainty may also arise due to instrument response time for equilibration if the required sampling time is not allowed. However, sufficient time was allowed to ensure equilibration during the field measurements (Figure 2.8). After stabilization, the fluctuations in readings were accounted through precision errors. The bias error (B_C) was calculated considering the instrument and calibration errors for each measurement, which was larger compared to W_C. Then the total uncertainty was calculated from Eq. (2.1) resulting in a maximum uncertainty of 1.5% for the TDG measurements. The corresponding error bars are shown in Figure 2.7 for the measurements at the tailrace of each dam. Eq. (2.2) indicates that the uncertainty associated with TDG measurement is proportional to the total gas pressure and inversely proportional to the barometric pressure. Therefore, the total uncertainty was comparatively lower for the downstream measurements.

2.4 Summary

A comprehensive and detailed measurement of total dissolved gas (TDG) was carried out in the Columbia River system for three different field work sessions. During July 25-30, 2016, a TDG monitoring survey was conducted at the Hugh L. Keenleyside Dam and downstream river. To further the research effort, two additional field work sessions were carried out at the Brilliant Dam from June 7-8, 2017 and at the Seven Mile and Waneta dams from June 19-20, 2017. The surveys covered the dam facilities as well as the downstream river reaches and included the Columbia River to all the way down to Canada-US border. The field works were carried out for different combinations of spill operations at various hydropower facilities and resulted in TDG measurements for eight different scenarios throughout the Columbia River system.

During the field work sessions, total gas pressure, barometric pressure and temperature data were measured to acquire TDG through combination of continuous monitoring at multiple locations and spot measurements across different cross-sections. For continuous monitoring, an innovative floating platform was designed that can effectively capture TDG levels representative of the main flow. The installation and deployment of these monitoring stations was often constrained by steep bank slopes, high velocity in the river and navigational issues. The spot measurements at different locations were taken from a boat which was extremely challenging due to turbulent river

conditions. Measurements were occasionally limited due to time and other facility-specific operational constraints, and appropriate measures were taken to ensure quality data collection. The combination of continuous and spot measurements provided temporal and spatial variation of TDG which were consistent with gate operational changes associated with spill operation of individual dams. Despite following strict protocol and careful measurement techniques, uncertainty in TDG measurement can arise due to instrument accuracy, inadequate sampling or measurement errors. A maximum uncertainty of 1.5% was quantified by considering precision and bias errors of individual measurements. The measurements during the field work sessions provided interesting and useful observations on TDG supersaturation in dam spillways and downstream rivers, and founded the basis of various research components of the current study.

Table 2.1: Summary of the field work sessions in the Columbia River hydropower system

Session	Period	Scenario	Facility	Spill rate (m^3/s)	Generation flow (m^3/s)
1	26 – 30 July, 2016	1A	HLK	1025.6	1085
		1B		934.8	1100
		1C		1110.6	1081
		1D		1023.3	1081
2	7 – 8 June, 2017	2A	Brilliant	1768.3	942.5
		2B		1807.1	946.9
3	19 – 20 June, 2017	3A	Seven Mile	246.4	1413.1
			Waneta	189.5	1470
		3B	Seven Mile	836.2	713.6
			Waneta	79.8	1470

Table 2.2: Precision uncertainty for TDG measurements at the continuous monitoring stations

Field Session	Scenario	Station Location	W_C (%)
26 – 30 July, 2016	1B	0.98 km d/s of HLK Dam	0.3
		4.39 km d/s of HLK Dam	0.2
		2.60 km d/s of Brilliant Dam	0.4
		11.30 km d/s of HLK Dam	0.5
		19.68 km d/s of HLK Dam	0.1
7 – 8 June, 2017	2B	2.60 km d/s of Brilliant Dam	0.4
		12.49 km d/s of HLK Dam	0.5
		17.62 km d/s of HLK Dam	0.2
19 – 20 June, 2017	3A	Seven Mile Dam forebay	0.5
		Seven Mile Dam tailrace	0.5
		Waneta Dam forebay	0.3

Figure 2.1: The Columbia River hydropower system

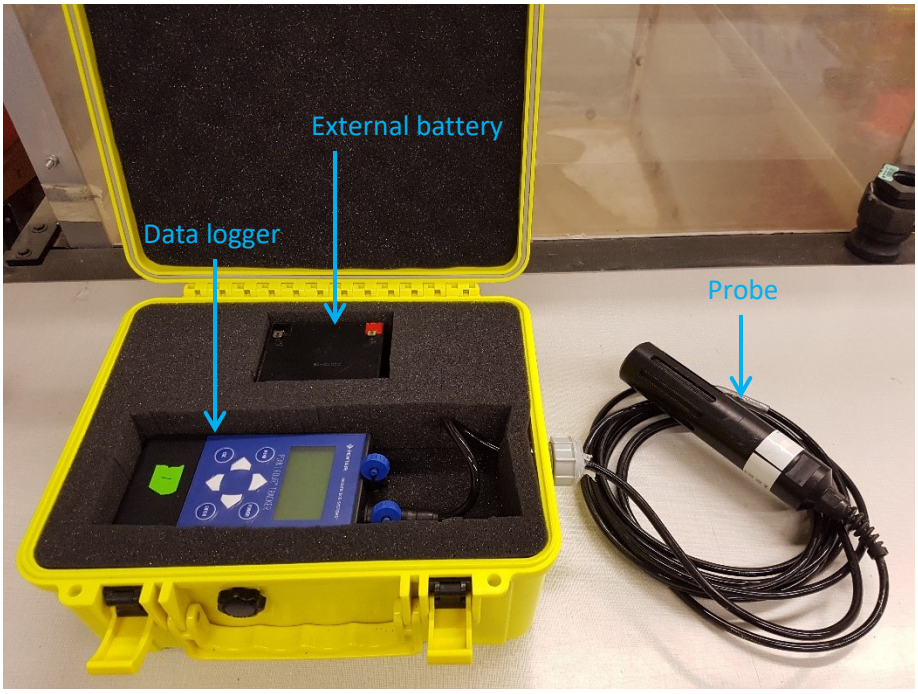

Figure 2.2: TDG measurement instrument (PT4 Smart/ Lumi4 DO-TGP probe) inside enclosure

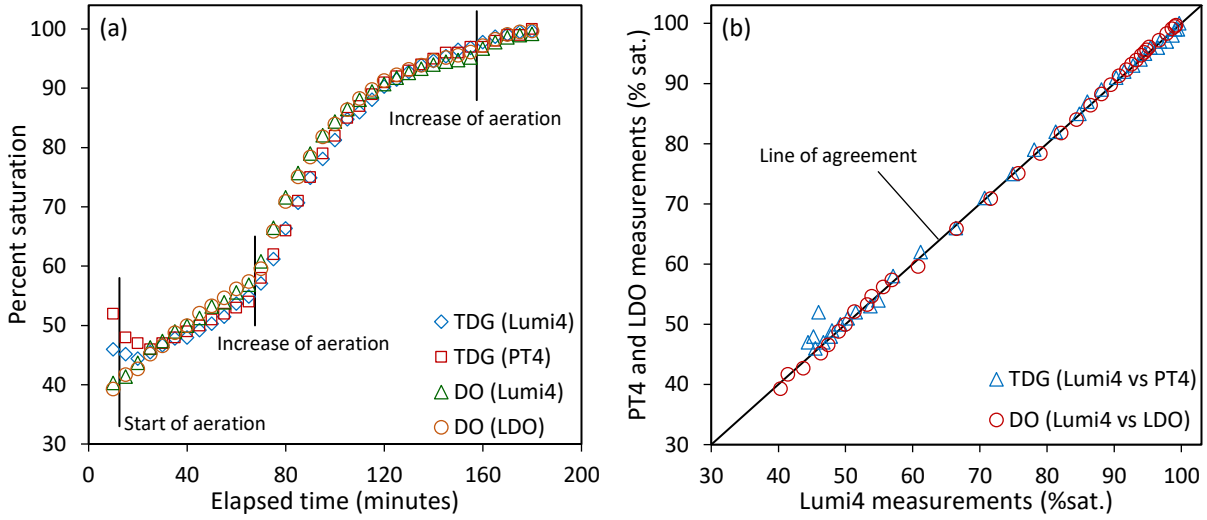

Figure 2.3: Laboratory measurement of (a) total dissolved gas and dissolved oxygen using different probes and (b) their comparison

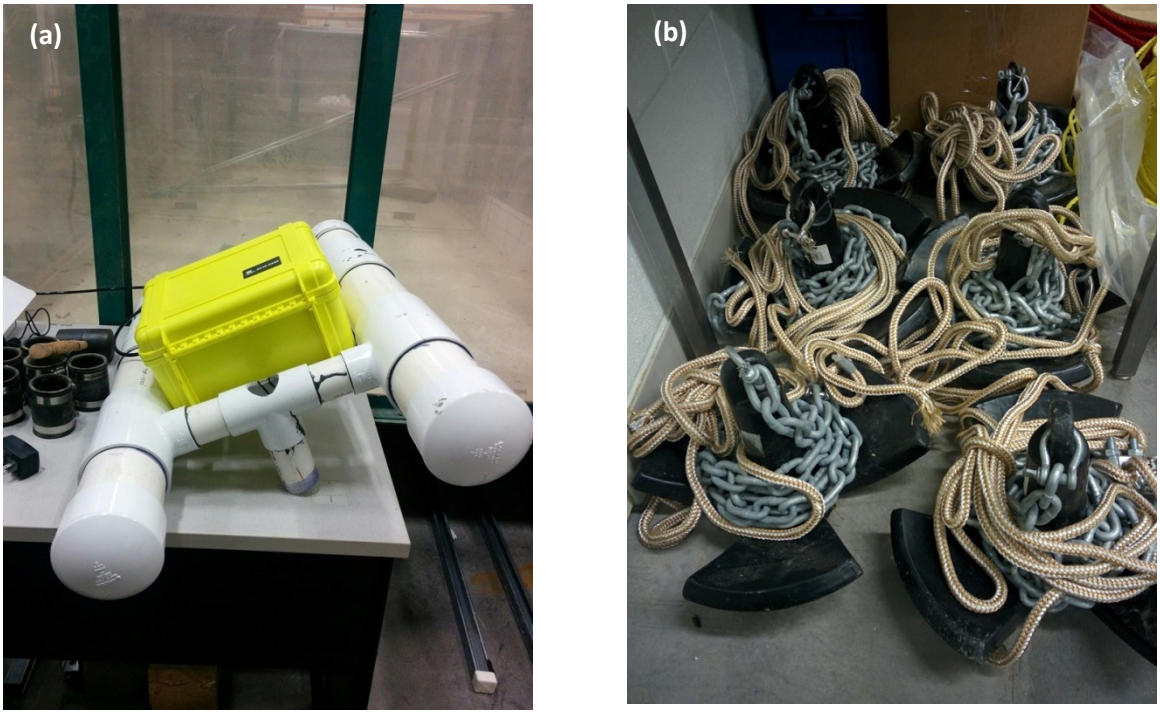

Figure 2.4: Floating platform (a) and anchors (b) for TDG probe deployment

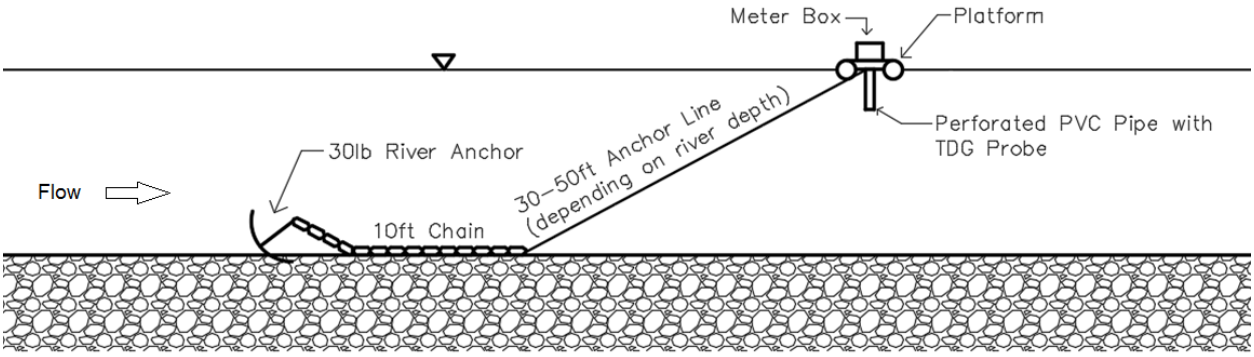

(a)

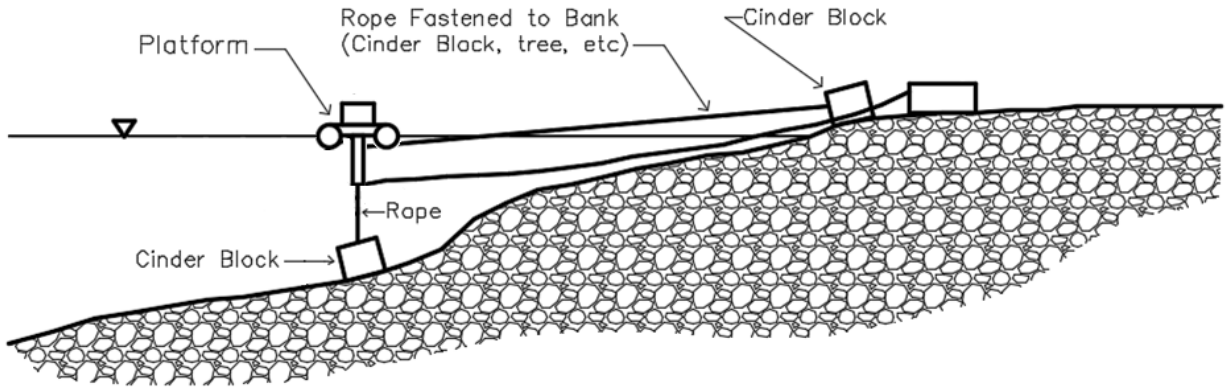

(b)

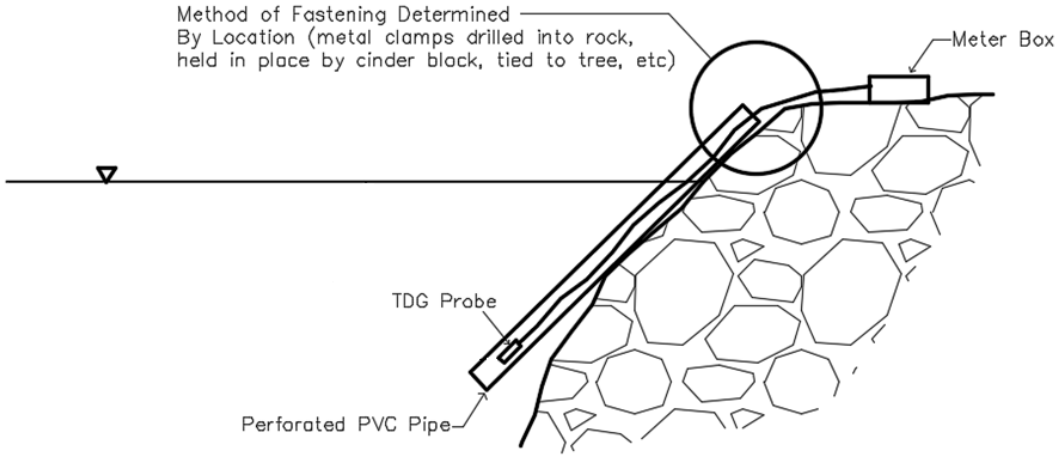

(c)

Figure 2.5: TDG probe installation for continuous monitoring (a) within river channel, (b) along shallow bank and (c) along steep bank

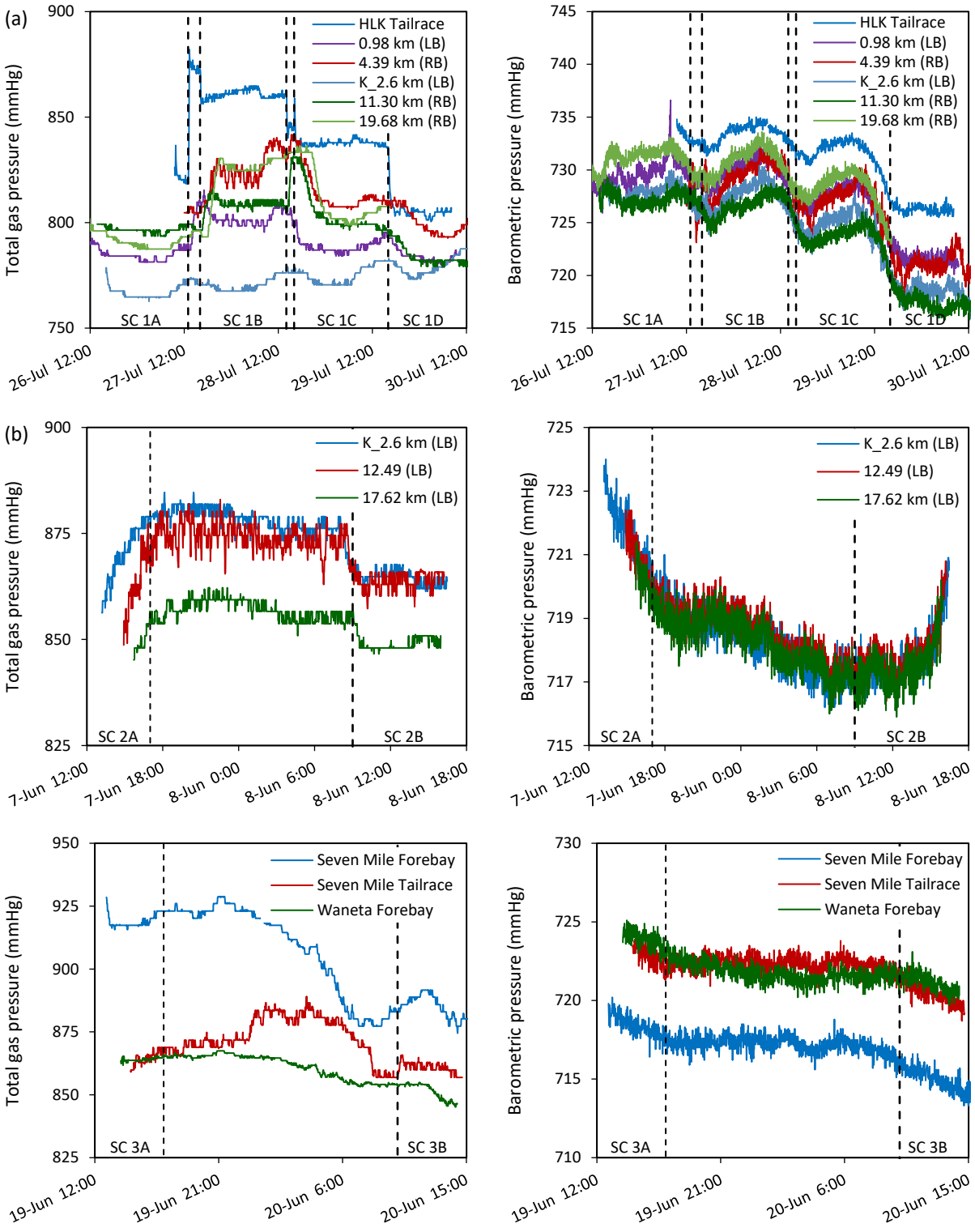

Figure 2.6: Continuous monitoring of total gas pressure and barometric pressure during different field work sessions

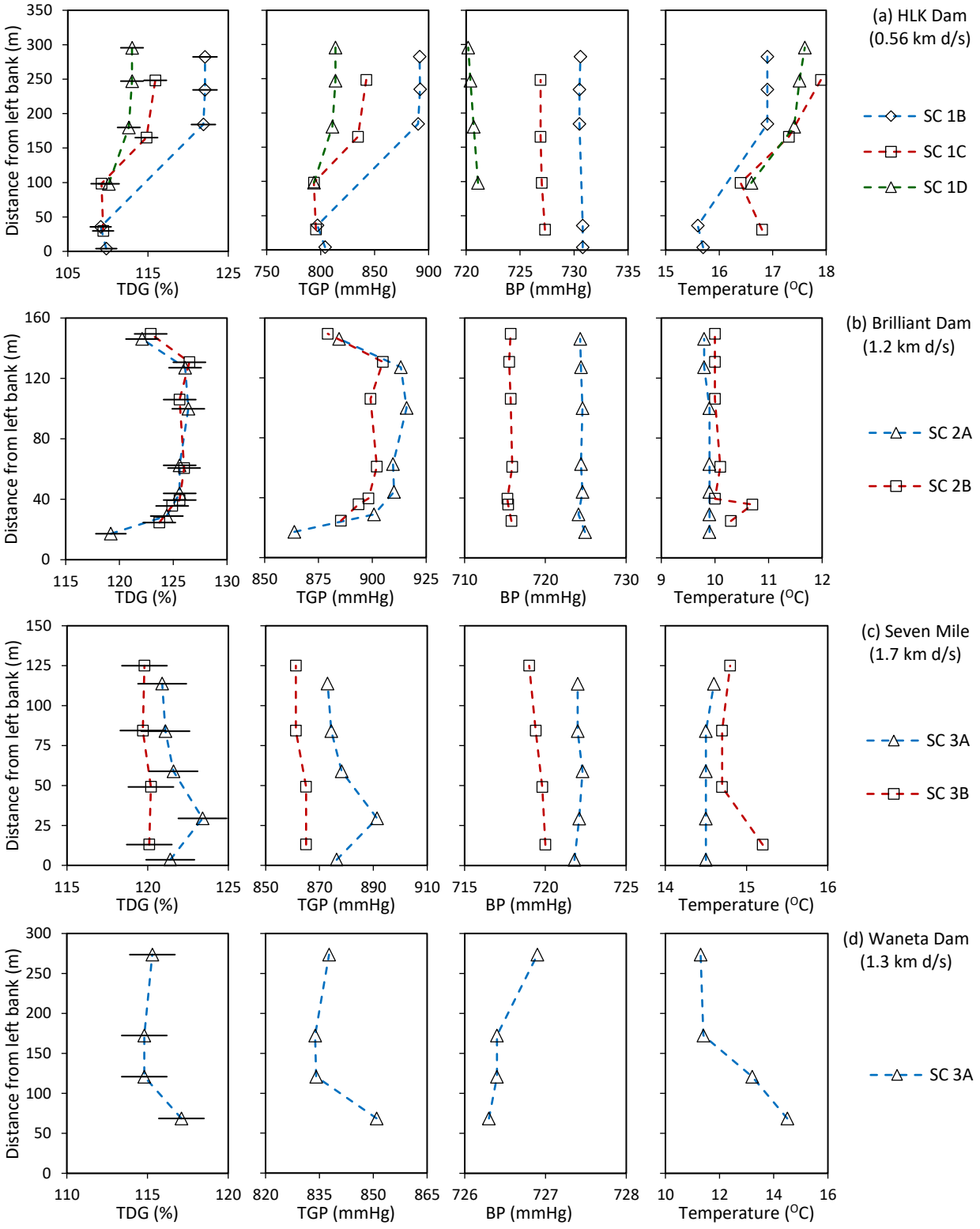

Figure 2.7: Spot measurements of TDG, total gas pressure, barometric pressure and temperature at the tailraces of (a) HLK, (b) Brilliant, (c) Seven Mile and (d) Waneta dams

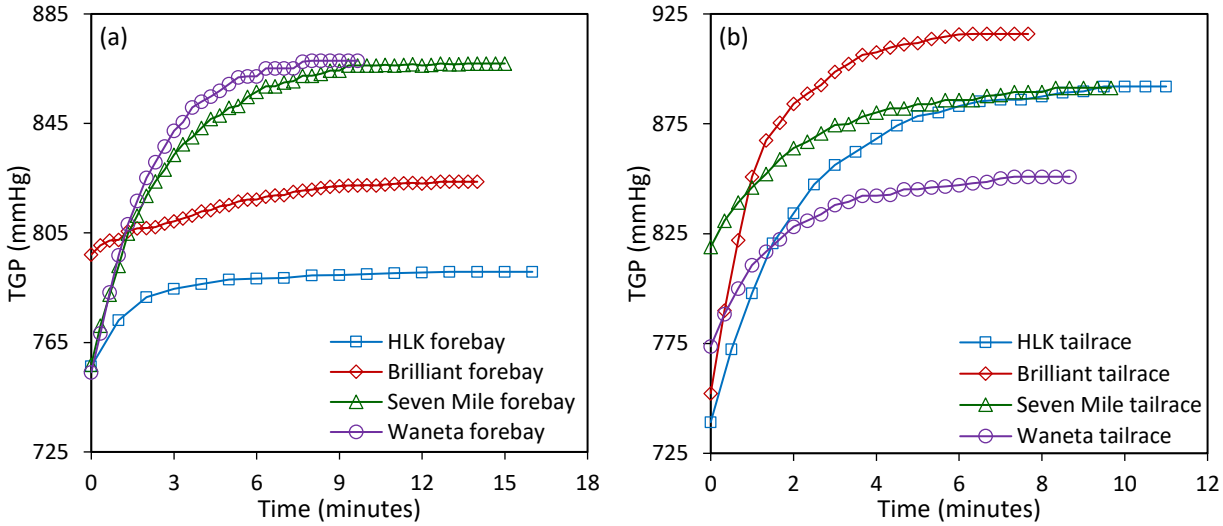

Figure 2.8: Elapsed time to acquire stable total gas pressure (TGP) during spot measurements in the (a) forebay and (b) tailrace of different dams

CHAPTER 3

Dissipation of Supersaturated Total Dissolved Gases in the Intermediate Mixing Zone of a Regulated River [*]

3.1 Introduction

Spill operations in hydropower facilities are known to cause supersaturation of total dissolved gases (TDGs) in the tailrace and downstream rivers, and often exceed the water quality standard of 110% (USEPA 1986; CCME 1999) or site-specific waived limit of 120% (Weitkamp 2008). Exposure to supersaturated water can cause gas bubble trauma (GBT) in fish, especially in early life, and lead to direct or indirect mortality (Ebel 1969; Weitkamp 2008). The likelihood of such exposure depends on the operational pattern at the dam site and can vary across and along the river affecting fish and aquatic environment. It is therefore necessary to understand the distribution and dissipation of TDG to address the risk of exposure to supersaturation at different spatial scales and identify operational mitigation measures for the conservation of fish habitat.

TDG distribution extending from the dam site to the downstream river can result from different physical processes. During spill releases, significant amounts of atmospheric gases can be entrained in stilling basins at the outlets of spillways (Gulliver et al. 1990) and low-level conduits (Mortensen et al. 2011), where the hydrostatic pressure is sufficient to produce supersaturated condition compared to ambient atmosphere. In general, TDG pressure is maximum at the stilling basin where the air content, depth, velocity and turbulence intensity are very high (Geldert et al. 1998). Beyond the plunging region of the tailrace, the net mass transfer reverses resulting in TDG dissipation. This process, along with mixing within water, causes the supersaturated dissolved gases (primarily nitrogen and oxygen) to re-establish equilibrium. However, elevated or even supersaturated gas levels may persist hundreds of kilometers from the source of supersaturation (USACE 2001; Feng et al. 2014).

[*] The content of this chapter has been published as: Kamal, R., Zhu, D.Z., Leake, A. and Crossman, J. (2019). "Dissipation of Supersaturated Total Dissolved Gases in the Intermediate Mixing Zone of a Regulated River". *Journal of Environmental Engineering, ASCE*, 145(2): 10.1061/(ASCE)EE.1943-7870.0001477.

The dissipation can be associated with various physical, biological and chemical processes (Weitkamp and Katz 1980), among which the interfacial gas exchange is usually considered as the key process for degassing supersaturated TDGs out of the river system. For low-solubility gases such as nitrogen and oxygen, the dissipation across the air-water interface depends on the turbulent transport in the water layer similar to the stream reaeration process (Moog and Jirka, 1999). Due to difficulty in direct field measurements, numerous empirical and semi-empirical methods have been developed to estimate the stream reaeration coefficient (O'Connor and Dobbins 1958; Churchill et al. 1962; Owens et al. 1964; Thackston and Krenkel 1969; Bennett and Rathbun 1972; Smoot 1988). These equations are site-specific and can result in large prediction errors in conditions different from which they were formulated (Bowie et al. 1985; Melching and Flores 1999; Gualtieri et al. 2002). Some previous studies considered the interfacial transfer of TDG by incorporating bulk hydrodynamics of flow (Geldert et al. 1998; Orlins and Gulliver 2000), dissolved oxygen transfer estimates (Politano et al. 2009), or utilizing mechanistic approach based on small-eddy model (Weber et al. 2004; Urban et al. 2008). However, these studies were limited in the tailrace bubbly region. When gas transfer is accompanied by bubble formation, it is no longer a reverse process of reaeration (Hikita and Konishi 1984; Woolf and Thorpe 1991). From experimental study, Li et al. (2013) found that TDG dissipation rates were different than the unsaturated reaeration estimates. The gas exchange of supersaturated TDG in rivers require further investigation as suggested by Orlins and Gulliver (2000), particularly in the field through direct quantification of dissipation rate.

The mixing between the spilled water with high TDG and generation flow is also important, as the powerhouse releases tend to dilute TDG pressures (USACE 2001). Additional mixing and dilution can result by flows from secondary sources, such as tributary inflows. In rivers, mixing across depth is quicker compared to the lateral width of the channel; hence transverse mixing is the dominant mechanism for spreading (Fischer et al. 1979; Rutherford 1994). Therefore for quantitative prediction of TDG, both mixing and dissipation rates should be accounted particularly in the downstream rivers in order to understand the TDG distribution process.

The Hugh L. Keenleyside Dam (HLK) and the Brilliant Dam are the lower-most of series of hydropower facilities in the Columbia and Kootenay Rivers respectively (Figure 3.1). The river reaches downstream of these dams inhabit a variety of fish species, including white sturgeon,

mountain whitefish, rainbow trout, and are typically subjected to supersaturation during spring freshet and summer (Bruce 2016). The cumulative contributions of these dams can result in high TDG concentrations and negatively impacts fish populations. Assessment of such impact can be very complex and require reliable estimation of TDG. Further, uncertainties surrounding impacts to the aquatic environment at varying distances downstream from the source of TDG generation also support the need for direct quantification of dissipation. In this study, our objective was to quantify the dissipation rate of supersaturated TDG in the regulated lower Columbia River and evaluate its consistency with known surface reaeration models and gas transfer theories.

3.2 Background

When supersaturation occurs, the exchange of gas at the air-water interface (i.e. dissipation) during transport through the river drives TDG levels towards equilibrium with the atmosphere. Considering control volume approach, the concentration of TDG can be obtained assuming first-order kinetics as follows:

$$C = C_{sat} + (C_i - C_{sat})\, exp(-kt) \quad (3.1)$$

where C_i and C are the initial and final concentrations respectively; C_{sat} is the saturation concentration (usually 100% at atmospheric pressure), k is the gas transfer coefficient associated with dissipation and t is the travel time of water. Typically in reaeration studies, the interfacial transfer rate is parameterized by gas flux which depends on the air-water concentration gradient and can be expressed as follows:

$$k = \frac{J}{H(C - C_{sat})} \quad (3.2)$$

where H is the mean depth of flow, and J is the gas flux per unit interfacial area which can be estimated from the mass flux difference between two consecutive sections. The mass flux at a given section can be estimated as $M = \int_0^Q C\, d\hat{q}$, where $\hat{q}$ is the cumulative discharge defined as $\int_0^y uhdy$ with $\int_0^y dy =$ channel width, B; u, h and y are local depth-averaged velocity, depth and transverse distance from bank respectively; and Q is the total discharge.

In reaeration studies, two widely used semi-empirical treatments are the surface renewal model and the energy dissipation model (O'Connor and Dobbins 1958; Tsivoglou and Wallace 1972).

These were later related to turbulence by considering the presence of a wide range of eddy sizes, ranging between flow domain (integral scale) to smallest sizes (Kolmogorov scale). These two extreme estimates are known as the large-eddy (Fortescue and Pearson 1967) and small-eddy (Lamont and Scott 1970) models respectively, and can be generalized as (Moog and Jirka, 1999):

$$kH/U^* \propto Sc^{-1/2} Re_*^{-n} \quad (3.3)$$

where U^* is the shear velocity; Sc is the Schmidt number = ν/D_m; ν is the kinematic viscosity; D_m is the molecular diffusivity of the gas in water and Re_* is the shear Reynolds number = U^*H/ν. The Reynolds number exponent (n) is ½ for large-eddy model and ¼ for small-eddy model. A number of experimental works supported the small-eddy model (Moog and Jirka 1999), while some others suggested the influence of large-scale motions in interfacial transport (Gulliver and Halverson 1989). From dimensional analysis, Li et al. (2015) showed that the TDG dissipation rate depends on the Schmidt number, the aspect ratio of the channel and the shear Reynolds number. Also temperature could affect the rate of dissipation (Shen et al., 2014), which can be incorporated with the simplified equation as follows:

$$k = k_{20}\theta^{(T-20)} \quad (3.4)$$

where k_{20} = dissipation rate at standard 20 ºC; T = river water temperature; and θ = temperature coefficient. The temperature coefficient could vary from 1.008-1.047, but generally reported to be 1.024 (Bowie et al. 1985).

3.3 Methodology

3.3.1 Field Work

The Hugh L. Keenleyside Dam (HLK) is located on the Columbia River approximately 57 km upstream from the BC-Washington border. The 52 m high dam impounds the Arrow Lakes Reservoir and helps regulate the flow as per the Columbia River Treaty between Canada and the United States. This facility consists of eight low level outlet gates (referred as northern and southern gates) located on either side of a four-bay spillway with the generating station being positioned directly north of the dam (Figure 3.1). The Kootenay River confluence is located approximately 10.5 km downstream, which is regulated by the Brilliant Dam (situated 2.8 km

upstream of the confluence) and five more facilities upstream in the Canadian part of the river. The run-of-the-river Brilliant Dam consists of a powerhouse on the right bank and an eight-bay, gated spillway adjacent to the left bank. The second generating station is located about 150 m downstream on the left bank. The region of field work for this study extended from the HLK Dam covering about 25 km stretch of the Columbia River and included the Brilliant Dam facility on the Kootenay River. The length of this study reach is on the order of 90 times the width of the river, which can be considered as the intermediate field where transverse mixing is dominant.

The first field work session was conducted from July 26-30, 2016 for four different low-level outlet gates operations at the HLK Dam (Table 3.1). Over the course of the field work period, the generation flow was set as consistent as possible between 1081 to 1100 m^3/s, while the spill through the individual units were varied to produce different TDG levels. For example, northern gates 2 and 3 were partially opened while gate 4 was fully opened during scenario 1A with average flows of 186.4, 188.4 and 650.8 m^3/s respectively. However for each of the scenarios, flows through the individual units and corresponding total spills (as outlined in Table 3.1) were held relatively constant except during the gate changes. Throughout this test period, discharge out of the Brilliant Dam only consisted of the powerhouse releases (no spills) and averaged from 482.6 - 585.2 m^3/s for individual scenarios.

The second field work session was conducted on June 7-8, 2017 during a spill event at the Brilliant Dam. For this scenario, spillway bays 1-3 (bay 1 partially opened; 2 and 3 fully opened) were operated to discharge at 1807.1 m^3/s. Generation flows from the two powerhouses were 404.5 and 542.4 m^3/s respectively. During this session, northern gates 2, 3 and 4 were in operation at the HLK Dam. For both field work sessions, discharge and water level information were also collected from the Water Survey Canada (WSC 08NE049 station, https://wateroffice.ec.gc.ca) located about 29 km downstream of the HLK Dam. This station included the combined releases from the upstream facilities, and measured an average of 2.3% higher discharge compared to the flow rates outlined in Table 3.1.

In order to capture the temporal and spatial variation of TDG, two collection methods were adopted – stationary continuous monitoring using floating platforms and spot measurements across transects from a boat. Total gas pressure (TGP), barometric pressure (BP) and water temperature

were measured by Lumi4 DO-TGP and PT4 Smart TGP probes (manufactured by Pentair Aquatic Eco-Systems, Apopka, Florida). During the spill events at the HLK Dam (scenario 1), measurements were carried out in seven downstream transects as shown in Figure 3.1. For continuous monitoring, five stations were set up near the left bank at 0.98 km; along the right banks at 4.39, 11.30 and 19.68 km and upstream on the Kootenay River (about 3-5 m away from the banks). In addition, another monitoring station was installed along the southern berm of the tailrace. In these cases, the probes were submerged approximately 1-1.5 m deep below a custom-built, floating PVC platform which contained the data logger in a water-tight enclosure and was anchored to the river (Figure 3.2). Before deployment, the probes were calibrated and set to record data continuously at 2 minutes intervals.

Figure 3.3 shows the measured TDG at the continuous monitoring stations for the first field work session. The consistent gate operation for individual scenarios resulted in a stabilized, steady-state condition which allowed carrying out spot measurements at transects downstream of the HLK Dam. Due to time limitation and other constraints, it was not possible to take measurements at 0.56 and 0.98 km for scenario 1A and at 11.30 and 19.68 km for scenario 1D. Additional measurements were also taken in the forebay and at a point near the tailrace. For scenario 2 (spill at the Brilliant Dam), spot measurements were taken across two transects on the Kootenay River and four transects on the Columbia River (Figure 3.1). All spot measurements were taken from a boat anchored at the survey location. The probe was kept at depth about 1-1.5 m for about 10-20 minutes, sufficient to acquire stable TGP readings. Occasionally, readings were taken using two different probes in order to ensure reliable measurements. Also, the measurement locations were recorded using a handheld GPS (Garmin GPSMAP 78) which had accuracy in the order of 1-2 m.

An Acoustic Doppler Current Profiler (600 kHz RiverRay manufactured by Teledyne RD Instruments) was used to carry out hydraulic measurements. The RiverRay measured the velocity (accuracy of ±2 mm/s) and depth (accuracy ±1%), which were utilized to estimate discharge (TRDI 2015). These measurements were completed by driving the boat slowly across the seven transects covered during scenario 1 (refer to Figure 3.1). The first two transects (0.56 and 0.98 km) were measured for scenario 1B, while transect at 19.68 km was covered during scenario 1C. The rest of the measurements were taken during scenario 1D. Each of these transects were repeated 3 to 4 times for accuracy and comparison purposes. Standard deviation of discharge for the repeated

measurements varied from 1.2% (0.98 km) to 5.1% (19.68 km). The mean discharges at the first five transects were similar to the combined releases from the HLK Dam for scenarios 1B and 1D (refer to Table 3.1), except for the transect at 0.98 km. In this location it was not possible to survey the whole river width due to log booms. At 11.30 km, the measured discharge was 2629.5 m^3/s for scenario 1D, indicating additional inflow coming from the Kootenay River. Due to presence of large eddies near the left bank at 19.68 km, the measured discharge was about 11% lower than the combined releases from the upstream dams for scenario 1C.

3.3.2 Hydraulic Calculation

Due to time constraint, it was not possible to carry out the ADCP measurements in all transects for individual scenarios. Therefore, HEC-RAS (www.hec.usace.army.mil) was used to obtain velocity-depth information for different scenarios. Flows released from the HLK and Brilliant dams were used as input boundary conditions with the model domain extending up to Water Survey Canada station (the downstream boundary). The model was calibrated for scenario 1D for which the maximum variation of water levels at the WSC station was about 3 cm. Field observation and previous studies (Bruce 2016) showed that the river reach upstream of the Columbia-Kootenay confluence could be backwater affected. Therefore the model calibration, i.e. adjustment of Manning's roughness coefficient, was performed in two steps. First the calculated water surface elevation was matched with the tailwater levels of both dams and then the modeled velocities were matched with the ADCP measured mean velocities. The final calibrated Manning's roughness varied from 0.023 to 0.068 which fell within the range of acceptable values found in the literature. The modeled velocities matched the measured velocities satisfactorily with a maximum variation of 4.2% (Figure 3.4a). Table 3.2 outlines some basic hydraulic parameters at various transects, in which only scenario averaged values were reported for the four operational conditions of scenario 1 (scenarios 1A-1D). For these cases, standard deviation of the calculated velocities and depths (obtained from HEC-RAS) ranged between 0.8-3.3% and 0.5-1.1% respectively compared to the scenario averaged values.

The cumulative discharge at individual transects were estimated from the mean velocity profile, which was obtained by fitting the ADCP measurements utilizing Manning's equation (as shown in Figure 3.4b for example). Use of Manning equation to estimate the local depth-averaged

velocity was suggested by Rutherford (1994) and Zhang and Zhu (2011). The calculated velocities were compared with the ADCP measurements by computing absolute relative error in each transects (Table 3). Overall the errors were within 13% except for transects at 0.56 and 19.68 km, where measurements were likely difficult due to re-circulation zone. To compute the cumulative discharge in locations where ADCP measurements were not done (e.g. transects covered for scenario 2) or in areas of incomplete (as in 0.98 km) and inaccurate (as in 19.68 km) measurements, a modified Manning's equation was utilized.

3.3.3 Analytical Modeling of Transverse Mixing

In rivers, complete vertical mixing occurs at a distance approximately fifty times the depth (Rutherford 1994). Beyond this distance, vertically well-mixed conditions are expected for TDG measured at downstream transects. In the intermediate field of a river, transverse mixing is dominant and hence Eq. (3.1) cannot be applied directly to estimate dissipation. To describe the two-dimensional distribution of TDG, an analytical method based on streamtube model (Yotsukura and Sayre 1976) was used in this study. Such method is useful, particularly for field applications where the data quality is difficult to control due to inadequate samplings or measurement errors (Zhang and Zhu, 2011). Using the concept of cumulative discharge, the steady-state distribution of a substance can be described as follows (Gowda 1984):

$$\frac{\partial C}{\partial x} = D\frac{\partial^2 C}{\partial \hat{q}^2} - \frac{kC}{U} \quad (3.5)$$

where x is the longitudinal distance; U is the mean velocity in the direction of flow and D is the factor of turbulent diffusion. Eq. (3.5) assumes uniform velocity in the direction of flow. The factor, D can be assumed constant at a given cross-section but can vary in the longitudinal direction (Gowda 1984). It can be related to the variances of concentrations based on the method of moments as follows (Rutherford 1994):

$$D = \frac{1}{2}\frac{d\sigma_{\hat{q}}^2}{dx} \quad (3.6)$$

where $\sigma_{\hat{q}}^2$ is the variance of concentration distribution with cumulative discharge $\hat{q}$. In order to evaluate transverse mixing coefficient, the factor of turbulent diffusion can be related to reach averaged hydraulic properties as follows (Rutherford, 1994):

$$D = \psi E_t U H^2 \quad (3.7)$$

where E_t is the transverse mixing coefficient and ψ is the dimensionless shape factor = $\int_0^Q uh^2 dq / UH^2 Q$. Following Fisher et al. (1979), distribution from a steady-state point source can be predicted from the analytical solution of Eq. (3.5) assuming a conservative case (k = 0):

$$C_i\,(x, \hat{q}) = C_{max}\, exp\left[-\frac{(\hat{q} - \hat{q}_o)^2}{2\sigma_{\hat{q}}^2}\right] + Image\ sources \quad (3.8)$$

where $\hat{q}_o$ = cumulative discharge at the source and C_{max} = peak concentration at a given x. Image sources were included to account the effect of banks on concentration distribution. For a distributed source at x = 0 stretching over a range of cumulative discharge from $\hat{q}$ = $\hat{q}_1$ to $\hat{q}$ = $\hat{q}_2$, the superposition principle gives:

$$C_i\,(x, \hat{q}) = \int_{\hat{q}_1}^{\hat{q}_2} \frac{C_o}{\sqrt{2\pi\sigma_{\hat{q}}^2}}\, exp\left[-\frac{(\hat{q} - \hat{q}')^2}{2\sigma_{\hat{q}}^2}\right] d\hat{q}' + Image\ sources \quad (3.9)$$

where C_o is the reference or maximum concentration at the initial section. Assuming uniform concentration at the source, Eq. (3.9) was integrated to obtain the following analytical solution:

$$C_i\,(x, \hat{q}) = \left(\frac{C_o}{2}\right)\left[erf\left(\frac{\hat{q} - \hat{q}_1}{\sqrt{2\sigma_{\hat{q}}^2}}\right) - erf\left(\frac{\hat{q} - \hat{q}_2}{\sqrt{2\sigma_{\hat{q}}^2}}\right)\right] + Image\ sources \quad (3.10)$$

In this equation, four image sources were included on either side of the banks. The concentrations obtained from this equation could be incorporated in Eq. (3.1) to estimate TDG dissipation rate.

3.4 Results

In the Columbia River, water was consistently supersaturated during the field work sessions. At the HLK Dam (scenario 1), marked distinction in concentrations were observed between the spill and generation flows, with spill releases containing high level of TDG near the right bank (Figure 3.5a). For different gate settings (scenarios 1A-1D as outlined in Table 3.1), discharge through the low-level gates and powerhouse were similar. Due to consistent gate operation of the individual scenarios, steady TDG concentrations were observed at the tailrace continuous monitoring station

(Figure 3.3) which indicated that the operation of three northern gates (scenario 1A) generated 112% TDG. Measurements at this station for other scenarios were relatively lower compared to the spot measurements at 0.56 km. Such variation might arise because of the near-bank placement of the station or calibration difference between the measuring probes. Near the tailrace (about 250 m downstream), spot measurements were taken at different depths during the operation of three southern gates (scenario 1B). For this scenario, the TDG at 1.5 m depth was 120%, while it increased to 124% and 126% at the mid and maximum depth respectively. At 0.56 km downstream, the maximum TDG (at 1.5 m depth) was 122% near the right bank (corresponding to spill flow) indicating vertically well-mixed condition further downstream. For scenarios 1C and 1D (combined operation of northern and southern gates), the maximum TDG dropped to 116 and 113% respectively. For all scenarios, initial TDGs near the left bank (corresponding to generation flow) were in the range of 108-110%, which were similar to that in the forebay.

Due to subsequent mixing and dissipation, the concentration decreased in the upstream reach of the confluence and was least variable at 6.70 km (Figure 3.5b-e). The maximum TDG at this transect was 117% for scenario 1B and 113% for scenario 1C. Downstream of the confluence, the distribution was affected by the two converging rivers of different TDG levels. Continuous monitoring indicated that the Kootenay River inflow had TDG concentrations in the range of 106-109% (Figure 3.3). At 11.30 km, the concentrations were relatively higher along the right bank (corresponding to HLK Dam flow as shown in Figure 3.5f), with maximum TDG of 110, 114 and 112% for scenarios 1A, 1B, and 1C respectively. The continuous observations at 11.30 and 19.68 km were more or less consistent with the tailrace TDG pattern, except for scenario 1B where the concentrations were higher at 19.68 km than at 11.30 km (Figure 3.3). Such variation might result from the complex flow pattern (deep pool with large re-circulation zone) at this section, and was not included in the analysis.

During the second field work session (scenario 2), the spill rate at the Brilliant Dam was high with a spill-to-generation ratio of about 1.9. Because of the orientation of the facility (powerhouses located on either side of the spillways), the spill created a plume of high TDG water along the mid-channel of Kootenay River with maximum concentration of 126% at 1.20 km, which only reduced by 1% at 2.60 km. The high TDG water was transported downstream of the confluence where marked concentration gradients were observed due to two converging rivers (Figure 3.5h). Spot

measurements taken at the upstream of the confluence (at 10.10 km) showed that the Columbia River inflow had TDG concentrations of about 111%. At 12.49 km, TDG near the left bank (corresponding to Brilliant Dam flow) was 125%, while it decreased to 120% at 24.19 km.

The rate of dissipation can be assessed directly by considering the changes in total mass flux in a control volume. Assuming net flux across the air-water interface (J) equals the mass flux difference between two consecutive sections, Eq. (3.2) could be employed to estimate the rate. However, the calculated mass fluxes were not always consistent between two sections. For example, mass flux at 0.98 km was overestimated by 0.23% compared to 0.56 km for scenario 1C. Such error resulted from the insufficient samples collected between the left and right banks and straight-line interpolation between these points (Figure 3.5a). For scenarios 1B-1D, the calculated mass flux at 6.70 km was higher than at 4.39 km due to some scattered individual point measurements. Similarly TDG fluxes were not consistent between 11.30 and 19.68 km, with the latter located in a deep pool with complex flow structure and might lead to error in subsequent calculation of mass flux. Despite the variations, the dissipation rate was evaluated using Eq. (3.2) considering control volumes stretching from 2.03-6.70 km for scenarios 1A and 1C, 0.56-6.70 km for scenario 1B, and 0.98-4.39 km for scenario 1D. These relied heavily on raw field data and were only used as a first estimate in analyzing transverse mixing.

Given the uncertainty with individual point measurements, the step-function based analytical approach was utilized to estimate the mixing and dissipation rate in the Columbia River. Considering line sources downstream of the dam (corresponding to spill and generation flows) or downstream of the confluence (representing two converging rivers), Eq. (3.10) was used to obtain the transverse TDG distribution. In the upstream reach, maximum TDGs measured for different gate settings of scenario 1 were taken as the reference concentration for the spilled plume. Since the concentrations could also change by dissipation, Eq. (3.10) in conjunction with Eq. (3.1) was used to calculate the theoretical profile by assuming an initial rate obtained from the mass flux approach. Then the variances ($\sigma_{\hat{q}}^2$) of the C-$\hat{q}$ distribution were estimated from the comparison with the measured TDG across individual sections. When $\sigma_{\hat{q}}^2$ is plotted with the longitudinal distance, half of the slope of the fitted straight line would be the factor of turbulent diffusion, D (Figure 3.6). With the estimated D, the dissipation rates for different scenarios were obtained by fitting the calculated concentrations with measured data based on least square method. The mean

concentration of TDG plume calculated upstream of the confluence was then utilized together with Kootenay River TDG to estimate D and dissipation rate in the downstream reach following similar procedure. For this reach, line sources of high TDG water from the Kootenay River (measured at K2.6 km – K indicates the distance on the Kootenay River) and Columbia River (measured at 10.10 km) were considered as the reference concentration during the spill operation at the Brilliant Dam (scenario 2).

For the spill operations at the HLK Dam, the factor of turbulent diffusion was estimated considering all four operational conditions (scenarios 1A-1D). The total discharge for these cases ranged from 2,035-2,192 m^3/s and 2,601-2,722 m^3/s in the two sub-reaches with maximum variations of 3.9 and 2.7% respectively compared to a scenario averaged value. Therefore D was assumed constant for scenario 1, although it can vary with river discharge (Gowda 1984; Zhang and Zhu 2011). The dimensionless transverse mixing coefficient (E_t/U^*H) in the two sub-reaches was 0.85 and 0.82 respectively (Table 3.4). In natural rivers, it can vary from 0.3-0.6 for regular channel, 0.6-0.9 for gently meandering channel and 1-3 for sharp curved channel (Fischer et al. 1979; Rutherford 1994). During the spill at the Brilliant Dam, E_t/U^*H in the downstream of the confluence was 1.09 which was considerably higher than scenario 1. The total discharge (4,111 m^3/s) for this scenario was about 1.6 times greater compared to the average flow in scenario 1. Also the flow condition was very turbulent as most of the water (about 67% of total flow) was discharged through the spillway bays. The effect of river discharge on mixing coefficients is still subjected to uncertainty (Rutherford 1994; Zhang and Zhu 2011). Rutherford (1994) summarized that E_t increased with discharge while the dimensionless coefficient remained constant. The mixing downstream of the confluence could also be accelerated due to secondary currents for high discharge (Chen et al. 2017).

Assuming first-order kinetics, the calculated and measured TDG were matched to obtain appropriate dissipation rate (k) for the corresponding scenarios (as shown in Figure 3.7 for scenarios 1A-1D). Considering the transverse mixing between spilled plume and powerhouse releases in the upstream reach, the dissipation rates for different gate operations of scenario 1 were 0.002, 0.007, 0.004 and 0.003 hr^{-1} respectively. In the downstream of two converging rivers, the rates for scenarios 1A-1C were 0.016, 0.024 and 0.019 hr^{-1} respectively. The dissipation in the upstream of the confluence was comparatively slower due to different hydraulic conditions

between the two reaches. The velocities in the upstream reach varied from 0.43-0.62 m/s with an average depth of 13.36 m, while the mean velocity increased to 1.74 m/s in the downstream with additional inflow (from Brilliant Dam) passing through comparatively shallower sections of mean depth of 6.29 m.

During the high discharge condition at the Brilliant Dam (scenario 2), the dissipation rate in the downstream of the confluence was 0.031 hr^{-1} which was larger than the rates of scenario 1. The mean velocity for this scenario increased to 2.29 m/s, while the depth-velocity ratio (H/U) dropped to 3.1 (as opposed to 3.6 in scenario 1). However, such variation might not be the only reason for higher dissipation which has been discussed later. Overall, the computed profile matched quite well with the measured TDG for this scenario except at the right bank at 12.49 km (shown by point P in Figure 3.8) where the measured TDG was significantly higher. This could be attributed due to rapid mixing in the confluence (Chen et al. 2017) which was not considered in the simplified analytical model of this study. However, sensitivity analysis indicated that the reach downstream of the confluence was less sensitive to estimated factor of turbulent diffusion than the upstream. Also, the factor would be higher when dissipation was neglected. Hence the approach of using initial dissipation rates based on mass flux approach provided better prediction in terms of reliable estimation of the diffusion factors.

The uncertainty in dissipation rates was evaluated based on the method of first-order, second moment uncertainty analysis. For a given reach, the uncertainty in TDG dissipation rate, δ_k, was quantified utilizing Eq. (3.1) which relates the potential sources of uncertainty such as travel time of water (t) and TDG measurements (C_i or C). An order of magnitude analysis showed that the uncertainty associated with t was small, and greater uncertainty resulted from C_i or C measurements. Measurements indicated that the fluctuation of TDG saturation over time (precision uncertainty) was typically ≤ 0.1% once the readings were stabilized. The bias uncertainty was calculated from the errors associated with instrument, probe and calibration. The accuracy of dissolved gas and barometric pressure measurement is ±2 mmHg (Pentair Aquatic Eco-Systems, 2014), which corresponds to a bias uncertainty <0.3% at 95% confidence interval. Laboratory tests indicated that typical variability of TDG probes exposed to the same water was about 2 mmHg (≈ 0.3%) in terms of calibration. In this study, multiple measurements (refer to Figs. 3.7 and 3.8) were utilized to estimate the dissipation rate, which led to significant reduction in total uncertainty

associated with C_i or C. The analysis indicated higher uncertainty for small (C_i - C) which was the case for scenarios 1A, 1C and 1D. However discharge slightly varied for scenarios 1A-1D, with maximum variations in depths and mean velocities of 0.19 m and 0.03 m/s and 0.15 m and 0.02 m/s for the two sub-reaches respectively. Therefore these scenarios can be considered as repeated experiments with different TDG levels which resulted in reduced uncertainty estimates as outlined in Table 3.5. The average dissipation rate of these repeated experiments for the two reaches was 0.004 and 0.020 hr^{-1} respectively. The corresponding uncertainty estimates were 0.0017 and 0.0087 hr^{-1} respectively at 95% confidence interval (as shown by error bars in Figure 3.9).

During the field work sessions, the average water temperature in different reaches varied depending on the operational condition. For scenario 1, the generation flows near the left bank were relatively cooler (15.6–16.9 ºC) compared to the spills from the HLK Dam (16.9–17.9 ºC), which was expected considering intake withdrawal from the upstream deep reservoir. Downstream of Brilliant Dam (scenario 2), about 2 ºC difference were observed initially between the two converging rivers. At 24.19 km, the average temperature was 11.2 ºC. The observed dissipation rates were temperature corrected using Eq. (3.4) and are outlined in Table 3.5.

3.5 Discussion

In the Columbia River, the TDG dissipation rate in the upstream of the confluence (average k_{20} = 0.004 hr^{-1}) was relatively slower compared to the downstream reach. The hydraulic conditions in these two sub-reaches were quite different. The upstream reach was deeper (mean depth 13.36 m) with an average velocity of 0.49 m/s for scenario 1. On the contrary, the mean depth and velocity in the downstream reach were 6.29 m and 1.74 m/s, and 7.12 m and 2.29 m/s for scenarios 1 and 2 respectively, where the bottom stress generated turbulence would be higher resulting in increased surface renewal rate. Both these factors (lower depth and higher velocity) would contribute to the faster dissipation rates (k_{20} = 0.021 and 0.038 hr^{-1} respectively) in the downstream reach. These rates were compared with some field observations of TDG dissipation (Li et al. 2015) and reaeration (Churchill et al. 1962). Since depth and velocity are the key factors affecting gas transfer (reaeration or dissipation), these observations were scaled to H/U ratios for comparison purpose (Figure 3.9). Li et al. (2015) summarized a number of field observations in China, where the dissipations rates varied by two orders of magnitude ranging from 0.003-0.652 hr^{-1}. For similar

H/U ratios, the dissipation rates obtained in this study were comparatively lower, which was likely due to the unique hydraulic conditions in the Columbia River. The mean H/U (in m/ms) in the upstream of the confluence was 27.1, while it varied from 3.1-3.6 in the downstream reach depending on the scenario. Also the dissipation rates in Li et al. (2015) were analyzed assuming uniform mixing conditions across the rivers, which was not the case in this study. Comparison at similar H/U also indicated that the dissipation rates were relatively higher than the observations of Churchill et al. (1962) where the reaeration rates varied from 0.009-0.232 hr^{-1} with H/U ranging between 0.7-3.9. Overall the dissipation rate tended to decrease with H/U, which was consistent with the TDG dissipation rates in Chinese rivers as well as the reaeration observations.

Similar to surface reaeration, the dissipation of TDG is usually conceived as the physical process involving gas exchange at the air-water interface. To estimate dissipation, the US Army Corps of Engineers employed the form of surface renewal theory based on O'Connor and Dobbins' (1958) model (USACE 2001). Most of the semi-empirical reaeration models were developed as a function of depth and velocity (O'Connor and Dobbins 1958; Churchill et al. 1962; Owens et al. 1964); with channel slope as an additional variable (Bennett and Rathbun 1972; Smoot 1988); or dimensionally correct form of equations (Thackston and Krenkel 1969; Gualtieri et al. 2002). Some studies have also included the effect of wind (Chu and Jirka 2003). Review of Raymond and Cole (2001) suggested that the wind-driven turbulence can dominate the surface transfer in systems deeper than 10 m. Although the Columbia River had deeper sections at the upstream of the confluence, the velocities were sufficiently high (refer to Table 3.2) to propagate bottom stress generated turbulence; and therefore the effect of wind was not considered in this study. A positive relation between dissipation rate and water velocity provided further evidence that water currents are an important driver of gas exchange in the Columbia River.

To investigate the predictive capabilities of reaeration models to estimate TDG dissipation, some of the most widely used stream-driven formulae were evaluated in this study (Figure 3.10). The models that incorporated depth and velocity as the key variables produced similar but underestimated dissipation rates in the Columbia River. The applicability of these equations differs depending on the depth-velocity condition of a stream (Bowie et al. 1985). The equation of O'Connor and Dobbins (1958) was developed for deep and low-velocity rivers, while the Owens et al. (1964) model would be applicable for shallow channels (about 0.6 m). In the deepest reach

upstream of the confluence, the k value based on O'Connor and Dobbins (1958) model was 0.002 hr^{-1}, while it was lower in the downstream reach (0.014 and 0.013 hr^{-1} for scenarios 1 and 2 respectively). Churchill et al. (1962) provided best estimate (in terms of relative error) in the downstream reach for scenario 1. The methods of Bennett and Rathbun (1972) and Gualtieri et al. (2002) presented similar results, with the latter being on the lower bound for scenario 2. The equation of Smoot (1988) performed better for high H/U ratio (k = 0.004 hr^{-1} in upstream reach), while the model of Melching and Flores (1999) led to over prediction for all scenarios. In the reach downstream of the confluence, Thackston and Krenkel (1969) and the TDG dissipation model by Feng et al. (2014) resulted in overestimation for scenario 1, but produced comparable k value for scenario 2 (0.040 and 0.038 hr^{-1} respectively). Except Thackston and Krenkel (1969), Smoot (1988) and Melching and Flores (1999), most of the methods presented low estimates of dissipation rate. For scenario 1, the average rate based on these models was 0.002 ± 0.001 hr^{-1} in the upstream reach as opposed to the observed rate of 0.004 hr^{-1}. The reaeration models provided similar estimates for the two scenarios in the downstream reach (0.014 ± 0.002 and 0.013 ± 0.004 hr^{-1} respectively), which were about 1.5 and 3 times smaller than the observed dissipation rate.

To relate the surface transfer rate of TDG with mechanistic gas transfer models, Geldert et al. (1998) considered the large-scale motion by scaling it with U/H, while Weber et al. (2004) and Urban et al. (2008) accounted smallest-scale motion related to energy dissipation rate. In this study, the relevant size of turbulent motions affecting interfacial exchange of TDG were evaluated using the general form provided by Eq. (3.3). In the Columbia River, the shear Reynolds number (Re_*) varied from 7.79×10^5 to 1.07×10^6 depending on the scenario. Sc was calculated based on the value of D_m obtained from the molar weightage diffusivities of individual gas components (Broecker and Peng 1974) along with temperature corrected viscosity. Considering n = 1/2 and 1/4 in Eq. (3.3), the corresponding large-eddy and small-eddy models were compared with dissipation rates obtained in the present study along with the data set provided by Li et al. (2015) where the Re_* ranged between 7.9×10^5 to 7.5×10^6 (Figure 3.11). Because of limited observations within narrow range of Re_* in the Columbia River and unique features of individual reaches, direct comparison with these models were not possible. The observations of Li et al. (2015) showed n = 0.86 which was higher than the large-eddy model prediction. Laboratory studies on gas transfer indicated consistency of the exponent with small-eddy model prediction at low Reynolds number (Moog

and Jirka 1999). Gulliver and Halverson (1989) identified large streamwise vortices controlling surface renewal rate, which were scaled with the large-eddy model for Re_*> 4500. Beyond this value, the normalized transfer rate would depend on the shear Peclet number and the large-eddy model could be re-arranged in the following form:

$$Sh/\sqrt{Pe_*} = const \qquad (3.11)$$

where Sh is the Sherwood number = kH^2/D_m, and Pe_* is the shear Peclet number = U^*H/D_m. Eq. (3.11) is very similar to the O'Connor and Dobbins' (1958) formulation for non-isotropic turbulence, according to which the value of the constant would be 1.58 while Gulliver and Halverson (1989) reported it as 0.63 for moving bed flume. Such formulation could be useful for deep rivers like the Columbia River system where integral length scales might influence the interfacial gas transfer (i.e. dissipation of TDG) due to high Reynolds number range.

The dissipation rates observed in the present study were higher compared to most of the reaeration estimates. The rate was about two times higher for scenario 2 than scenario 1 in the downstream of the confluence, where the differences in mean depth and velocity were 0.83 m and 0.55 m/s respectively. Such hydraulic variations cannot explain the large difference in dissipation rates as indicated by the reaeration estimates which were similar for these two conditions (refer to Figure 3.10). This suggested that the net gas transfer could be attributed to another mechanism in addition to the direct (diffusive) transfer across the air-water interface. Transfer through small bubbles (microbubbles), caused by the supersaturation of the liquid phase, could potentially mediate gases between air and water. Bubbles can form at pre-existing gas cavities (nucleation sites) provided by suspended particles (e.g. sediments), or the surface of the contacting liquid in a process known as heterogeneous nucleation. Such nucleation can prevail in any environmental system subjected to supersaturation, even when the degree of supersaturation is low (Jones et al. 1999).

Bubble-mediated mass transfer can be substantial for gases of low solubility such as N_2 and O_2 (Woolf and Thorpe 1991) and enhance the net degassing compared to diffusive transfer (Hikita and Konishi 1984; Kierzkowska-Pawlak and Chacuk 2010). In the absence of bubbles, the dissipation can be regarded as the reverse process to reaeration, and the contribution of direct transfer can be approximated by Eq. (3.11). To estimate mass transfer in bubble swarms, Azbel

(1981) and Gulliver et al. (1990) proposed a similar form of equation which can be rearranged in a general form as follows:

$$Sh_b/\sqrt{Pe_*} = \alpha\, f\,(\phi)\, Re_*^{0.25} \qquad (3.12)$$

where Sh_b is the Sherwood number of bubbles = kHd_b/D_m (d_b = bubble diameter); ϕ is the void fraction and α is a coefficient that depends on the bubble size distribution of the flow, and was reported to be 0.21 by Azbel (1981). Gulliver et al. (1990) indicated that the functional form of void fraction, $f(\phi)$ remains independent of the size distribution. Assuming net gas transfer is the sum of diffusive and bubble-mediated component, the role of individual mechanisms can be conceptualized utilizing Eq. (3.11) and (3.12) (Figure 3.12). It was evident that for a given shear Reynolds number, the contribution of bubbles to net dissipation was greater when relative supersaturation (defined as $(C_o - C_{sat})/ C_{sat}$) was high which might result due to increased void fraction. This is consistent with Hikita and Konishi (1984) and Kierzkowska-Pawlak and Chacuk (2010) which reported that the desorption rate of carbon dioxide enhanced rapidly with relative supersaturation compared to diffusive transfer. For arbitrary void fractions (ϕ_1, ϕ_2, ϕ_3, …), the bubble-mediated transfer increased with shear Reynolds number as opposed to a constant value of direct transfer. Because of the micro-scale bubbles, the void fractions would likely be very small (<< 1%) and the corresponding coefficient in Eq. (3.12) would be different than Azbel (1981) and Gulliver et al. (1990).

The role of bubble-mediated transfer can be utilized to explain the variability in observed dissipation rates in the downstream reach of Columbia River. Among different gate settings of scenario 1 (similar hydraulic condition with different TDG levels, refer to Table 3.5), the dissipation rate was found to increase with relative supersaturation and was maximum for scenario 1B which corresponded to a relative supersaturation of 0.15. For scenario 2, the relative supersaturation increased to 0.25 although the increase in depth and velocity were only 0.83 m and 0.55 m/s respectively. The higher supersaturation for this scenario had the potential to form more bubbles resulting in increased void fraction and subsequent dissipation. Also about 67% of the total flow was discharged from the Brilliant Dam for scenario 2 as opposed to 26% for scenario 1. The run-of-the-river Brilliant Dam might contain higher sediment concentrations compared to the HLK Dam flow which is regulated by the large Arrow Lakes reservoir. Higher turbidity can provide more nucleation sites (Jones et al. 1999) resulting in enhanced dissipation of TDG.

3.6 Conclusions

In this study, the dissipation rate of supersaturated total dissolved gases in the regulated Columbia River was quantified directly through a combination of field measurements and analytical modelling. Detailed field monitoring during spill operations at the HLK Dam and the Brilliant Dam indicated differential TDG concentrations between the spill and the generation flows as well as between two converging rivers downstream of Kootenay River confluence. Within the study area, the maximum concentrations dropped by about 2-8% depending on the operational scenarios, as the supersaturation reduced through mixing within water and dissipation across the air-water interface. To analyze dissipation, an analytical approach incorporating transverse mixing was utilized to obtain two-dimensional distribution of TDG. This method is advantageous in terms of reliable estimates for sparsely measured data with limited number of samplings, particularly in hydropower facilities where measurements are often limited by time and other constraints.

The two sub-reaches (upstream and downstream of the confluence) in the Columbia River were hydraulically different, with deeper sections and low-velocity waters in the upstream resulting in slower rate of TDG dissipation. For four different operational conditions at the HLK Dam, the average dissipation rate in the two reaches was of 0.004 and 0.021 hr^{-1} respectively at 20 ºC. Despite measurement uncertainties, the rates were quite consistent between individual operational conditions (similar hydraulic condition with different TDG levels) in a given reach. Also the dimensionless transverse mixing coefficient (E_t/U^*H) remained similar in these reaches (0.84 and 0.82 respectively). During the high discharge condition at the Brilliant Dam, the dissipation rate in the downstream of the confluence increased to 0.038 hr^{-1} with corresponding E_t/U^*H of 1.09. Overall the dissipation rates tended to decrease with depth-velocity (H/U) ratio, which was consistent with the general reaeration theories as well as with the field observations in some other rivers. This also suggested that water currents are an important driver of gas exchange in the Columbia River.

In order to compare the dissipation with mechanistic models of gas transfer, the large-eddy and the small-eddy models were evaluated using the rates obtained in the present study. Because of the limited observations within narrow Reynolds number range, no discernible trend was observed comparable to these models. Evaluation of some widely used reaeration models showed limited applicability to estimate dissipation, with the observed rates being 1.5-3 times higher compared to

most of the models. This indicated the potential of bubble-mediated transfer that might result in faster dissipation rates compared to the direct transfer predicted by reaeration models. Such transfer could be substantial for low soluble gases (such as nitrogen and oxygen) and affected by the liquid phase supersaturation and presence of pre-existing gas cavities (e.g. sediments). Based on theoretical considerations, a conceptualization was presented to account the role direct and bubble-mediated transfer which indicated that the contribution of bubbles to net dissipation could be greater for high supersaturation as a result of increased void fraction.

Because of the limited data available, the role of different gas transfer mechanisms on the dissipation rate is not conclusive and needs further investigation. However unlike traditional approaches of reaeration, the contribution of direct and bubble-mediated transfer should be accounted for TDG prediction and dissipation rate estimation with considerations of bubble formation and distribution in rivers subjected to supersaturation. In order to relate dissipation with different parameters, systematic experiments should be conducted in rivers with variable hydraulic conditions.

Table 3.1: Hugh L. Keenleyside (HLK) Dam and Brilliant Dam gate operation scenarios

Scenario	HLK Dam		Brilliant Dam		Gate operation
	Spill (m^3/s)	**Generation** (m^3/s)	**Spill** (m^3/s)	**Generation** (m^3/s)	
1A	1025.6	1085	-	585.2	L2, L3, L4
1B	934.8	1100	-	566.2	L5, L6, L7
1C	1110.6	1081	-	530.4	L3, L4, L5, L6
1D	1023.3	1081	-	482.6	L3, L4, L6
2	320.2	1037.2	1807.1	946.9	L2, L3, L4, S1, S2, S3

Note: L = low-level gate at Keenleyside Dam; S = spillway at Brilliant Dam

Table 3.2: Hydraulic parameters at transverse sections for different scenarios

Scenario	Reach	Transect (km)	B (m)	H (m)	U (m/s)	U^* (m/s)	ψ
1[a]	u/s of confluence	0.56	309.7	15.93	0.43	0.068	2.34
		0.98	259.7	13.21	0.62	0.062	1.63
		2.03	339.1	13.65	0.46	0.064	2.59
		4.39	329.2	13.45	0.48	0.063	1.89
		6.70	409.9	10.35	0.50	0.056	1.96
	d/s of confluence	11.30	199.7	7.48	1.79	0.187	1.83
		19.68[b]	200.0	17.36	0.78	0.278	3.25
2	d/s of confluence	12.49	310.5	6.18	2.14	0.170	1.27
		17.62	199.2	8.41	2.46	0.198	1.88
		24.19	356.3	5.51	2.10	0.160	2.13

[a] scenario averaged values are presented

[b] not used in the reach average calculation

Table 3.3: Comparison of calculated velocities with ADCP measurements

Transect (km)	**Absolute Relative Error (%)** [a]							
	Measurement 1		Measurement 2		Measurement 3		Measurement 4	
	Avg.	St. Dev.	Avg.	St. Dev.	Avg.	St. Dev.	Avg.	St. Dev.
0.56	17.51	7.01	16.42	8.46	15.53	6.77	14.55	8.54
0.98	11.27	7.22	10.04	8.94	11.10	7.56	-	-
2.03	11.38	9.52	11.80	8.76	12.40	7.91	11.07	7.97
4.39	10.93	7.97	9.47	7.79	9.86	6.63	10.16	7.32
6.7	7.90	6.01	8.83	5.47	9.21	6.33	7.00	5.92
11.3	9.68	7.81	10.38	6.08	8.06	5.98	11.04	7.59
19.68	12.73	8.82	17.46	8.42	16.06	6.68	-	-

[a] Absolute relative error = (|calculated velocity – measured velocity| / measured velocity × 100%)

Table 3.4: Estimation of transverse mixing coefficients

Reach	***Scenario***	D	H_{avg}	U_{avg}	U^*_{avg}	ψ_{avg}	E_t	E_t/U^*H
		(m^5/s^2)	(m)	(m/s)	(m/s)		(m^2/s)	
u/s of confluence	1	130.10	13.36	0.49	0.063	2.08	0.715	0.85
d/s of confluence	1	110.90	6.29	1.74	0.170	1.83	0.880	0.82
	2	286.02	7.12	2.29	0.181	1.76	1.400	1.09

Table 3.5: Results of observed dissipation rates of TDG for different scenarios

Reach	*Scenario*	U	H	T	k	δ_k	k_{20}	Sc	Re_*	kH/U^*	$Sh/\sqrt{Pe_*}$
		(m/s)	(m)	(ºC)	(hr^{-1})	(hr^{-1})	(hr^{-1})		($\times 10^{-6}$)		
u/s of confluence	1A	0.49	13.39	16.5	0.002	0.002	0.002	658.7	0.79	0.426	2.70
	1B	0.48	13.28	16.5	0.007	0.001	0.008	658.7	0.78	1.484	9.34
	1C	0.51	13.47	17.4	0.004	0.002	0.004	628.0	0.81	0.854	5.36
	1D	0.50	13.31	17.2	0.003	0.002	0.003	634.7	0.79	0.637	3.97
d/s of confluence	1A	1.75	6.31	17.3	0.016	0.010	0.017	631.3	1.03	0.591	4.19
	1B	1.73	6.20	17.5	0.024	0.007	0.025	624.7	1.01	0.879	6.13
	1C	1.75	6.35	18.5	0.019	0.009	0.020	592.8	1.07	0.704	4.93
	2	2.29	7.12	11.2	0.031	0.006	0.038	880.1	1.05	1.217	10.30

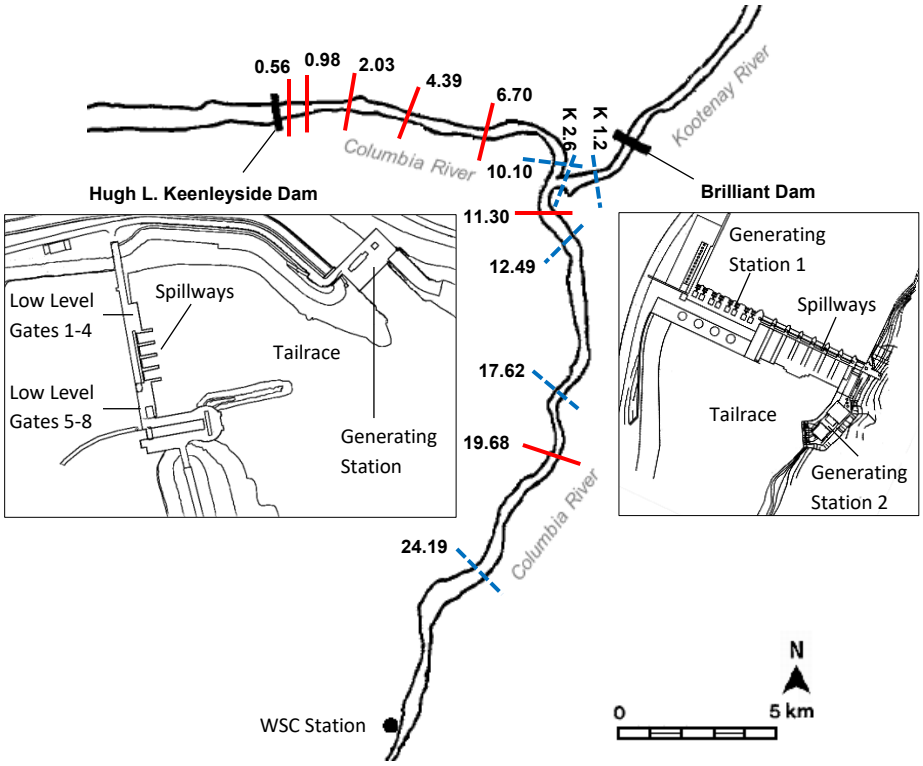

Figure 3.1: Study area in the Columbia River with measurement locations for scenario 1 (solid lines) and scenario 2 (dashed lines)

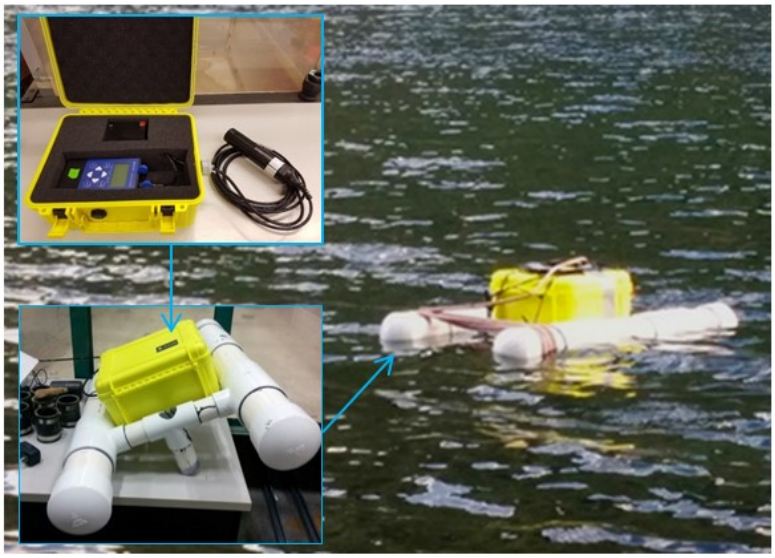

Figure 3.2: Instrumentation and field deployment configuration of continuous monitoring platform

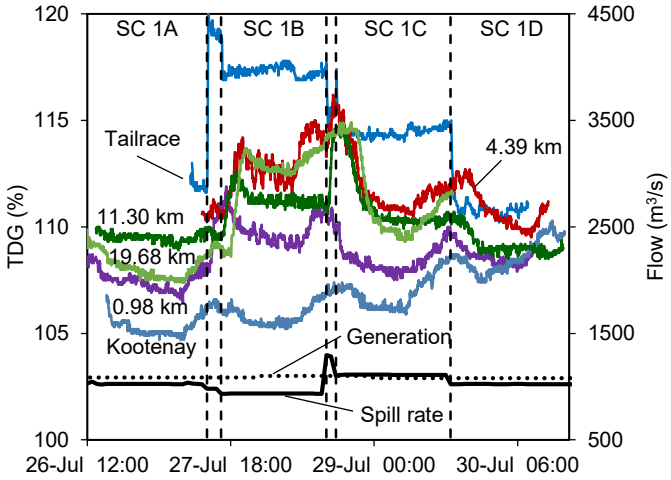

Figure 3.3: TDG measured at the continuous monitoring stations during HLK Dam spills (vertical dashed lines indicate transition between gate changes)

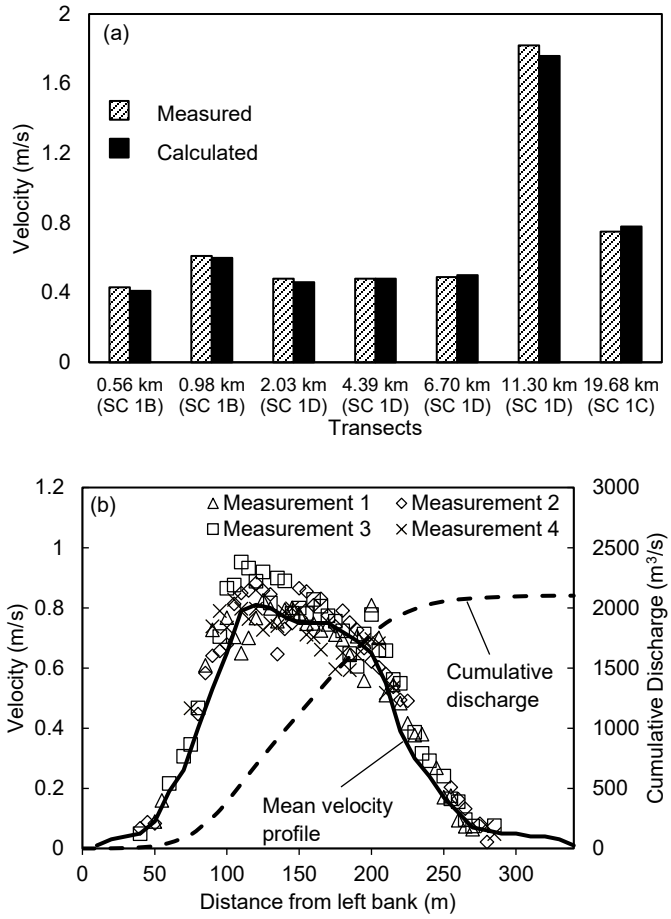

Figure 3.4: Comparison between measured and calculated velocity: (a) mean velocity at different transects; (b) velocity distribution at 2.03 km for scenario 1D

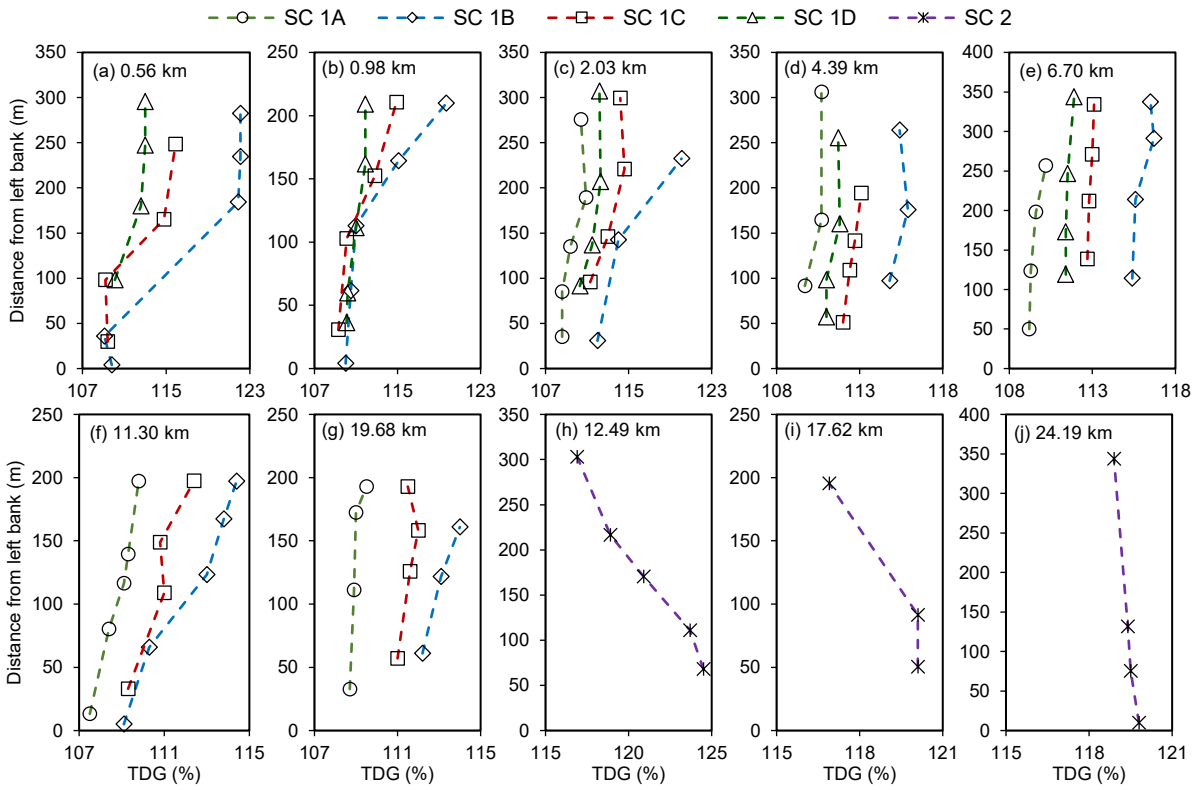

Figure 3.5: Measured TDG at the Columbia River for different scenarios

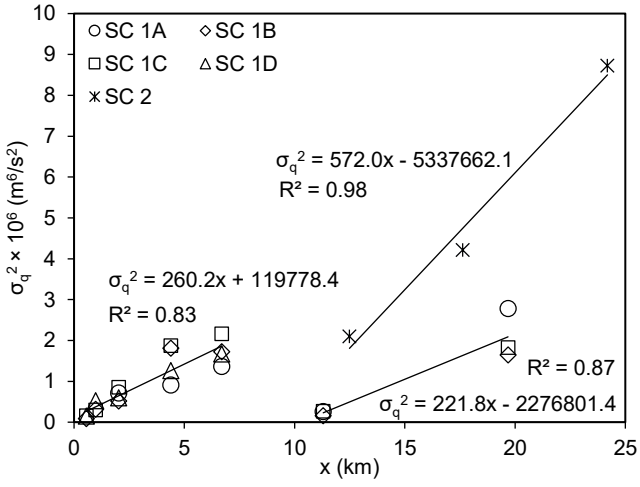

Figure 3.6: Variances of TDG concentrations along the river

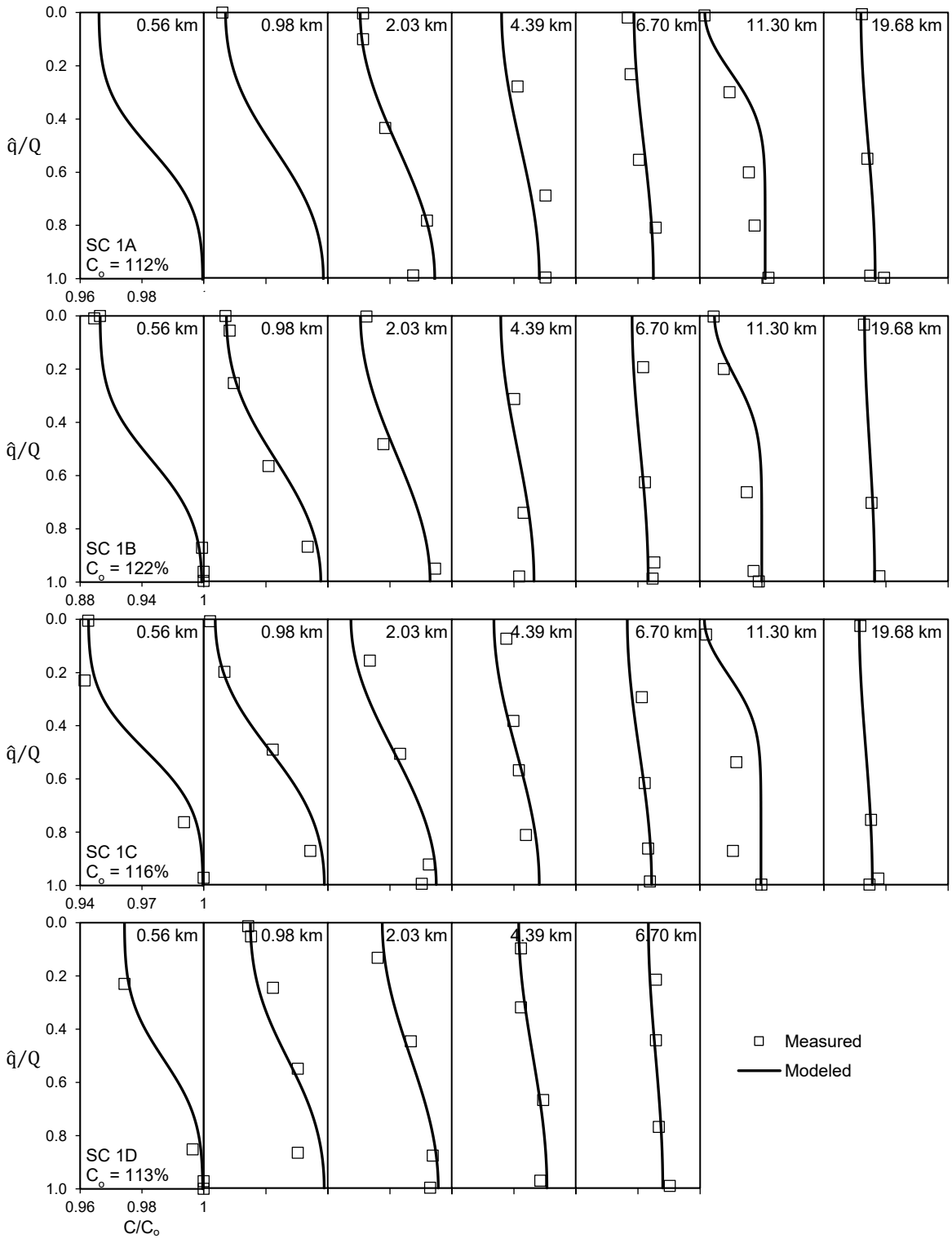

Figure 3.7: Concentration-cumulative discharge (C-$\hat{q}$) distribution of TDG based on analytical approach for different gate settings of scenario 1

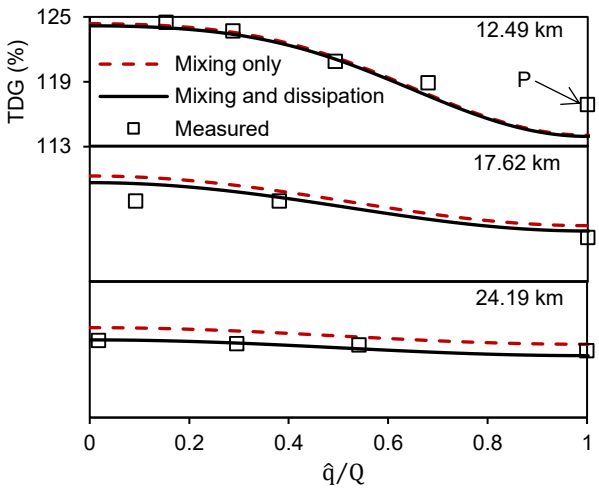

Figure 3.8: Calculated TDG incorporating mixing and dissipation in the downstream of confluence for scenario 2

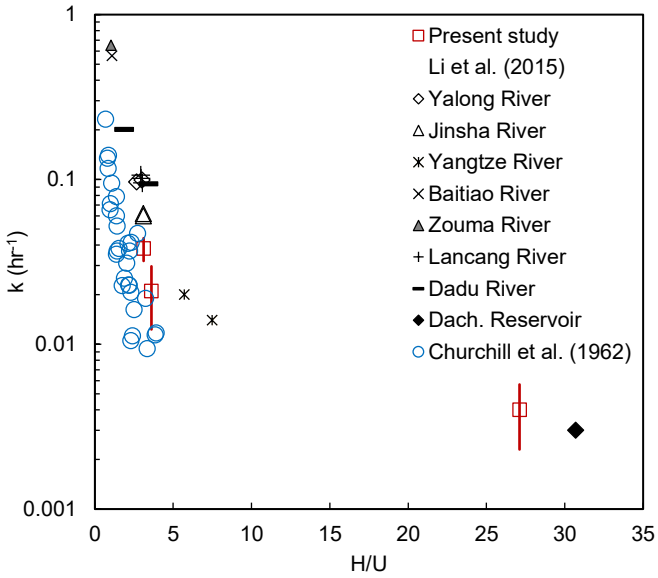

Figure 3.9: Effect of depth-velocity ratio on the dissipation rate with reaeration observations of Churchill et al. (1962)

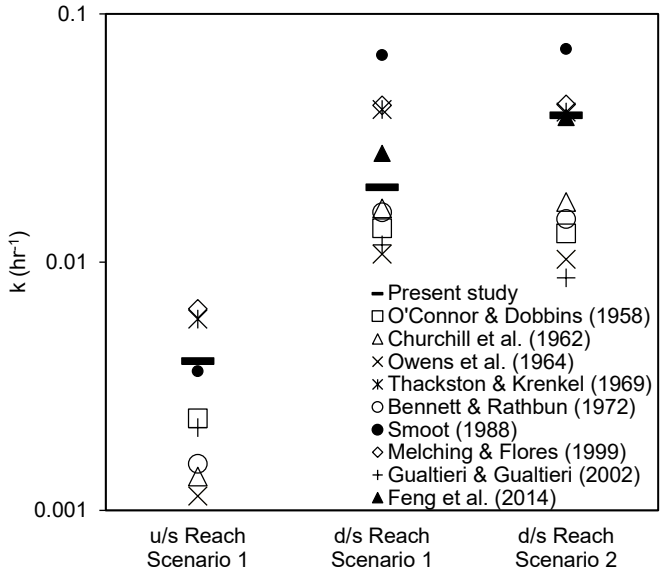

Figure 3.10: Comparison of dissipation rates with empirical reaeration models

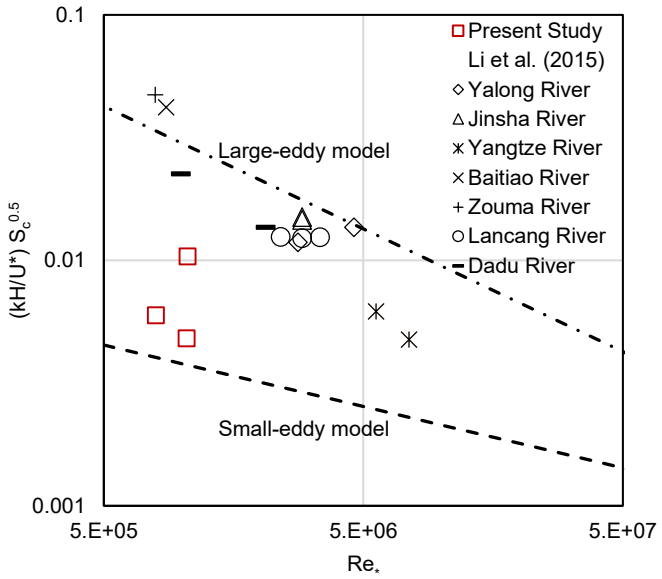

Figure 3.11: Comparison of dissipation rates with turbulence-based gas transfer theories

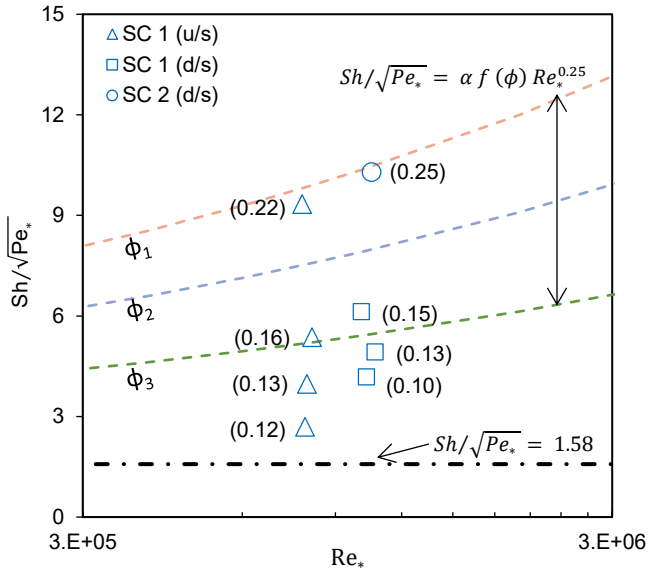

Figure 3.12: Conceptualization of the contribution of bubble-mediated transfer to estimated dissipation rates. The bracketed values indicate relative supersaturation, while dashed lines represent arbitrary void fractions

CHAPTER 4

Modeling Total Dissolved Gas Transfer in a Ski-jump Spillway *

4.1 Introduction

Operations at hydroelectric facilities can generate elevated levels of total dissolved gases (TDGs) as a result of air entrainment during spill events. In a cascading hydropower system, high TDG waters released from upstream dams have the potential to dissipate, remain unchanged, or be increased at downstream facilities (USACE 2001), and can exacerbate adverse impacts of TDG supersaturation on aquatic environment. Elevated levels of TDG often extends far from the source of supersaturation (Kamal et al. 2019) and can cause gas bubble trauma in fish leading to direct or indirect mortality (Ebel 1969; Weitkamp 2008). Recognizing this environmental risk, an allowable water quality criterion for TDG of 110% is established in the United States and Canada (USEPA 1986; CCME 1999). Therefore, understanding the gas transfer processes associated with spill operations is crucial to evaluate the fate of supersaturated water in a given facility and identify operational alternatives that can mitigate TDG risk.

Ski-jump spillways consisting of a chute and a flip bucket are energy dissipation elements usually provided at high-head dams to convey large discharges into a distant pool (Vischer and Hager 1998; Khatsuria 2005). The high-velocity jet released from the bucket experiences surface instabilities which leads to 'self-aeration' along jet surface spreading the initial compact flow (Rajaratnam 1976; Chanson 1996). If the trajectory is long enough, the jet breaks up and the corresponding break-up length defines the air concentration distribution along the jet (Ervine and Falvey 1987; Pfister et al. 2014). On relatively long and steep chutes with small discharges, air can be entrained on the spillway face if the turbulent boundary layer intersects free surface at a location called the inception point (Keller and Rastogi 1975). Beyond this point, the entrained air concentration gradually increases (Wood 1991; Chanson 1996; Wilhelms and Gulliver 2005). This results in pre-aeration of the approach flow upstream of the jet, affecting jet-air features (Schmocker et al. 2008; Pfister and Hager 2012). The entrained bubbles in the chute and jet flows

* The content of this chapter has been submitted as a journal manuscript: Kamal, R., Zhu, D.Z., Crossman, J. and Leake, A. (2019). "Modeling Total Dissolved Gas Transfer in a Ski-jump Spillway." *Journal of Hydraulic Engineering, ASCE,* Manuscript ID HYENG-12160, under review.

significantly increase the surface area available for gas transfer. In addition to direct transfer across the free surface, the bubble-mediated exchange can contribute greatly to reaeration (when oxygen is deficit) or degassing (for oxygen and nitrogen supersaturation).

Predictive relationships to estimate gas transfer and corresponding efficiency of hydraulic structures are typically site-specific and have limited generality (Gulliver et al. 1998). To obtain useful insight, physically based relationships should be utilized. To predict TDG downstream of spillways, mechanistic models were developed considering mass transfer across the free surface and at the bubble-liquid interface (Geldert et al. 1998; Urban et al. 2008). Orlins and Gulliver (2000) and Weber et al. (2004) implemented this approach into multi-dimensional domain incorporating complex hydrodynamics and air bubble distribution in the tailrace. In recent years, computational fluid dynamics (CFD) models were utilized to predict TDG exchange and spillway jet regimes considering bubble dissolution and bubble density equation (Politano et al. 2009; Wang et al. 2018). However, such modeling effort is extremely complicated due to two-phase flow and can be time consuming and computationally expensive which limits its practical application to multi-reservoir systems in real time (Politano et al. 2017). Also most previous studies focused on TDG generation in the tailrace without considering gas transfer before plunging in the pool. In a cascading hydropower system, supersaturation may occur in the upstream of a dam and the plunge pool transfer could be affected by the incoming high TDG water associated with the changes in spillway face and free jet (Lu et al. 2019). Wilhelms and Gulliver (2005) used entrained air distribution on the spillway face to estimate bubble-mediated transfer of oxygen. Such transfer is of greater importance for the jet since more bubbles are exposed to high level of turbulence (Davies and Ting 1967; Xue et al. 2019). Therefore, independent consideration of gas transfer on the spillway, free jet and plunge pool is needed to evaluate the change of TDG concentrations. Mechanistic modeling of various physical processes in these regions can be a necessary supplement to current TDG prediction methods.

The objective of this study is to evaluate gas transfer in a ski-jump spillway. Specifically, the change in TDG was quantified while transporting through the spillway by developing a physically based model related to air entrainment, bubble characteristics and mass transfer. The model development is discussed in the next section by introducing related studies in the literature. The model was calibrated using the field tests conducted at the Seven Mile Dam located on the Pend

d'Oreille River in southeastern British Columbia, Canada. The dam has a ski-jump spillway (Figure 4.1a) that frequently receives high TDG water during high flow periods of the year due to spill operations at upstream projects. Information from the field observations and modeling efforts were utilized to investigate gas transfer on the spillway face, free jet and plunge pool and quantify TDG concentration change associated with different physical processes.

4.2 Gas Transfer Computation

In hydropower facilities, the generation discharges usually do not contribute directly to the gas exchange due to limited scope of air entrainment in turbines, and the gas transfer is dominated by the aeration processes associated with spill operations. The gas transfer efficiency of spilled water E_s, which is termed by the ratio of total gas transfer at the spillway to total potential gas transfer, can be expressed as follows (Wilhelms and Gulliver 2005):

$$E_s = \frac{C_{spill} - C_u}{C_{sat} - C_u} = 1 - \exp\left(-\int_0^x \frac{k_L a}{U} dx\right) \quad (4.1)$$

where C_u and C_{spill} are the dissolved gas concentrations of spilled water in the upstream and downstream respectively, C_{sat} is the saturation concentration for equilibration with the gas phase, U is the mean velocity in flow direction x, k_L is the liquid film coefficient, and a is the specific interfacial area. This transfer efficiency usually depends on the spill rate, water temperature, project head and tailwater depth (Gulliver et al. 1998).

In aerated flow, gas transfer occurs across two interfaces: bubble-water interface and free surface interface. For bubbles entrained in turbulent flow, a theoretical expression for the liquid film coefficient $(k_L a)_b$ can be adopted (Azbel 1981; Urban et al. 2008):

$$(k_L a)_b = 6\beta \frac{D_m}{L_t} \frac{\phi}{d_b} \frac{(1-\phi)^{1/2}}{(1-\phi^{5/3})^{1/4}} \left(\frac{\nu}{D_m}\right)^{1/2} \left(\frac{U_t L_t}{\nu}\right)^{\eta} \quad (4.2)$$

where D_m is the diffusivity of the gas in water, ν is the kinematic viscosity of water, U_t is the characteristic turbulence velocity, L_t is the characteristic length of turbulence, ϕ is the gas void ratio (entrained air volume per unit volume of air-water mixture), and d_b is the bubble diameter. In this equation, interfacial area a_b of uniform spherical bubbles was considered by $6\phi/d_b$. β and η are coefficients which would be 1/4π and 3/4 respectively based on Azbel's relationship for

bubble swarms. The exponent η is related to the turbulent flow features and depends on the appropriate selection of velocity and length scales (Geldert et al. 1998). With similar scaling, the exchange coefficient for surface transfer $(k_L a)_s$ can be considered by incorporating eddy dissipation model (Lamont and Scott 1970):

$$(k_L a)_s = \beta \frac{D_m}{L_t} \left(\frac{\nu}{D_m}\right)^{1/2} \left(\frac{U_t L_t}{\nu}\right)^{\eta} \frac{A}{V} \quad (4.3)$$

where A is the free surface area for transfer, and V is the volume of water. A/V results in a free surface interfacial area (a_s) of $1/h$ for the spillway face and plunge pool and $2/h$ for the free jet, where h is the flow depth.

For ski-jump spillways, the area over which transfer is occurring can be divided into three regions: the spillway face (region 1), the free jet in the atmosphere (region 2) and the plunge pool (region 3), as shown in Figure 4.1(b). The pool region extends from the jet plunge point to the downstream river distance travelled by bubbles. Gas transfer across the free surface and bubbles and subsequent change in concentration varies with distance in these regions. Considering Eq. (4.1), a control volume approach results the following one-dimensional equation:

$$\frac{\Delta(UC)}{\Delta x} = (k_L a)_b \left(C_{eff} - C\right) + (k_L a)_s (C_{sat} - C) \quad (4.4)$$

where C is the average dissolved gas concentration in a control volume, and C_{eff} is the effective saturation concentration at bubble-water interface at some depth. The modeling framework described herein was developed based on the following assumptions:

- typically measurements are carried out in a downstream section where spill and generation discharges contribute to overall concentration. Since direct measurement is not possible, the concentration of spilled water was obtained assuming complete mixing as $C_{spill} = (C_d Q - C_u Q_g)/Q_s$, where C_d is the downstream dissolved gas concentration, and Q_s, Q_g and Q are spill rate, generation discharge and total flow respectively.
- the flow hydrodynamics and corresponding turbulent scaling is expected to be similar for both bubble-water and free surface interfaces, and the β and η coefficients in Eqs. (4.2) and (4.3) would be similar for both interfaces.
- dissolved gas components are considered identical to air, and the diffusivity (D_m) was obtained from the molar weightage values of individual gas components (Broecker and Peng 1974).

- bubbles are assumed to be uniformly distributed across the depth. Majority of the gas transfer occurs in regions where turbulence is sufficiently high to balance bubble rise velocity and keep the bubbles vertically well mixed (Urban et al. 2008).

In Eqs. (4.2) and (4.3), the void ratio, characteristic length and velocity are influenced by flow hydrodynamics at the spillway face, free jet and plunge pool. These variables need to be estimated for the individual regions as discussed in the following section.

4.3 Air-Flow Features in Ski-Jump Spillway Regions

4.3.1 Pre-Aeration in Spillway Face

Wood (1991) developed semi-empirical relations to predict the location of inception point, x_I:

$$x_I = 13.5(q^2/gsin\theta)^{1/3}(sin\theta)^{0.08}\left(q^{2/3}/(gsin\theta)^{1/3}k_s\right)^{0.069} \quad (4.5)$$

where θ is the angle of the chute face, q is the discharge per unit width of spillway, k_s is the equivalent roughness height of the spillway surface (= 1.5 mm for concrete), and g is the acceleration due to gravity. Eq. (4.5) is applicable for spillway slopes of 5º to 70º (Wood 1991). As shown in Figure 4.2(a), the location of inception point obtained using this equation agrees reasonably well with prototype observations (as tabulated in Chanson 1996) for 45-60º chutes. Wilhelms and Gulliver (2005) showed that the mean concentration of entrained air (i.e. void ratio ϕ_s) gradually increases as a function of θ and depth at the inception point h_I (refer to Table 4.1 for the equation), asymptotically approaching an equilibrium void ratio ϕ_{eq}. Downstream of the inception point, bulking of flow due to entrained air affects the local depth and the corresponding length scale would be $h_I/(1-\phi_s)$. A relevant turbulent velocity scale would be shear velocity $\sqrt{gh_IS}$, where *S* is the slope of the spillway. The depth and velocity at the inception point, spillway toe and bucket lip were calculated using standard energy and continuity equations.

4.3.2 Jet Air Features

The jet surfaces of a high-speed air-water flow are usually defined at air content of 0.90 and the jet void ratio, ϕ_j, involves the integration of concentrations between these boundaries (Heller et al. 2005; Pfister and Hager 2012). Pfister et al. (2014) presented a relation for the streamwise

variation of void ratio in a plane jet of a ski jump (refer to Table 4.1), which essentially consists relevant parameters like break-up distance and trajectory length. This equation can be applied directly when air is not entrained on the spillway face. For pre-aeration, ϕ_j was assumed herein to be the air content on the spillway plus the air entrained by the jet itself.

The trajectory of the free jet is usually defined by the standard projectile profile (Vischer and Hager, 1998; Khatsuria, 2005). The jet thickness along this trajectory increases in proportion to $1/(1-\phi_j)$. However, prototype trajectory lengths are always shorter than the theoretically derived distance due to jet break-up, deviation in take-off angle and aerodynamic interaction (Heller et al. 2005). To account for these effects, the theoretical equation was modified as:

$$L_j = K_a \frac{U_j^2 sin2\Omega}{2g}\left[1+\left(1+\frac{2g\Delta z}{U_j^2 sin^2\Omega}\right)^{1/2}\right] \qquad (4.6)$$

where L_j is the trajectory length, Ω is the bucket angle, U_j is the take-off velocity, Δz is the elevation difference between bucket lip and tailwater surface, and K_a is a coefficient introduced for air resistance. L_j calculated using Eq. (4.6) was fitted with the prototype data of Kawakami (1973) to yield K_a = 0.82 (Figure 4.2b). This value could vary from 0.75-0.9 when computing real trajectory (Wahl et al. 2008). The jet velocity at plunge pool impact is $U_{j(x_j)} = \sqrt{(U_j^2 + 2g\Delta z)}$. The turbulent velocity scale was approximated by Blasius solution (Davies and Ting 1967) as shown in Table 4.1.

The break-up length, L_b, is usually of the order of 50-100 times the jet thickness for circular jets and comparatively shorter for rectangular jets (Ervine and Falvey 1987). Castillo et al. (2015) proposed the following relation for rectangular jet break-up length:

$$\frac{L_b}{h_j F_j^2} = \frac{0.85}{\left(1.07 T_u F_j^2\right)^{0.82}} \qquad (4.7)$$

where h_j is the jet thickness, F_j is the jet Froude number and T_u is the turbulence intensity at the issuance. Castillo et al. (2015) suggested an estimate of T_u~1.2% for prototype flows. The break-up length becomes shorter when pre-aeration occurs on the approach chute flow. However, Pfister and Hager (2012) showed that L_b/h_j remained unchanged for small void ratio up to 0.15. Under normal spillway operating conditions, the void ratio is expected to be in this range.

4.3.3 Plunge Pool Region

As the aerated jet plunges into the pool, the momentum of the jet carries bubbles deep into the water. At normal spillway operations, the streamwise velocity (U_p) is much higher than bubble rise velocity (u_b, typically 0.25 m/s) and bubbles can travel further downstream to the river. For uniform distribution across depth, the loss of bubbles to the atmosphere and subsequent reduction in plunge pool void ratio (ϕ_p) can be described by an exponential relation (Geldert et al. 1998), as shown in Table 4.1. Using this relation and assuming ninety percent of the initial air has left the river, the length of this bubbly aerated zone can be estimated as $L_p = -(U_p h_p/u_b)\ ln\ (0.1)$ where h_p is the average pool depth. For this region, a depth integrated scale of $0.62h_p$ (Nezu and Nakagawa 1993) and a velocity scale of $U_p\sqrt{f/8}$ was used, where f is the friction factor.

Due to increased hydrostatic pressure, atmospheric equilibration is not applicable for plunge pool bubbles and the effective saturation concentration can be estimated from $C_{eff} = C_{sat}\left(1 + \rho g d_{eff}/P_{atm}\right)$ (Hibbs and Gulliver 1997). This depends on the effective depth d_{eff} which represents the average depth that bubbles experience in a control volume and the can change with distance. Following a simplified bubble trajectory (Politano et al. 2017), this can be estimated as $d_{eff} = h_{pen}/2\,(1 - x_p/L_p)$, where h_{pen} is the bubble penetration depth at plunge point. The penetration depth is a function of impact velocity, jet thickness and unit discharge (Ervine and Falvey 1987; Hibbs and Gulliver 1997) and is physically limited by the plunge pool depth. However when the impinging jet is aerated, total resistance and buoyancy forces of the bubbles spreads the jet wider with shorter penetration depth compared to momentum driven pure water jet (van de Sande and Smith 1975). Therefore, h_{pen} was modeled considering the amount of entrained air as follows:

$$h_{pen} = MIN\left[h_p\ , \alpha_p U_j^{4/3} h_j \left(\frac{\phi_{jd}}{1-\phi_{jd}} Q\right)^{-1/4}\right] \quad (4.8)$$

where ϕ_{jd} is the void ratio of the jet at impact, and α_p is coefficient for penetration depth. The value of α_p was 0.42 in the original equation proposed by van de Sande and Smith (1975), and was used as a fit parameter in the present study.

4.3.4 Bubble Size in Different Regions

The bubble size in self-aerated flow depends on the balance between surface tension and shear forces and could vary depending on the turbulence level of a location. The representative bubble diameter for a given region could be estimated as (Hinze 1955):

$$d_b \approx \left(\frac{\sigma}{\rho}\right)^{3/5} \varepsilon^{-2/5} \quad (4.9)$$

where σ is the surface tension of water, ρ is the density and ε is the turbulent energy dissipation rate. The proportionality constant of this equation is close to unity. This value was 0.725 for Hinze's (1955) experiment, while Sevik and Park (1973) found a value of 1.15 for plunging jets. The energy dissipation rate can be approximated by U_t^3/L (Nezu and Nakagawa 1993), which led to a scaling of $\sqrt{(g^3 h_I S^3)}$ for the spillway face (Wilhelms et al. 2005). For the free jet, ε was scaled by $(U_j sin\Omega)^3/L_j$ assuming energy was dissipated along the jet length. These scaling correspond to homogeneous and isotropic turbulence, and were assumed to be applicable in the presence of bubbles.

4.4 Field Tests

The Seven Mile Dam is an 80-m-high concrete gravity dam that consists of a powerhouse near the right bank and five spillway bays with 15.24-m-wide vertical lift gates. Spilled water is discharged over ogee crests into a divided chute with two flip buckets. The left chute profile (bays 3 to 5) merges into an 18.3 m radius flip bucket with a lip angle of 30º (Figure 4.1). The right chute profile (bays 1 and 2 adjacent to the powerhouse) is similar, with an additional 23 m long downward straight section before the lower-elevation flip bucket (Table 4.2). Bays 1-4 are operated under normal conditions, while bay 5 is for emergency use. There are ten hydroelectric facilities on the Pend d'Oreille River upstream (in the U.S.) of this facility. The Seven Mile dam is a run-of-the-river facility operated in hydraulic balance with upstream Boundary Dam and downstream Waneta Dam, eventually discharging water in the Lower Columbia River near the Canada-US border.

A field survey at the Seven Mile Dam was conducted from June 19-20, 2017 to determine the change in TDG during the operation of ski-jump spillways for two different scenarios. For the first scenario (scenario A), water was spilled through bays 1 and 2 to discharge at 246.4 m^3/s. For the

second scenario (B), bays 1-4 were operated at the same time spilling water at a rate of 836.2 m^3/s. During the survey, total gas pressure, barometric pressure and water temperature were measured at multiple locations using Lumi4 DO-TGP and PT4 Smart TGP probes (manufactured by Pentair Aquatic Eco-Systems, Apopka, Florida). These probes are capable of recording gas pressure and temperature with accuracy of ±2 mmHg and 0.2 ºC respectively (PentairAES 2014).

The temporal and spatial variation of TDG was measured through a combination of continuous monitoring as well as spot measurements across transects. To monitor the TDG continuously, two stationary platforms were deployed in the forebay (about 550 m upstream) and tailrace (about 1.7 km downstream) of the dam. Custom-built floating platforms were used to house the data logger. The probes were calibrated and set to record data continuously at 2-minute intervals and then deployed at a depth of about 5 m. Spot measurements were carried out in the forebay and tailrace locations as well as across a transect 5.7 km downstream of the dam. These measurements were taken from a boat which was anchored at each survey location. The probe was kept below water for about 10-20 minutes to acquire stable TGP readings. To ensure reliable measurements, readings were taken using two different probes which were consistent with a maximum variation of 6 mmHg. The measurement locations were recorded using a handheld GPS (Garmin GPSMAP 78) which had accuracy in the order of 1-2 m.

To obtain detailed description of gas transfer in the dam, additional TDG data were collected for spill events in 1995, 1997, 1998 and 2011 (refer to Table 4.3). This dataset covered a wide range of discharges, forebay and tailrace concentrations. The spill rates for these conditions varied from 201-3023 m^3/s, while the generation flow remained more consistent between 997-1435 m^3/s. The TDG concentrations were recorded continuously in the forebay and at a location in the tailrace.

4.5 Results and Discussion

During the 2017 field monitoring, water was consistently supersaturated at the forebay of Seven Mile Dam (Figure 4.3a). Depth measurements indicated that the TDG concentrations were lower for scenario B compared to scenario A, which was consistent with observations recorded at the continuous monitoring stations. On June 19 (scenario A), TDG near the surface was 121%, while it increased at 8 m depth followed by relatively stabilized distribution with an average

concentration of 124.9%. For scenario B, the average concentration was 123.5% (Figure 4.3b). The maximum variation of temperature with depth for these scenarios was 1.0 ºC and 0.5 ºC respectively, indicating no significant evidence of stratification. This was further supported by the fact that water residence time in Seven Mile Reservoir is typically < 1 day (Bruce et al. 2018), which limits the possibility of differential heating. The tailrace TDG for the two scenarios was comparatively lower than the forebay which indicated the potential for degassing during the dam operations. Spot measurements at 1.7 km downstream showed that the concentrations were almost uniform across the channel for both scenarios (Figure 4.3c). Mean TDG at this location was 122.1 and 120.0% respectively. Similarly no significant transverse variation was found at 5.7 km downstream. These observations were representative of well-mixed conditions and supported the assumption of complete mixing between the spill and generation flow.

Due to spill operations at the upstream Boundary Dam, high TDG conditions were frequently observed in the Seven Mile Reservoir. In 2011, forebay TDG reached as high as 150% during freshet, while the tailrace concentrations were much lower. Analysis of the dataset (as outlined in Table 4.3) indicated 1-11% drop in mean TDG levels for varying spill conditions compared to forebay concentrations of 114.7-144.9%. Measurements during no-spill event showed no appreciable change in dissolved gas concentration as the generation flows pass through the turbine (Bruce et al. 2018). Therefore, the reduction (i.e. degassing) of supersaturated TDG would be associated with the spill discharges at the Seven Mile Dam.

The transfer efficiency of spilled water E_s was obtained using Eq. (4.1). From Eq. (4.5), the characteristic discharge, q_c = 17.2 m^2/s was estimated for the Seven Mile Dam, beyond which self-aeration does not occur on the chute face. As shown in Figure 4.4, the transfer efficiency varied with spill rate and depended on the operational features associated with q_c. When unit discharge was less than q_c, pre-aeration occurred on the spillway face for which transfer efficiency was highly variable. Particularly due to pre-aeration in bays 1-2 only, E_s varied from 0.31-0.69 for a narrow range of unit discharge (q_1) from 7.0-12.3 m^2/s. For no pre-aeration on the chute face (q_1, q_2 > 17.2 m^2/s), E_s was comparatively lower and ranged from 0.27-0.32 at higher spill rates (Table 4.3). For individual chute profiles, the efficiency varies depending on the spill rate and geometric configuration, and the tailrace concentrations for bays 1-2 and bays 3-4 can be related to spilled

water concentration as $C_{spill} = (C_1Q_1 + C_2Q_2)/(Q_1 + Q_2)$, where Q_1 and Q_2 are the spill rates of bays 1-2 and 3-4, and C_1 and C_2 are the corresponding tailrace concentrations, respectively.

4.5.1 Estimation of Coefficients

TDG degassing in the Seven Mile Dam was evaluated using Eq. (4.4) considering the transfer at the spillway face, free jet and plunge pool. The flow dynamics and corresponding turbulence scaling were different for these regions, and the β and η coefficients of Eqs. (4.2) and (4.3) were evaluated separately for individual regions (denoted as β_s, β_j and β_p for the transfer coefficient, and η_s, η_j and η_p for the exponent, respectively). In the spillway face, η_s was set to 0.75 following the work of Wilhelms and Gulliver (2005). The remaining parameters were estimated using the field data collected during 1995, 1997, 1998 and 2011 spill events which covered a wide range of discharge conditions (refer to Table 4.3). A nonlinear regression was performed to minimize the error between predictions with Eq. (4.4) and field observations. Considering the simplifications made in this study, the coefficients for the free jet (β_j and η_j) were surprisingly consistent with Azbel's (1981) theoretical predictions (Table 4.4). β_s was also very close to 1/4π and neared the range of Wilhelms and Gulliver's (2005) observations at Kost Dam. The plunge pool estimates were smaller than the theoretical values, although η_j was within the range of values found in Geldert et al. (1998) and Urban et al. (2008). Sensitivity analysis indicated that the predicted downstream TDG was mainly dependent on the variation of η_j and η_p (see Appendix). The coefficient for bubble penetration depth (α_p = 1.92) was higher than the experimental value suggested by van de Sande and Smith (1975). For high α_p, the effective depth of bubbles and corresponding C_{eff} increases in the plunge pool resulting in higher TDG downstream.

As shown in Figure 4.5(a), the predicted and measured TDG concentrations in the downstream agreed very well (R^2 = 0.993). The predictive relationships were able to capture the field conditions with and without pre-aeration for the 1995-2011 dataset. The standard error of the predicted to measured TDG was 0.82%. The capability of the model to predict TDG was verified with the 2017 field scenarios (Figure 4.5b). The absolute error for the prediction of two conditions (scenarios A and B) was 0.30% and 1.38% respectively.

4.5.2 Surface and Bubble-mediated Transfer

The two mechanisms of gas exchange, i.e. transfer over the free surface and via entrained bubbles, were evaluated for the Seven Mile Dam using Eqs. (4.2) and (4.3). For a given region, the liquid film coefficient k_L depended on the turbulence scaling, flow hydraulics and air-bubble features. The corresponding transfer coefficients $(k_L a)_b$ and $(k_L a)_s$ differed considerably in the presence of bubbles. When there was no pre-aeration on the spillway (q_1, q_2 > 17.2 m^2/s), k_L varied from 1.69×10^{-4} to 1.92×10^{-4} m/s and the TDG change due to surface transfer was less than 0.1% for typical travel times. The surface transfer was smaller for pre-aerated conditions, but the concentrations dropped by 0.4-5.1% as a result of bubble-mediated exchange attributed by high interfacial area a_b. Similarly for the jet, the interfacial area contributed by bubbles was 660-1850 times higher than the jet surface area, and $(k_L a)_s$ was very small relative to $(k_L a)_b$. Along the jet length, $(k_L a)_s/(k_L a)_b$ decreases and gas exchange is dominated by the bubble-mediated transfer (Figure 4.6).

In the plunge pool, a_b decreases as the air bubbles leave the flow while traveling downstream, and $(k_L a)_s/(k_L a)_b$ increases particularly in the shallow pool (for bays 3-4). However, degassing through the pool surface was not significant in the bubbly region. This could be important at the end of aerated zone, reducing TDG in the downstream river. However in deep, regulated rivers like the Pend d'Oreille, this process is typically very slow (Kamal et al. 2019) and would take many river miles for any noticeable change to occur. As shown in Figures 4.3(c) and 4.3(d), mean TDG for scenario B reduced by 0.1% while traveling from 1.7 to 5.7 km downstream.

Figure 4.7 shows the predicted TDG profile as a function of distance from the dam crest. For q < 17.2 m^2/s, bubbles were entrained on the spillway face with void ratio ranging from 0.08-0.19. Since forebay TDG was greater than atmospheric saturation (C_{sat} = 100), gas transfer dominated by bubble-mediated exchange led to degassing of supersaturated water. Bubbles were further entrained along the free jet, increasing interfacial area and jet thickness available for gas transfer. The transfer increased along the jet and degassing was maximum within the aerated jet (for $(x - L_s)/L_j$ between 0 and 1) as a result of higher gas void ratio (Figure 4.7a). On the other hand, minimal change due to surface transfer occurred at the chute for high flows (unit discharge > q_c). Without pre-aeration, the mean jet void ratio varied from 0.24-0.38 and bubble-mediated transfer

began once the water was discharged from the flip-bucket. The TDG profile and the pattern of change in concentrations were similar for bays 3-4 (Figure 4.7b).

The evolution of TDG in the plunge pool was affected by both dissolution and degasification depending on the bubble penetration depth and corresponding saturation concentration. In bays 1-2, the jet plunges into a deep pool where the mean depth varied from 13.8-17.1 m. For high discharge conditions, bubbles were carried to the bottom ensuing C_{eff} as high as 180% (for q_1 = 55.6 m^2/s). The bubble dissolution associated with high gas void ratio (mean ϕ_p = 0.15) and hydrostatic pressure led to a rapid increase of TDG, followed by a gradual degasification due to change in effective depth of bubbles. This resulted in a net increase in TDG in the tailrace (i.e. TDG generation) compared to the plunge-in concentration of the jet. The additional generation of dissolved gas was limited for low flow condition (q_1 = 5.7 m^2/s) due to smaller h_{pen}. For bays 3-4, degassing was dominant at the plunge pool due to shallower depths (refer to Table 2). The aerated zone was shorter for this bay as bubbles escaped quickly, reducing the TDG concentrations for both low and high flow conditions.

4.5.3 Transfer in Individual Regions

The gas exchange in the spillway face, jet and plunge pool affects the net degassing of TDG in the Seven Mile Dam. Figure 4.8 shows the change in TDG in individual regions (ΔC defined as the difference between initial and final concentration of a given region) compared to forebay concentration. For pre-aerated conditions, TDG concentrations in the spillway face dropped by 1.1-4.2% for bays 1-2 and 0.3-2.5% for bays 3-4. Although smaller bubble size and higher turbulence facilitates gas transfer, the degassing reduced with unit discharge as the aeration length was shortened and less bubbles were available for transfer. For a given flow rate, the transfer was higher in bays 1-2 because of longer chute length (refer to Table 4.2). The degassing was substantial in the aerated jet, leading to 6.1-9.1% reduction of TDG in bays 1-2. For these cases, the concentrations dropped to 104.6-106.5% compared to forebay TDG of 114.7-119.1%. For no pre-aeration, the jet length increases and high turbulence shears the bubbles into smaller size, thus enhancing the degassing to 13.1-15.0%. Complete degassing was not achieved for these conditions due to shorter residence time of bubbles. Because of the elevated bucket, L_j was longer in bays 3-4 and the corresponding transfer was comparatively higher (up to 18.4%).

Due to shallow plunge pool, TDG was degassed by 0.1-2.5% in bays 3-4 for q_2 = 4.7-29.8 m^2/s. On the other hand, TDG was increased by 1.0-8.9% in the deep pool of bays 1-2 which tended to increase with spill rate q_1. This was consistent with previous studies (Geldert et al. 1998; Urban et al. 2008; Politano et al. 2017), even though the inflow was highly supersaturated for this case. For q_1 > 42 m^2/s, TDG degassing in the free jet slightly reduced due to smaller L_j/L_b and void ratio, while the corresponding generation in the plunge pool increased. This resulted a net decrease in degassing which explains the lower transfer efficiency in high flows as shown in Figure 4.4.

4.5.4 Bulk Estimate of Transfer Rate and Efficiency

Since the aerated jets were the largest contributor of TDG degassing, Eq. (4.2) could be utilized to estimate the corresponding transfer rate in the jet. Using Eq. (4.9), the bubble size in the jet was scaled as $d_b \sim (\sigma/\rho)^{3/5}(L_j/U_j^3 sin^3\Omega)^{2/5}$. The time over which gas transfer occurs depends on the jet length. Assuming uniform velocity along the jet, the residence time would be $T \sim L_j/U_j cos\Omega$. Incorporating the time factor and substituting d_b, Eq. (4.2) was rearranged to obtain the following non-dimensional form for jet transfer coefficient $(k_L aT)_j$:

$$(k_L aT)_j \propto f(\phi_j)\alpha_\Omega We^{3/5} Sc^{-1/2} R_j^{\zeta} \qquad (4.10)$$

where $f(\phi_j)$ is a functional form of jet void ratio, α_Ω is a coefficient for bucket angle = $sin^{6/5}\Omega/cos\Omega$, We is a form of jet Weber number = $U_j^2 L_j \rho/\sigma$, Sc is the Schmidt number = ν/D_m, R_j is the jet Reynolds number = $U_j h_j/\nu$, and ζ is the Reynolds number exponent. Since the jet void ratio is a function of L_j/L_b and the break-up length is proportional to h_j, the functional form could be approximated by $(L_j/h_j)^{\lambda}$, where λ is another adjustable coefficient that takes into account of the non-linear form of $f(\phi_j)$. Then Eq. (4.10) was simplified into:

$$(k_L aT)_j = \alpha_1 We^{3/5} Sc^{-1/2} R_j^{\zeta} (L_j/h_j)^{\lambda} \qquad (4.11)$$

where α_1 is a proportionality constant that also included α_Ω (α_Ω is constant for a given spillway bucket). To obtain the adjustable coefficients α_1, ζ and λ, regression analysis was performed to fit the $(k_L aT)_j$ associated with TDG degassing in the free jet. These coefficients were 1.02×10^{-5}, -0.0197 and 0.5724 respectively, where the Reynolds number exponent was very small. Setting ζ= 0, another regression was performed to yield $\alpha_1 = 6.51\times10^{-6}$ and λ = 0.5983 (≈ 0.6). The predictive

form of Eq. (4.11) was consistent with $(k_L aT)_j$ estimates for bays 1-2 and bays 3-4 (Figure 4.9). Some of the scattered data corresponded to pre-aerated conditions for which the jet void ratio not only depended on L_j/h_j, but also on the aeration characteristics (i.e. location and depth at inception point) on the spillway face. The simplified form can be expressed as:

$$(k_L aT)_j = 6.47 \times 10^{-6} \, (\nu/D_m)^{-1/2} (U_j^2 L_j \rho/\sigma)^{3/5} (L_j/h_j)^{3/5} \qquad (4.12)$$

The temperature for the field test conditions varied from 10.1-14.9 ºC. The values of ρ and σ do not change significantly within these range and can be assumed constant. The jet thickness can be approximated as $h_j = \frac{q}{U_j} = \frac{q}{\sqrt{2gH}}$, where H is the head difference between forebay water level and bucket invert. Simplifying and rearranging Eq. (4.12) results in:

$$(k_L aT)'_j = 0.00156(\nu/D_m)^{-1/2} (q\sqrt{2gH})^{3/5} (L_j\sqrt{2gH}/q)^{6/5} \qquad (4.13)$$

When there is no pre-aeration, the forebay concentration would remain unchanged on the chute and Eq. (4.13) can be used directly. For pre-aerated conditions, TDG degassing in the spillway face was lower than the jet (refer to Figure 4.8). Considering net degassing in these regions, Eq. (4.13) was fitted to obtain the transfer coefficient for pre-aerated conditions:

$$(k_L aT)'_j = 0.00172(\nu/D_m)^{-1/2} (q\sqrt{2gH})^{3/5} (L_j\sqrt{2gH}/q)^{6/5} \qquad (4.14)$$

The plunge pool gas transfer process also affects the net transfer efficiency of the ski-jump spillway. In addition to air-water features of incoming jet, the change in TDG is governed by C_{eff} and corresponding bubble penetration depth h_{pen}. Also depending on the pool depth, dissolved gases can be generated (in bays 1-2 with h_p = 13.8-17.1 m) or degassed (in bays 3-4 with h_p = 2.6-5.9 m). Therefore using Eqs. (4.13) and (4.14) and introducing a factor relating h_{pen} and h_p, the transfer efficiency of individual bays, E was approximated as:

$$E = 1 - exp\left[-(k_L aT)'_j \left(1 + \frac{0.25 h_{pen}}{h_{avg} - h_p}\right)\right] \qquad (4.15)$$

where h_{avg} is the mean depth of flow in the pool. When $h_p > h_{avg}$, additional dissolved gas is generated in the plunge pool (bays 1-2) and vice versa (bays 3-4). The comparison between modeled transfer efficiency and that calculated by Eq. (4.15) is shown in Figure 4.10. The equation provided a reasonable estimate of transfer efficiency for bays 1-2 and 3-4 (R^2 = 0.95), particularly

when there was no pre-aeration. For pre-aerated conditions in bays 3-4, TDG change in the plunge pool was 0.1-0.4% which was much smaller than the degassing in the jet. The additional depth term in Eq. (4.15) resulted in an overestimation of E for these conditions. As indicated by Eqs. (4.13)-(4.15), the gas transfer rate increased with jet velocity ($\approx \sqrt{2gH}$) and trajectory length and the corresponding transfer efficiency was affected by plunge pool depth variations, which was compatible with the physical processes of gas transfer in ski-jump spillway.

4.6 Conclusions

In this study, the transfer of supersaturated total dissolved gases in a ski-jump spillway was evaluated through a combination of field observations and modeling. Due to flip buckets designed to aerate water with a large surface area, substantial degassing of TDG was observed in the Seven Mile Dam during spill operations. Analysis of 26 field test conditions showed that the high TDG water, received at the forebay due to upstream spill operations, decreased significantly in the tailrace with a maximum reduction of 11%. The corresponding gas transfer efficiency varied depending on the aeration characteristics of flow associated with the spill rates and operational conditions of individual bays.

The modeling effort in this study utilized physical relationships related to air entrainment, bubble characteristics and mass transfer over the free surface and bubbles, and allowed the independent evaluation of TDG transfer in the spillway face, free jet and plunge pool of the ski-jump spillway. Results indicated that the degassing of TDG was dominated by the bubble-mediated transfer in the Seven Mile Dam. The entrained bubbles significantly increase the interfacial area available for gas transfer and the corresponding concentration change is much higher than the transfer at free surface. The free jet is the major contributor of degassing, where the change in concentration was 1.5-7.7 times higher compared to spillway face of bays 1-2. When forebay water is highly supersaturated, dam operating at spill rate less than the characteristic discharge for pre-aeration facilitates degassing in the spillway face and jet. The degassing can be enhanced by spilling through longer chute and jet trajectory. The plunge pool region was found to generate additional dissolved gases as well as degas TDG depending on the spill rate, tailwater depth and geometric features of the dam. Based on these observations, operational alternatives could be considered to minimize the dissolved gas supersaturation in the downstream environment.

To estimate the degassing in the dam, a simplified relationship of gas transfer efficiency was presented for practical applications. This indicated that the transfer and corresponding degassing in the ski-jump spillway increased with jet velocity and trajectory length, and depended on spill rate, plunge pool depth and water temperature. This was consistent with the physical processes of aerated flows and the well-founded theories of bubble-mediated mass transfer. The methodology presented herein with independent consideration of the spillway face, free jet and plunge pool can be very useful for real-time decision support. Direct measurement in these regions is not possible, and the transfer in individual region was evaluated based on measurements carried out in the upstream and downstream of the dam. Therefore, data for similar ski-jump spillways are needed to verify its application for the assessment of dissolved gas transfer.

Appendix. Sensitivity of Adjustable Model Coefficients

For the sensitivity check of the fitted model coefficients, the downstream dissolved gas concentrations were estimated by varying each coefficient while keeping the others constant. As shown in Figure 4.11, the downstream TDG concentrations increase for smaller β_j and η_j due to less degassing along the free jet. For smaller β_p and η_p, the concentrations drop as the effect of plunge pool dissolved gas generation becomes less pronounced. It should be noted that the predicted concentrations were particularly sensitive to η_j and η_p, which represents turbulence in the jet and plunge pool respectively. For η_j = 0.9, the transfer in the jet increases and lead to 3.6-9.3% reduction in TDG as result of high degassing (Figure 4.11b). When η_p is higher, the degassing is complemented by additional dissolved gas generation in the plunge pool with a net increase in downstream concentrations. For high flow rates, degassing in the plunge pool becomes dominant and the TDG changes little (Figure 4.11d). The variation with β_s was only applicable for pre-aerated conditions (q_1, q_2 < 17.2 m^2/s) with minimal change in concentration (Figure 4.11e). The coefficient α_p determines the bubble penetration depth in the plunge pool. As α_p increases, bubbles travel deeper generating higher TDG downstream. For higher flows, the penetration depth equals the plunge pool depth and tailrace concentrations remain unchanged (Figure 4.11f).

Table 4.1: Definition of gas void ratio, turbulent velocity and length scale in different regions of the ski-jump spillway

Property	Spillway face	Free jet	Plunge pool
Void ratio, ϕ	$\phi_s = \phi_{eq}\left[1 - \exp\left(-0.01\frac{x_s}{h_i}\right)\right]$ $\phi_{eq} = 0.656[1 - e^{-0.0356(\theta - 10.9)}]$	$\phi_j = \phi_s + tanh\left[0.4\left(\frac{x_j}{L_b}\right)^{0.6}\right]$	$\phi_p = \phi_j \exp\left(-\frac{u_b x_p}{q}\right)$
Characteristic velocity, U_t	$\sqrt{g h_i S}$	$0.2 U_j Re_j^{-1/8}$	$U_p\sqrt{f/8}$
Characteristic length, L_t	$\frac{h_i}{1-\phi_s}$	$\frac{h_j}{1-\phi_j}$	$0.62 h_p$

Notation:

Subscripts s, j and p denotes spillway face, free jet and plunge pool.

x_s = distance from the inception point to the location of interest along the spillway

x_j = distance from the bucket lip to a location on the jet

x_p = distance from the plunge point in the pool along the flow direction

Table 4.2: Geometric information of Seven Mile Dam spillways

Bay	Slope	Length	Ogee crest elevation	Bucket invert elevation	Bucket lip elevation	Plunge pool bed level
	(deg)	(m)	(m)	(m)	(m)	(m)
1-2	51.3	100.6	511.76	470.92	474.13	450.58
3-5	51.3	76.2	511.76	473.96	477.18	461.78

Table 4.3: Conditions of the Seven Mile Dam field tests across 5 years of TDG studies. Data provided by BC Hydro for all years except 2017

Date	No. of cases	**q** (m^2/s)		C_u (%)	C_d (%)	Temperature (ºC)	E_s
		q_1 (bays 1-2)	q_2 (bays 3-4)				
May 31– June 04, 1995	4	9.5-11.7	0-5.3	114.7-119.1	113.6-116.3	10.1-10.6	0.19-0.40
June 11 – June 13, 1997	4	53.8-55.6	29.6-29.8	144.7-146.2	135.4-135.7	10.9-11.3	0.27-0.32
June 01 – June 03, 1998	3	17.8-18.5	13.3	130.0-132.2	125.1-125.4	10.4-10.6	0.30-0.43
June 12 – June 18, 1998	6	5.7-12.3	0	116.7-118.7	115.5-116.6	10.8-11.3	0.32-0.69
June 01 – June 16, 2011	7	34.5-42.3	13.0-25.4	140.9-144.9	132.3-134.5	10.4-11.3	0.32-0.40
June 19 – June 20, 2017	2	7.0, 12.5	0, 11.0	124.9, 123.5	122.1, 120.0	14.5, 14.9	0.60, 0.34

Table 4.4: Summary of model coefficients

Region	β *	η *	α_p *	K_a	T_u
Theoretical/ expected value	1/4π	0.75 / 0.55 – 1.3	0.42	0.75-0.9	1-5
Spillway	1.09/4π	0.75	-	-	-
Free jet	1.13/4π	0.77	-	0.82	1.2
Plunge pool	0.86/4π	0.69	1.92	-	-

* adjustable model coefficients

Figure 4.1: (a) Seven Mile Dam during spill operation, and (b) schematic representation of different regions in ski-jump spillway

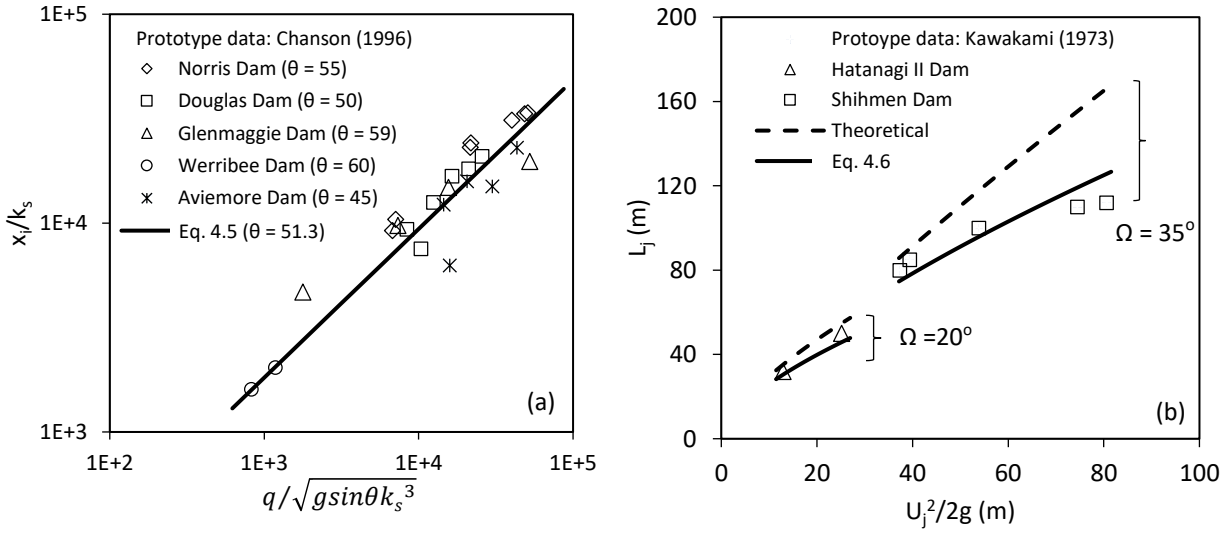

Figure 4.2: Comparison with prototype data for the calculation of (a) inception point using Eq. 4.5 and (b) jet trajectory length using Eq. 4.6

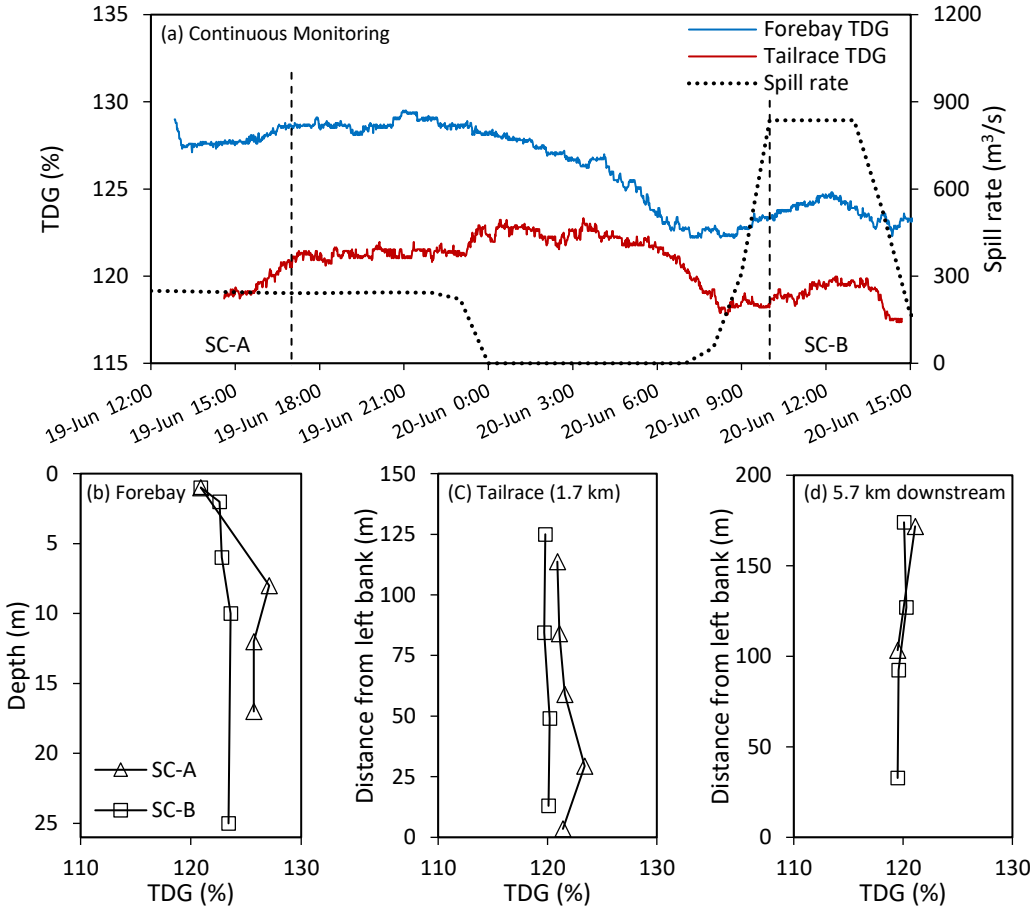

Figure 4.3: Measured TDG during 2017 field work: (a) continuous monitoring, and spot measurement at the (b) forebay, (c) tailrace and (d) 5.7 km downstream

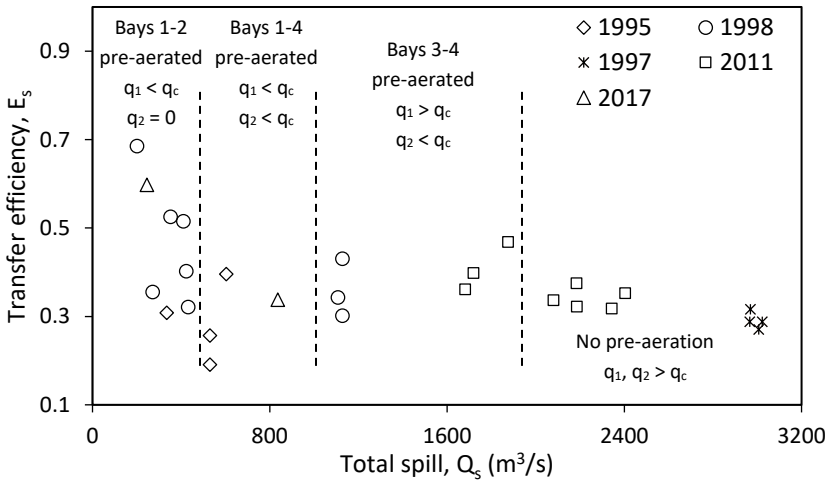

Figure 4.4: Transfer efficiency of spillways for field tests

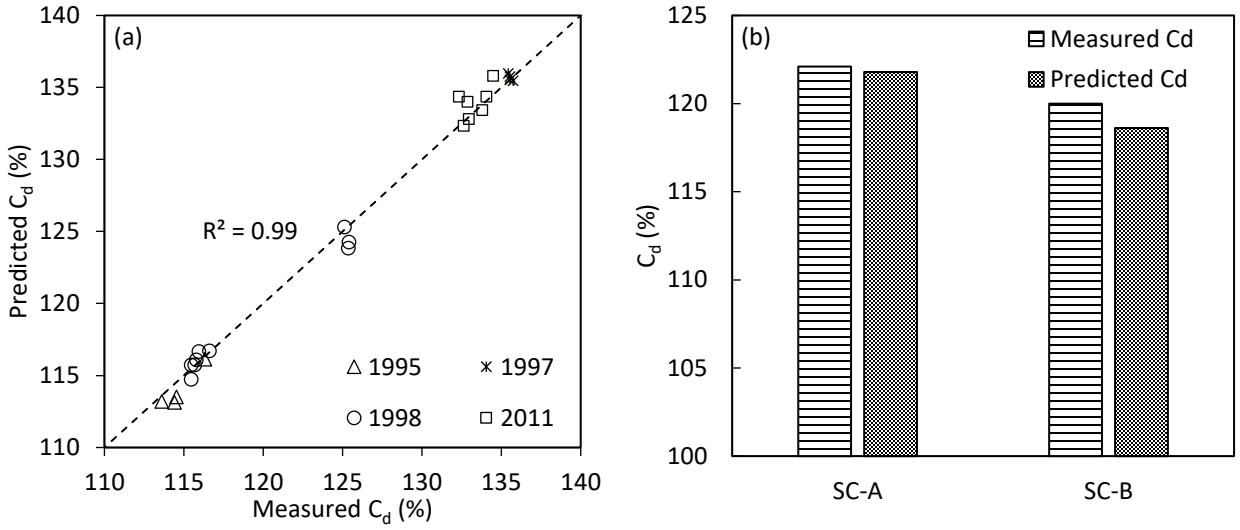

Figure 4.5: (a) Comparison between the measured and calculated TDG, and (b) verification with 2017 field data

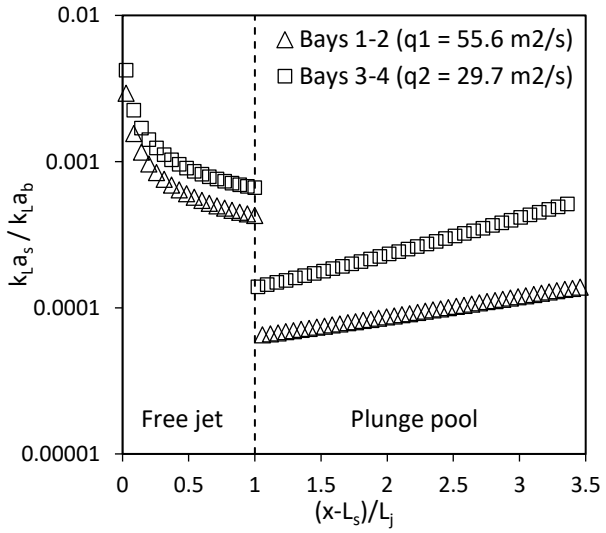

Figure 4.6: Relative variation of surface transfer ($k_L a_s$) and bubble transfer ($k_L a_b$) along the jet and plunge pool region

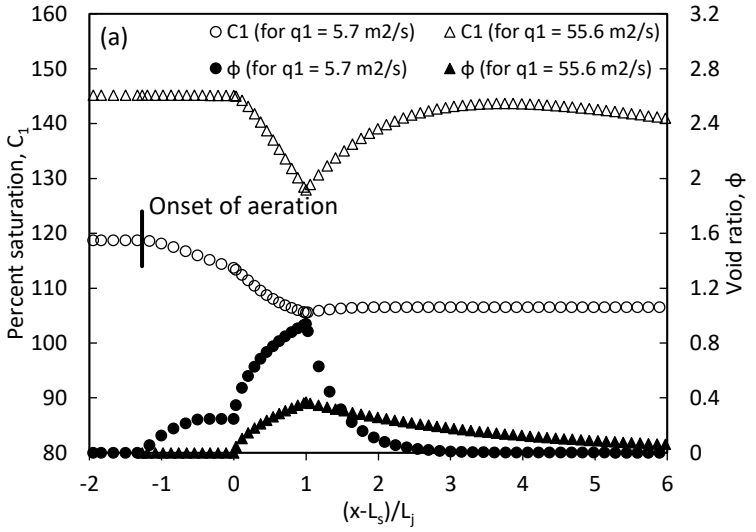

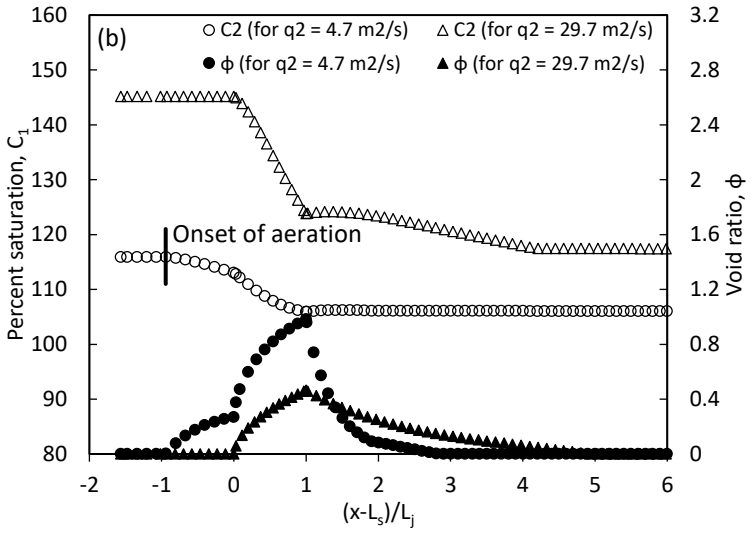

Figure 4.7: TDG profile and void ratio with distance for (a) bays 1-2 and (b) bays 3-4

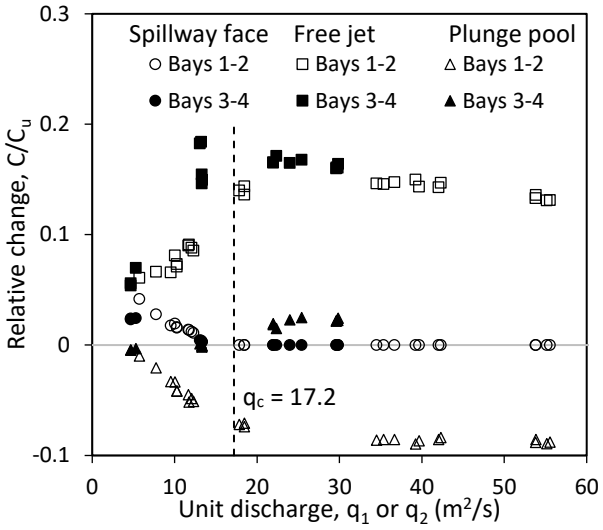

Figure 4.8: Change in TDG concentration in individual regions

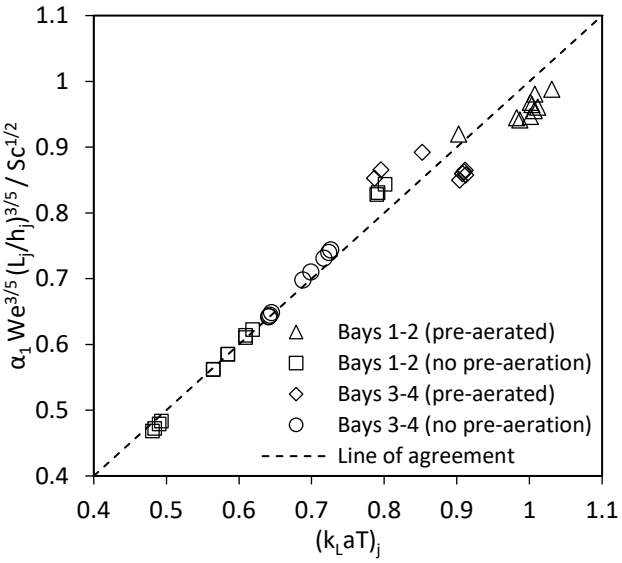

Figure 4.9: Correlation between jet gas transfer coefficient and non-dimensional prediction parameter

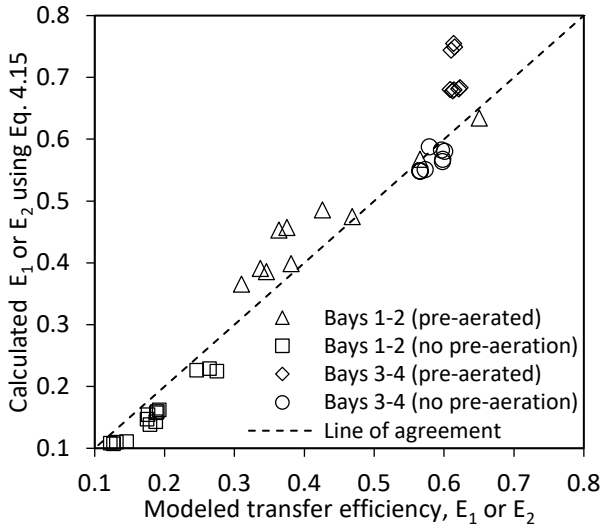

Figure 4.10: Comparison of gas transfer efficiency calculated using Eq. 4.15 with modeled efficiency

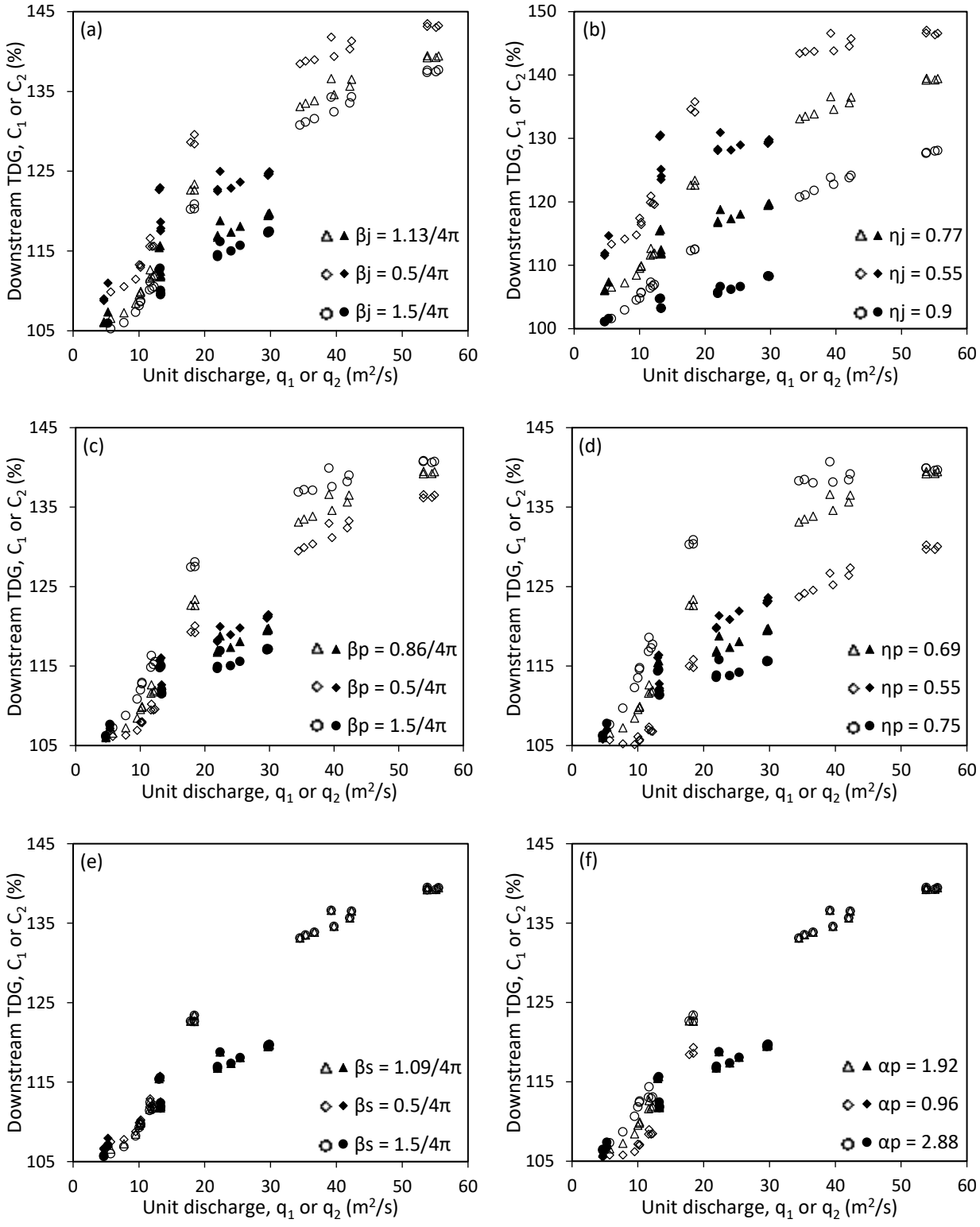

Figure 4.11: Sensitivity of downstream dissolved gas concentrations to fitted model coefficients. Open symbols represent bays 1-2 and solid symbols represent bays 3-4

CHAPTER 5

A System Model for Total Dissolved Gas Risk Assessment *

5.1 Introduction

Hydropower facilities greatly impact regional water resources balance as well as the physical, chemical and biological features of an aquatic environment and habitat ecosystem (Richter and Thomas 2007; Anderson et al. 2015). Nowadays one of the major concerns in this aspect is the supersaturation of total dissolved gases (TDGs) produced downstream of spillways that can negatively impact aquatic life and fish population (Fidler and Miller 1997; Weitkamp 2008). Typically, hydropower facilities are developed in a cascade manner and high TDGs generated in a dam affects other facilities below and downstream river-reservoir environment resulting in cumulative impacts in the system (USACE 2001; Ma et al. 2018). During spill operations, supersaturated waters released from upstream dams have the potential to dissipate, remain unchanged, or be increased (Urban et al. 2008; Kamal et al. 2019), and can impose environmental and ecological risk to downstream habitat. Understanding such consequences can be very complex and becomes more complicated when multiple facilities are involved in series on a single river system, in parallel on multiple river systems, or both.

In hydropower dams, water is often spilled voluntarily as a part of management strategy to aid non-turbine fish passage. Involuntary spill, in contrast, is the release of excess water when river discharge exceeds powerhouse generation capacity or demand for electricity. When water is spilled via non-power release (NPR) structures like spillways and low-level outlets, atmospheric air is entrained at the plunge pool in the form of bubbles where hydrostatic pressure is sufficiently high to enhance mass transfer and subsequent gas dissolution (Hibbs and Gulliver 1997; Geldert et al. 1998; Politano et al. 2009). This results in dissolved gas (primarily nitrogen and oxygen) supersaturation in water compared to ambient atmosphere (Colt 1984). Such supersaturation poses a conflict with the voluntary spill management due to the effects of gas bubble disease or gas bubble trauma (GBT) in fish which results from bubble formation in tissues and body. Acute GBT can result in fish mortality through tissue damage, cardiac blockage, hemorrhaging, and increase

* The content of this chapter is being prepared to be submitted as a journal manuscript.

risk of predation due to reduced mobility (Fidler and Miller 1997). The lethal effect of supersaturation and risk of GBT varies by fish species and life stage, TDG levels, swimming depth of fish, duration of exposure, past exposure to high TDG etc. (Weitkamp and Katz 1980). In downstream riverine environment, supersaturated TDGs tend to re-establish atmospheric equilibration through dissipation (gas exchange at air-water interface) and mixing with adjacent waters (Li et al. 2015; Kamal et al. 2019). However, the extent of supersaturation can reach far downstream exceeding the water quality standard for TDG of 110% (USEPA 1986; CCME 1999) and result in spatial variations in exposure levels and subsequent adverse impacts to fish and other biota downstream (Johnson et al. 2007). Assessment of corresponding risk is therefore crucial from hydro-environmental-ecological perspective as well as in regulatory context for habitat protection.

The adverse impacts of TDG supersaturation can be managed by operational regulations like reducing involuntary spill, maximizing NPR releases, changing sequence of spill bay operation or optimizing spill pattern and interval (Schneider and Wilhelms 2005; Gulliver et al. 2009; Feng et al. 2014; Politano et al. 2017). Such operation to ensure water-quality constraints while maintaining power demand can be challenging, particularly in complex river systems involving multiple dams. A number of studies demonstrated the superposition of impacts on the hydrology, water temperature, sediment and water quality parameters due to multi-facility operations (Liang et al. 2012; Chen et al. 2015; Todorova et al. 2016; Wen et al. 2018). The cumulative TDG impacts for such operations are merely reported. Witt et al. (2017) presented a simplified model to assess tailrace TDG in a multi-reservoir system without considering the dissipation process in downstream environment. The model was used to optimize spill operations meeting state water-quality standards. The guideline of 110% saturation is often conservative, potentially resulting in costly mitigation when none is required. An alternative management strategy can be achieved by defining thresholds incorporating factors like the compensatory effect of depth and exposure duration (BC Hydro 2014). Detailed assessment is needed to evaluate the effect of these impacting factors and identify their role in specific river reaches exposed to TDG risk. Ma et al. (2018) utilized numerical models to simulate TDG distribution in reservoir and river as a result of cascade operations. This study considered the magnitude and duration to evaluate potential TDG risk. However, running simulation models for multi-reservoir systems can be very complicated due to various physical processes associated with air-water, two-phase flow (Politano et al. 2017), and precludes required mitigation actions in time. Hydropower operators are in urgent need of a

reliable tool to predict and manage TDG, and produce energy in environmentally sustainable manner.

Management of TDG in multi-facility hydropower systems requires a coordinated approach and decision-support tools to assess TDG and corresponding risk during spill operations. Therefore, a risk assessment framework was developed in this study to examine spill-TDG responses by means of both mechanistic and whole-system approaches and identify potential habitat risk zones for the combined operation of multiple facilities. The study was carried out based on the field observations at the Columbia River hydropower system in British Columbia, Canada. Given the complexity of the TDG generation process, gas transfer in individual facilities was modeled for downstream impact assessment. As TDG level changes in downstream, its mixing and dissipation was evaluated through an analytical transport model. These were integrated into a single analytical platform with objectives towards the evaluation of degree and extent of risk of GBT on resident fish, and development of a framework for real-time use by system managers to improve operational efficiency while maintaining environmental regulations. A ranking process was developed to address TDG risks at hydropower facilities in relation to wider management priorities throughout the river system and provide strategic assessment of the relative need for mitigation action.

5.2 Modeling Framework

The modeling framework developed in this study can be described by a multi-stage approach incorporating hydraulic analyses, TDG modeling, geospatial mapping and risk assessment (Figure 5.1). The system-wide distribution of TDG, a key component of this framework, is affected by TDG generation in individual facilities and its subsequent evolution in the downstream which essentially depends on the air-flow features of spillway and river hydraulics. The outcome is then utilized to map TDG across different spatial scales and assess its exposure risk to habitat ecology.

5.2.1 TDG Modeling in Spillways

Due to inherent complexity of various physical processes involving air entrainment, bubble characteristics and mass transfer and complicated air-water two phase flow, the generation of TDGs in spillway is usually site specific (USACE 2001). A mechanistic approach incorporating

meaningful physical processes can provide reliable estimates of TDG for wide range of operational conditions. The transfer of dissolved gases can be modeled as:

$$C_{spill} = C_{eff} + (C_u - C_{eff})exp(-k_L at) \qquad (5.1)$$

where C_u and C_{spill} are the total dissolved gas concentrations of spilled water in the upstream and downstream respectively, C_{eff} is the effective saturation concentration accounting increased hydrostatic pressure (Hibbs and Gulliver 1997), k_L is the liquid film coefficient, a is the specific interfacial area, and t is the residence time of the bubbles in the tailrace. C_{eff} increases transfer potential across interfaces and depends on the effective depth of bubbles. Typically, this depth is physically limited by the plunge pool bottom and can be considered by two-thirds of the tailwater depth, h_p (Roesner and Norton 1971; Hibbs and Gulliver 1997). The residence time depends on the depth and velocity of the flow, as well as rise velocity of the bubbles (Geldert et al. 1998).

In the plunge pool, gas transfer is dominated by the bubble-mediated exchange and the corresponding transfer rate coefficient, $k_L a$, estimation improves on previous research (Geldert et al. 1998; Urban et al. 2008) and this study (refer to Chapter 4). Considering residence time $t \approx h_p/u_b$ and incorporating Hinze's (1955) relationship for bubble size, Azbel's (1981) theoretical relationship for mass transfer across spherical bubbles can be written as:

$$k_L at \sim \phi \frac{(1-\phi)^{1/2}}{(1-\phi^{5/3})^{1/4}} We^{3/5} Sc^{-1/2} Re^{\eta} \left(\frac{\nu}{d_j u_b}\right) \qquad (5.2)$$

where ϕ is the gas void ratio; We is the Weber number = $\rho q^2/\sigma d_j$; Sc is the Schmidt number = ν/D_m; Re is the Reynolds number = q/ν; η is an exponent; q is the unit discharge; ρ, σ, ν and D_m are density, surface tension, kinematic viscosity and gas diffusivity in water, respectively; u_b is the bubble rise velocity (≈ 0.25 m/s); d_j is the jet thickness = $q/\sqrt{2gH_z}$; and H_z is the hydraulic head. The void ratio in the plunge pool is typically small and the functional form of ϕ in Eq. (5.2) can be approximated by $\phi_{av} = \lambda Fr/(1+\lambda Fr)$ (Azbel 1981; Sene 1988) where Fr is the Froude number = $q/g^{1/2}h^{3/2}$, g is the acceleration due to gravity and λ is a coefficient. After simplifying and incorporating in Eq. (5.2), the gas transfer coefficient can be obtained as:

$$k_L at = \alpha \left(\frac{q}{A+q}\right) We^{3/5} Sc^{-1/2} Re^{\eta} \left(\frac{\nu}{d_j u_b}\right) \qquad (5.3)$$

where α and A are model coefficients that can be adjusted with field observations. Depending on the flow field and turbulence scaling, the Reynolds number exponent can be different than Azbel's (1981) relation and was set to η = 0.69 following the work at the Seven Mile Dam (Chapter 4).

5.2.2 TDG Modeling in River

When supersaturation occurs, TDG change in the downstream riverine environment is strongly coupled with hydraulic processes of dissipation and mixing. Beyond the plunging/bubbly region of the tailrace, gas exchange at the air-water interface during transport through the river dissipates TDG levels towards equilibrium with the atmosphere. The mixing between high TDG spilled water and powerhouse flow as well as secondary sources like tributary inflow can result in dilution and cause transverse variation across the river (Kamal et al. 2019). To describe the two-dimensional distribution of TDG, an analytical method based on streamtube model (Yotsukura and Sayre 1976) can be utilized using the concept of cumulative discharge for steady-state case as follows:

$$C(x,\hat{q}) = C_{sat} + \left[\frac{C_o}{2}\left\{erf\left(\frac{\hat{q}-\hat{q}_a}{\sqrt{4Dx}}\right) - erf\left(\frac{\hat{q}-\hat{q}_b}{\sqrt{4Dx}}\right)\right\} - C_{sat}\right] exp\left(-k\frac{x}{U}\right) \qquad (5.4)$$

where C is the TDG concentration at a given location; C_{sat} is the saturation concentration (100% at atmospheric pressure); x is the longitudinal distance; $\hat{q}$ is the cumulative discharge = $\int_0^y uhdy$; u, h and y are local depth-averaged velocity, depth and transverse distance from bank respectively; U is the mean velocity in flow direction; D is the factor of turbulent diffusion; and k is the first-order dissipation rate. The reference concentration, C_o, corresponds to an initial distributed source stretching from $\hat{q}$ = $\hat{q}_a$ to $\hat{q}$ = $\hat{q}_b$. The factor, D is related to transverse mixing coefficient E_t and can be made non-dimensional in the form (Gowda 1984; Rutherford, 1994):

$$\frac{DB}{Q^2} = \psi\frac{E_t}{BU} \qquad (5.5)$$

where B is the channel width = $\int_0^y dy$; Q is the river discharge; ψ is the dimensionless shape factor = $\int_0^Q uh^2 d\hat{q}/UH^2Q$; and H is the mean depth of flow.

Dissipation of dissolved gas components is the key process for degassing of supersaturated TDG out of the river system. The dissipation rate can vary from 0.003-0.652 hr^{-1} depending on the river-reservoir hydraulics (Li et al. 2015). Empirical relationships available to estimate this rate (Feng

et al. 2014) can result in prediction errors when applied to other river systems (Kamal et al. 2019). The dissipation of TDG is usually conceived as the physical process involving gas exchange at the air-water interface. In surface reaeration studies, two widely used semi-empirical treatments are the surface-renewal and the energy-dissipation models (O'Connor and Dobbins 1958; Tsivoglou and Wallace 1972), and most of the models were developed in the form (Gualtieri et al. 2002):

$$k \sim U^a H^{-b} \qquad (5.6)$$

where a and b are model exponents which varies from 0.5-1.0 and 0.67-1.85 respectively among the usual reaeration equations found in the literature (as reviewed by Palumbo and Brown 2014). Typically, these models have limited generality and can result in large prediction errors in conditions different from which they were formulated (Bowie et al. 1985). Also transfer through small bubbles, formed at pre-existing gas cavities provided by suspended particles and sediments due to liquid phase supersaturation, can potentially contribute to net dissipation along with the direct transfer across the free surface (Kamal et al. 2019).

5.2.3 TDG Mapping

The intermediate stage of the framework is the development of TDG maps for the river system, based on the estimated concentration distribution. The analytical model described above considers cumulative discharge, $\hat{q}$, instead of transverse distance, y, to represent variation across channel width. The cumulative discharge at a cross-section can be estimated from Manning's equation by dividing it into a number of subsections (Rutherford 1994; Zhang and Zhu 2011). At each section, Q and local depth, h , are known and the local velocity can be estimated from $u/U \propto (h/H)^{2/3}$. The estimated velocity distribution is then utilized to relate cumulative discharge at a given distance and transform $(x, \hat{q})$ coordinates to (x, y). Next, the coordinates of every section are processed to convert into WGS84 UTM zone 11U reference system for real-time latitudes and longitudes. To develop standalone concentration maps, the data are exported to spatial mapping tools and interpolated for raster representation of TDG distribution of the entire river system.

5.2.4 TDG Management Thresholds and Risk Rating

The system-wide TDG mapping provides spatial distribution for different spill incidents and aids identification of potential risk-zones in the habitat ecosystem. However, the severity of exposure

and risk of GBT depends on many factors (Weitkamp and Katz 1980; Jensen et al. 1986; Fidler and Miller 1997; Weitkamp 2008). In general, fish mortality increases with total dissolved gas level although the response is highly variable depending on the species type and life stage. A major mitigating factor in this regard is the water depth which compensates the effect of supersaturation. Each additional meter of depth reduces effective gas pressure by approximately 10% saturation (Colt 1984). Access to deep waters slow or minimize bubble formation and reduces GBT risk (Antcliffe et al. 2002). The movement of dissolved gas from ambient water to fish tissues also depends on the duration of exposure. Longer exposure at high degree of supersaturation poses greater risk to mortality.

The TDG criterion of 110% saturation establishes a safe limit for total dissolved gas in water. This level of exposure results in little to no mortality regardless of water depth and exposure duration (Fidler and Miller 1997; Weitkamp 2008). A less conservative alternative management approach can be adopted by setting tolerance thresholds based on depth compensation and duration (BC Hydro 2014). Fish with access to water deeper than 0.5 m can tolerate the limit up to 115%. If fish are restricted to shallower waters (< 0.5 m), a threshold of 10 days is assumed to be conservative above which mortality can occur. The next threshold is up to 120% for which fish residing below 1 m depth are believed to survive for < 2 days. Fish mortality is more likely to occur after 2 days for water < 1 m deep. TDG level exceeding 120% are considered harmful to fish in all cases except for deep water regions (Fidler and Miller 1997; BC Hydro 2014). Based on these threshold levels, severity of each of the impacting factors can be ranked from low to high (Table 5.1). The assigned rank scores are utilized to evaluate a potential TDG event risk.

The factors affecting TDG risk, i.e. supersaturation level, depth and duration, are not independent and are implicitly interrelated with each other. For example, 120% saturation at 1 m depth poses more risk to fish than 130% at 3 m depth. Similarly 115% saturation exposure for more than 10 days can be riskier than short duration exposure to 120%. To account these effects, a ranking process is developed for overall TDG risk assessment based on the following relation:

$$TDG\ Risk = w_1 R_1 (w_2 R_2 + w_3 R_3) \qquad (5.7)$$

where R_1, R_2 and R_3 are the severity ranking scores for supersaturation level, water depth and exposure duration respectively and w_1, w_2 and w_3 are the corresponding weightage factor. Severity

rank scores (as outlined in Table 5.1) of each impacting factor is considered in Eq. (5.7) to obtain overall risk for a given TDG event. A TDG event is defined as a period of time when concentrations are above thresholds described in Table 5.1.

5.3 Case Study Region and Field Data

Over the past decade, there have been increased concerns regarding the possible effects of high TDG on fisheries resources in rivers within British Columbia. The Columbia River below Hugh L. Keenleyside Dam (HLK), which is also the outlet of Kootenay and Pend d'Oreille rivers regulated by the Brilliant and Waneta dams respectively, has been identified as having some of the highest TDG levels in the province (Bruce 2016). Spill operations in these facilities and their cumulative contributions in the river basin exceed Provincial and Federal water quality guideline (BCMOE 1997; CCME 1999) of 110% TDG, particularly during spring freshet and summer. The dams have been listed as 'Priority Facility' in BC Hydro's TDG Management Strategy (BC Hydro 2014) as the downstream river reaches inhabit a variety of fish species, including white sturgeon, mountain whitefish, rainbow trout, kokanee etc. (RL&L Environmental Services 2002). The domain of the system model for this study encompassed the Canadian portion of the transboundary reach of the Columbia River from the HLK Dam to the Canada-USA border and included lower reaches of the Kootenay and Pend d'Oreille rivers (Figure 5.2). The confluences are located 10.5 km and 55.6 km downstream of HLK respectively and divide the 56.6 km stretch of the Columbia River (from HLK to international border) into three hydraulically different reaches. The HLK Dam, with aid of the Brilliant and Waneta facilities, helps regulate the flow as per the Columbia River Treaty between Canada and the United States.

In the Columbia River System, the HLK Dam forms the lower-most of three hydroelectric projects on the Canadian portion of the river. This facility consists of eight low-level gates (denoted by HL1-8) located on either side of a four-bay spillway (HS1-4) with the generating station being positioned directly north of the dam. Flows are spilled through these outlets as per the Facility Operating Order depending on forebay elevation and head differential. For higher project heads, spillway bays 4 and 3 are used preferentially, followed by 2 and as a last resort 1. The low-level gates are opened in the order: 4-3-2-5-6-7-1-8, with the last two being only used for emergency. The run-of-the-river Brilliant Dam, located 2.8 km upstream from the confluence, is the furthest

downstream of six hydropower facilities on the Kootenay River. The facility consists of a powerhouse on the right bank, an adjacent gated spillway and a second powerhouse about 150 m downstream on the left bank. The spillway is an eight-bay, ogee-type structure with gates numbered (denoted by BS1-8) from the bay closest to the powerhouse. During spill operation, bay 8 is operated in order with 2, 3, 4 and 5. Once these gates are fully opened, bay 5 is operated in sequence with 7 and 6. Bay 1 is only used for emergency. The Waneta Dam is located on the Pend d'Oreille River about 0.5 km upstream of its confluence, and has a gated spillway and two powerhouse units. Both powerhouses draw water from the reservoir operated in hydraulic balance with the upstream Seven Mile Dam. There are ten more hydroelectric facilities on this river upstream (in U.S.). The ogee-type Waneta spillway consists of nine bays (WS1-9) with bay 1 located closest to the powerhouse. The priority sequence of spillway use is as follows: 2-3-4-5-7-8-9-6-1, where bays 4 and 5 are operated concurrently. Bay 6 is reserved for emergency operations while bay 1 is not used for reservoir management.

In response to predicted high flows during the 2011 freshet, a system-wide TDG monitoring was initiated in the Columbia River Basin around major hydroelectric facilities (Golder Associates 2011). Within the area of current study, continuous real-time TDG were measured at six different locations on the Columbia, Kootenay and Pend d'Oreille rivers from 27 May to 07 July. The monitoring stations were deployed in the forebay and tailrace of Brilliant Dam and Waneta Dam, as well as along the right banks of the Columbia River near Breakwater Island and Teck Water Quality Station located about 8.9 km and 56.4 km downstream of HLK Dam (Figure 5.2). Total gas pressure (TGP), barometric pressure (BP) and water temperature was recorded continuously at 15-minute intervals. In addition, TDG data were also collected from the U.S. Army Corps of Engineers at the CIBW station located about 3.5 km downstream from the international border on the Columbia River. Discharge and operations data of the individual dams were provided by BC Hydro and FortisBC. During the monitoring period, there was no spill in the HLK dam for most of the time. The spill through the Brilliant and Waneta dams varied from 1175-2423 m^3/s and 1556-3083 m^3/s respectively. The measured TDG at different locations in response to the spill operations is shown in Figure 5.3.

To obtain detailed description of TDG generation in individual dams, some dam specific data were collected for the Brilliant and Waneta dams (Table 5.2). For TDG evaluation below Brilliant Dam,

a series of predefined spill tests for individual bays were conducted on November 1997 (Aspen Applied Sciences 1998). During this survey, each of the spill bays was operated at a specified gate opening and the corresponding forebay and tailrace TDG were measured. TDG monitoring upstream and downstream of Waneta Dam was carried out through a series of measurements collected during 1995-1997 (RL& L Environmental Services 1997; Bruce 2016). The tailrace TDG was sampled at about 750 m downstream on the south bank of Columbia River. Although the site was within the confluence area, it was sufficiently close to the dam to consider TDG concentrations representative of spill operations.

5.4 Results and Discussion

Due to low power demands and above-average snowpack in headwaters of the Columbia, Kootenay and Pend d'Oreille rivers, the hydropower facilities experienced higher than usual discharges during 2011 freshet (Golder Associates 2011). High spills through non-power release (NPR) structures, like spillways and low-level outlets, resulted in high TDG throughout the Canadian portion of the Columbia River Basin. Over the monitoring period, there was little or no spill in the HLK Dam and flows from the Arrow Reservoir were passed through the generating station. As a result, TDG levels at 8.9 km downstream in the Columbia River (upstream of Kootenay confluence) were low and varied from 104.7-109.0% (Figure 5.3). Within the Kootenay River, the TDG of water released from Kootenay Lake increased due to the cumulative impact of series of dams. The forebay TDG of the Brilliant Dam varied from 112.8-123.6% due to operation of five more facilities upstream in the river. Furthermore, an increase in TDG occurs downstream of Brilliant Dam depending on the spill rate and proportion of total flow passed as generation discharge through the two power plants. TDG in the dam tailrace monitored at about 1.5 km downstream on the left bank varied from 120.6-130.6%.

In the Pend d'Oreille River, water entering Canada from the United States was highly supersaturated due to spill operations at upstream projects and TDG concentrations reached as high as 150% in the Seven Mile Reservoir (Golder Associates 2011). Due to flip-bucket design of spillways, degassing was observed in the Seven Mile Dam (refer to Chapter 4) that resulted in TDG levels from 127.1-135.8% in the Waneta Dam forebay. At the Columbia-Pend d'Oreille confluence downstream of Waneta Dam, the TDG levels ranged between 126.2 and 139.1%.

During the monitoring period, TDG at the CIBW station on the Columbia River (about 3.5 km downstream of international border) varied from 125.0-134.6%.

As shown in Figure 5.3, the tailrace TDG of individual dams varied depending on the spill rate. Considering spill rate, gate operation, powerhouse releases and total flows at the Brilliant and Waneta dams, four steady-state operational conditions were identified for the present study. Details of these conditions are outlined in Table 5.3.

5.4.1 TDG Generation at Individual Facilities

TDG measurements are usually carried out in a downstream section where spill and generation discharges contribute to the overall concentration. Since direct measurement of spilled water is not possible, it is necessary to develop predictive TDG generation models specific to each of the facilities. Previously some empirical models were developed for the HLK, Brilliant and Waneta dams (Bruce 2016). However, a mechanistic approach based on Eqs. (5.1) and (5.3) incorporating different physical processes was utilized to develop TDG models that are not only meaningful, but also predict the concentrations beyond the range of model inputs. The α and A coefficients of Eq. (5.3) were estimated by fitting the TDG measurements conducted at the Brilliant Dam in 1997 and at the Waneta Dam during 1995-1997 period (refer to Table 5.2). This resulted in facility-specific TDG generation curves for the Columbia River hydropower system (Figure 5.4). In general, TDG concentrations in these facilities increased with spill rate q which was consistent with previous studies (Geldert et al. 1998; Urban et al. 2008; Politano et al. 2017).

The Brilliant Dam spillway bays are ogee shaped with chute bottoms ending in bases with little or no inclination (Bruce 2016). The geometry and flow pattern is different for each of the bays and produce different levels of TDG (Figure 5.4b). The estimated α and A coefficients for bays 1-7 varied from 0.0024-0.0058 and 7.81-13.14 respectively (Table 5.4). These coefficients were not significantly different between the bays and the corresponding predicted TDG provided excellent agreement with the 1997 individual gates tests (overall $R^2 = 0.90$). In terms of TDG generation, bays 1-3 are the major contributor with gate 1 being the highest followed by 2 and 3. Bays 1 and 2 have similar chute profile with relatively long base and the spilled water plunges into the pool soon after leaving the base. This increases the depth and residence time of bubbles as well as void

ratio (with comparatively low A values of 9.58 and 8.78) resulting in higher TDG concentrations. Bay 3 has a deflector pad at the end with shorter base length. Bays 4 and 5 had similar TDG responses to unit discharge q which have bases located at deeper elevation with shorter plunging depth. This results in less air entrainment and lower void ratio with higher A coefficients of 10.76 and 12.55 respectively. Compared to these bays, TDG generation in bay 6 is higher. Bay 7 produces the least amount of TDG (A = 13.14) among all of the gates. Bay 8 spills onto bedrock benches and does not contribute to additional TDG generation.

The TDG responses of each gate of the Brilliant Dam is independent of each other and the concentration corresponding to a given spill volume (C_{spill}) was obtained by assuming complete mixing between individual bays for the four conditions of 2011 case study (as outlined in Table 5.3). For condition 1, bay 2 was fully open while gates 3 and 8 were partially opened in sync (according to facility operating order) which generated TDG of 126.0%. To accommodate additional spill, bays 2-5 and 8 were operated for conditions 2 and 3 that resulted 130.3 and 130.0% TDG respectively. Although spill rate for condition 4 was comparatively lower than the previous two, C_{spill} was 130.0% for the operation of gates 2-4 and 8 since TDG responses are similar for bays 4 and 5 (Figure 5.4b).

TDG measurements in the Waneta Dam during 1995-1997 periods were carried out for multiple gate operations and data for individual gates were not available. Therefore, TDG generation curves for this dam were developed considering single bay, two bays, four bays and six bays operation based on facility operating sequence (Figure 5.4c). For these cases, the unit discharge was considered by total spill divided by width of the operating bays, and the model coefficients, α and A, varied from 0.0017-0.0052 and 12.22-25.59 respectively (Table 5.4). The predicted TDG agreed reasonably well with the measurements with R^2 = 0.96. Spillway bays 2-4 discharge water into tailrace via a shallow-angled flip bucket structure and generates similar TDG responses for single-bay (WS 2) and two-bays (WS 2, 3) operation. Bays 5 and 6 have deeper chute bottom with a deflector pad at the end. The combined operation of four-bays (WS 2, 3, 4, 5) produces relatively higher TDG due to deeper plunge depth and increased void ratio (A = 12.22). The highest TDG generation occurs for six-bay operation (WS 2-5, 7, 8) when additional spill through bays 7 and 8 merge onto bays 5 and 6 due to angled abutment wall. Bays 1, 6 and 9 are used for emergency purpose and were not considered here. For conditions 1 and 4, TDG generation for the operation

of four-bays was 133.2 and 133.8% respectively. With higher spills of conditions 2 and 3, C_{spill} was 136.1 and 135.8% respectively for the operation of six-bays.

For the case conditions considered in this study, there was no spill at the HLK Dam. In case of spill operations, TDG generation can be estimated by the predictive relationships of Bruce (2016) (Figure 5.4a). Since there was no spill and the forebay TDG remains unchanged while passing through the generation units, the measured TDG at 8.9 km was assumed as the forebay TDG at HLK Dam for this study.

5.4.2 Estimation of Mixing and Dissipation Rates

TDG generated at a given facility can vary across and along the river while transporting downstream as a result of mixing with generation flow and tributary inflow and its dissipation across the water-atmosphere interface. The two-dimensional distribution of TDG, as described by Eq. (5.4), requires reliable estimates of mixing and dissipation rates for variable hydraulic and dam operational conditions. Based on extensive field work in the Columbia River, Kamal et al. (2019) showed that the factor of turbulent diffusion (D) and dissipation rate (k) varied from 110.9-286.0 m^5/s^2 and 0.002-0.031 hr^{-1} respectively for different operational scenarios at the HLK and Brilliant dams. A number of factors affect the mixing rates, for example, river discharge, sinuosity, depth, width, shear velocity etc. (Zhang and Zhu 2011). Rutherford (1994) summarized 53 studies in 23 rivers and found that the transverse mixing coefficient E_t increased with Q. Analysis of this dataset indicated that the non-dimensional term E_t/BU remains approximately consistent with Q for deep rivers with $B/H < 50$ (Figure 5.5). Considering E_t/BU is constant and using the field observations of Kamal et al. (2019), the non-dimensional form of Eq. (5.5) was utilized to develop following generalized expression for the Columbia River system:

$$D = 0.0026\psi Q^2/B \qquad (5.8)$$

Depth and velocity are the key factors affecting TDG dissipation in rivers (Li et al. 2015; Kamal et al. 2019) and the rate of dissipation, in general, increases with U/H (Figure 5.6). This rate can be estimated using the form of Eq. (5.6) similar to typical reaeration models. From dimensional analysis, Lau (1972) formulated a relation for non-dimensional transfer coefficient as $kH/U \sim (U^*/U)^3$ where U^* is the shear velocity. Based on the shear velocity relations and

Manning's equation, U^*/U is inversely proportional to the one-sixth power of depth. Using this concept along with the field estimates of Kamal et al. (2019), the TDG dissipation rate in the Columbia River system was estimated from the following formulation:

$$k = 0.2625U/H^{1.5} \qquad (5.9)$$

which resulted in the exponents a = 1.0 and b = 1.5 in Eq. (5.6). The proportionality constant in Eq. (5.9) was obtained for water temperature at 15 ºC and the corresponding value of k can be corrected for different temperatures (Bowie et al. 1985).

The river discharge in the three reaches of the Columbia River (separated by the Kootenay and Pend d'Oreille confluences) varied for conditions 1-4 depending on the flow releases of individual dams. Hydraulic analyses in these reaches were carried out using Manning's equation and continuity equation based on the field measurements in 2016 (Kamal et al. 2019). The 2.8 km and 0.5 km sections between each of the Brilliant and the Waneta facilities and their respective confluences also form hydraulically different reaches. The estimated mixing and dissipation rates of TDG for different conditions in these reaches are outlined in Table 5.5.

5.4.3 TDG Distribution in the River System

Considering multiple streamtubes representing spill and generation flows in the HLK, Brilliant and Waneta Dams, Eq. (5.4) was used to estimate TDG distribution in the Columbia River system. Superposition principle was applied to obtain the combined distribution. Also image sources were included to account the effect of banks. Within the confluence, concentrations were estimated based on linear approximation between multiple streamtubes of the converging rivers. This streamtube based model accounted channel irregularities across a section (Yotsukura and Sayre 1976) and resulted in concentration-cumulative discharge (C, $\hat{q}$) plots that provided bank-to-bank ($\hat{q}$ = 0 at right bank and $\hat{q} = Q$ at left bank) TDG variation at different spatial location (Figure 5.7). As shown in the figure, the spilled high TDG waters in the Brilliant and Waneta dams (represented by sections K_1.2 km and P_0.2 km respectively) and their mixing with generation flows created differential concentrations across the Kootenay and Pend d'Oreille rivers. For a given condition, the combined operation of these facilities along with the HLK dam resulted in cumulative effect of TDG supersaturation in the main stem Columbia River. The transverse variation in TDG was

particularly high downstream of the confluences (sections 10.7 km and 56.4 km respectively). Due to concurrent mixing within waters and dissipation across the air-water interface, TDG concentrations decreased in the downstream river and eventually became fully mixed. As shown in Figure 5.8, the predicted TDG concentrations at the dam tailraces and downstream river agreed well with the 2011 field measurements. The measurements were taken near the river banks, and the model was able to capture field conditions considering the transverse variations. The absolute error for the prediction of the four cases (conditions 1-4) varied from 0.14-2.23%.

From the analysis of cumulative discharge distribution of 105 cross-sections considered in this study, the modeled (x, $\hat{q}$) coordinates were transformed into UTM projection system to obtain spatial mapping of TDG for different case conditions (Figure 5.9). The TDG levels below the HLK Dam were less than 110% for conditions 1-4 since there was no spill during these periods. For comparatively low flows (Q = 870-1019 m^3/s corresponding powerhouse release), the dissipation rate was slow (k = 0.002 hr^{-1}) and TDG concentrations remained unchanged in the Columbia River reach (reach 1) upstream of the Kootenay confluence. For spill operations at the Brilliant Dam, the generated TDG exceeded 125% for all four conditions (refer to Table 5.3) which affects the 2.8 km stretch of Kootenay River above the confluence. The spillway of this dam is located between two powerhouse units (Figure 5.2). Such orientation created distinct plume of high TDG water in the mid-channel for conditions 1 and 4 (Figures 5.9a and 5.9d) when both powerhouses were operational, and along the left bank for conditions 2 and 3 (Figures 5.9b and 5.9c) due to operation of generating station 1 alone.

Downstream of the confluence, TDG distribution in reach 2 of the Columbia River was affected by the two converging rivers of different concentration levels. The maximum TDG levels in this reach were lower than the Brilliant Dam tailrace due to mixing and dilution from the upstream river. At 10.7 km, the concentrations were higher along the left bank (corresponding to Brilliant Dam flow as shown in Figure 5.7), with maximum TDG of 122.3, 129.5, 129.2 and 125.8% for conditions 1-4 respectively. As the flow transported downstream, TDG levels as well as its transverse concentration gradient reduced as a result of mixing and dissipation (Figure 5.9). Due to combined inflow from the HLK and Brilliant dams, the river discharge varied from 3277-3869 m^3/s for conditions 1-4 and the corresponding factor of turbulent diffusion ranged from 192.5-261.0 m^5/s^2 resulting in dilution of high TDG water. Complete mixing within this reach was

achieved at 29.9-32.4 km downstream from the confluence. Further downstream, change in concentration was only associated with TDG dissipation through interfacial gas exchange. The reach is shallower with high-velocity flows compared to the other river segments (refer to Table 5.5) and the dissipation rates were higher for different conditions. For condition 1, the dissipation rate was 0.030 hr^{-1} for a mean depth and velocity of 6.49 m and 1.91 m/s respectively. The depth increased to 7.05 m for conditions 2 and 3 resulting in k = 0.030 hr^{-1}. This rate was 0.029 hr^{-1} for condition 4. The TDG at 55.6 km (upstream of Pend d'Oreille confluence) was 114.8-118.7% for these conditions resulting in 7.5-10.9% drop in concentrations compared to initial high TDG conditions in reach 2.

The Waneta Dam forebay water was highly supersaturated during the periods of conditions 1-4 (Table 5.3). Release of this water through the powerhouse units (both located on the right bank) as well as dissolved gas generation by spillways (situated on the left bank) created high TDG water plume exceeding 130% saturation within the short 0.5 km tailrace stretch at the Pend d'Oreille River (Figure 5.9). This plume continued downstream of the confluence along the left bank of the Columbia River (reach 3). The combined inflow of high TDG waters from the upstream Columbia and Pend d'Oreille rivers resulted supersaturated state at the international border with marked difference in concentrations between the banks. Although discharge in reach 3 was higher than the upstream reaches (Q = 6402-7494 m^3/s), limited mixing and dissipation occurred within the short stretch between the confluence and international border. For conditions 1-4, maximum TDG along the left bank varied from 133.1-136.0% while the right bank concentrations remained similar to the TDG upstream of the confluence. Similar variation was observed at the CIBW station, located about 3.4 km downstream from the border, with maximum TDGs of 130.1, 133.0, 132.5 and 130.9% for the four conditions respectively.

5.4.4 Risk Assessment for Different Conditions

Based on the TDG management thresholds and severity of the impacting factors (Table 5.1), a ranking process was developed to address cumulative TDG risks from the combined operation of hydropower facilities in the Columbia River system. This process involved estimation of risk scores from Eq. (5.7) considering the severity rank of supersaturation level, water depth and duration of exposure for a given TDG event. The factors were given equal weightage in the

equation ($w_1 = w_2 = w_3 = 1$) and resulted in a total of twenty eight possible combinations with risk scores ranging from 0 (TDG ≤ 110%) to 18 (TDG > 120%, depth < 0.5 m, duration > 10 days). These scores were rescaled and normalized with respect to the maximum value over a 0 to 1 range and grouped into four broadly defined risk categories: None (score = 0), Low (0 to 0.33), Moderate (0.33 to 0.5) and High (≥ 0.5). This grouping procedure was consistent with BC Hydro's TDG Management Strategy.

During the periods of the four case conditions, approximately 22% area of the Columbia River system had TDG concentrations below 110% as a result of no spill in the HLK Dam. This corresponded to the no risk zone for conditions 1-4, particularly in reach 1 upstream of the Kootenay confluence (Figure 10). TDG risk below this reach varied depending on the severity of the impacting factors. For condition 1 (duration 4 days), about 63% and 8% area was exposed to TDG thresholds of 115-120% and greater than 120% respectively. Fish can compensate for the effect of supersaturated conditions by moving to a greater depth. The Columbia River system is typically deep with 87% area deeper than 2 m. However, about 7% of the wetted habitat was < 1 m deep for this condition, particularly near the river banks where fish are more susceptible to high TDGs. As a result, 52% and 17% of the river were found to be in the moderate and high risk zones respectively (Figure 5.10a). Only 9% area was in the low risk zone for this condition. The risk map also identified local high risk zones where water depths were shallow.

TDG risk maps for conditions 2 and 3 produced similar spatial distribution pattern (Figures 5.10b and 5.10c) which were slightly different from their respective concentration maps. The latter shows supersaturation level for a given TDG event while the former accounts compensation depth and exposure duration as additional factors. For example, TDG generation at the Brilliant and Waneta dams was comparatively high for these conditions (refer to Table 5.3) and about 41% and 43% of the river was subjected to supersaturation greater than 120% respectively. However due to lack of depth compensation, about 45% and 47% area was exposed to high risk correspondingly. As a result of high TDG generation with moderately long exposure duration (2.5 and 2.8 days respectively), approximately 77% of the basin was at moderate to high risk of TDG-related exposure for conditions 2 and 3. The extent of such risk stretched from the Kootenay confluence to the international border. Spill operations at the Columbia facilities generated similar TDG levels for condition 4. About 61% river area had TDG in the range of 115-120% while 16% area exceeded

this threshold level. However, 52% area was at low risk zone due to short exposure duration of 1.7 days for this condition (Figure 5.10d). In this region, the gas levels are unlikely to produce GBT symptoms because of limited duration of exposure. Approximately 24% and 2% of the river system were found to be in the moderate and high risk zones respectively.

As expected TDG risk was high close to each facility during spill events and declined progressively downstream. The TDG effects from Brilliant Dam spills were attenuated below the confluence because of dilution with the Columbia River. Due to seasonal differences in the timing of spills between Brilliant and HLK dams, the mixture of flows usually reduces the risk downstream of the confluence (i.e., typically one has low TDG). Immediately below the confluence, the left bank generally had higher TDG risk during Brilliant Dam spills than the right bank which corresponded to HLK inflow (Figure 5.10). Thus, impacts on fish due to high TDG are not expected to be similar in both banks. The Columbia River reaches upstream and downstream of the Kootenay confluence have been identified as high use areas for rainbow trout, white sturgeon and kokanee. In the stretch between Kootenay and Pend d'Oreille confluences, TDG concentrations reduced due to mixing and dissipation and the corresponding risk varied spatially from low to high depending on the operational condition, compensation by depth of fish and duration. The fisheries value in the short tailrace of Waneta Dam is limited. Of greater concern are the fish present at the Columbia-Pend d'Oreille confluence and downstream river. The confluence is designated as Critical Habitat in relation to the Species at Risk Act (SARA) for the population of white sturgeon (RL& L Environmental Services 2002). Since the converging rivers were not immediately mixed at the confluence, long sections of river bank were exposed to high TDG risk while the opposite bank remained unaffected.

5.5 Conclusions

This study presented a risk assessment framework and decision support system for real-time management of TDG in complex hydropower system and its impact on downstream fish habitat. The framework included analytical modeling of the generation of elevated TDG concentrations in individual dam spillways, and its mixing with powerhouse releases and tributary inflow as well as dissipation across the free surface interface. The mechanistic TDG generation models comprised the main processes controlling gas transfer and had predictive capabilities for wide range of

operational conditions. To track TDG concentrations in downstream rivers, physical relationships describing mixing and dissipation were developed based on field observations. The facility specific predictive TDG models, the generalized mixing and dissipation relationships and the streamtube method based transport model were integrated into a single analytical platform to develop a two-dimensional TDG distribution model for the Columbia River system, which is not only physically meaningful but provides a rapid and accurate estimations for impact assessment. This phase of model development was limited to the effects of individual spill events and required forebay concentrations as model input. To test the functionality of this integrated model, system-wide TDG monitoring data was evaluated successfully for different case conditions involving multiple dam operations.

The cumulative contributions of Columbia River operators, particularly during periods of high inflows or soft energy markets, resulted in high TDG supersaturation which can risk impacting fish populations. Due to combined effects of the HLK, Brilliant and Waneta dams, TDG concentrations near the individual facilities, in the main-stem Colombia River and its confluences of the tributaries (i.e. Kooteany and Pend d'Oreille rivers) and at the international border often exceeded the allowable criterion of 110%. The system-wide TDG mapping based on the modeling approach provided spatial distribution for different spill incidents and aided identification of potential risk-zones in the habitat ecosystem. However besides supersaturation level, the severity of exposure and risk of GBT varies by fish species and life stage, depth of compensation, duration of exposure, past exposure to high TDG etc. Based on the TDG management thresholds and severity of the impacting factors, a ranking process was developed to address cumulative TDG risks from the combined operation of hydropower facilities in the system. This process involved estimation of risk scores considering the severity rank of supersaturation level, water depth and duration of exposure for a given TDG event. These scores were rescaled and grouped into four broadly defined risk categories: None, Low, Moderate and High, which resulted in a TDG risk assessment framework that identifies the potential risk zones in the Columbia River system. For the case conditions considered in this study, about 22% area of the river basin were found to be in the no risk zone. Approximately 52%, 32%, 30% and 24% area was at moderate risk, while 17%, 45%, 47% and 2% of the river system was exposed to high risk for conditions 1-4 respectively. The overall pattern and relative ranking of severity due to the effect of supersaturation level, depth compensation and exposure duration were reasonably represented by the framework, and provided

a broader perspective on TDG risk in the Columbia River ecosystem. Habitat use requirements for different life stages for each species can be incorporated in this framework to obtain more detailed risk assessment.

From an operational perspective, hydropower operators need reliable tools to assess system-wide TDG risk during spill events. The integrated framework presented here for developing standalone TDG concentration and risk maps can help inform the operators to manage environmental regulations in compliance with water quality criterion, and to distinguish potential risk zones that require additional monitoring and administration for habitat protection. It can be utilized to revise facility operating order and spill management scenarios by incorporating TDG-related constraints to avoid or minimize negative ecological consequences. Furthermore, trade-off assessments among water management, economic consideration, power demand and environmental requirements can be carried out in accordance with policy objectives. The integrated framework would provide hydropower operators and system coordinators a theoretical and quantitative platform to identify a set of feasible, 'least risk' TDG management alternatives and strategies and meet their own social and environmental targets, thereby enabling them to generate hydropower in a sustainable manner.

Table 5.1: Summary of criteria and severity ranks for TDF risk rating

Severity rank (R)	TDG threshold	Water depth	Exposure duration
0	TDG ≤ 110%	-	-
1	110% < TDG ≤ 115%	> 1.0 m	< 2 days
2	115% < TDG ≤ 120%	0.5 – 1.0 m	2 – 10 days
3	TDG > 120%	< 0.5 m	> 10 days

Table 5.2: Summary of data collected for the Columbia River system study

Dataset	Period	Spill rate (m^3/s)	Reference
System-wide TDG monitoring	27 May - 07 July, 2011	HLK: 0-454 Brilliant: 1175-2423 Waneta: 1556-3083	Golder Associates (2011)
Brilliant Dam TDG tests for individual spill bays	November 1997	130-675	Aspen Applied Sciences (1998)
Waneta Dam TDG measurements	31 May - 08 July, 1995 13 March - 04 June, 1996 08 June - 27 August, 1997	193-2992	RL& L Environmental Services (1997)

Table 5.3: Operational scenarios for the 2011 field test conditions

Cond.	Period	Duration (days)	Facility	Gate operation	Flow releases (m^3/s)		TDG (%)	
					Spill	Generation	C_u	C_{spill}
1	31 May – 04 Jun	4.0	HLK	-	-	870	106.9	-
			Brilliant	BS 2,3,8	1336	1072	117.8	126.0
			Waneta	WS 2-5	2082	1043	132.6	133.2
2	14 Jun – 17 Jun	2.5	HLK	-	-	1019	105.8	-
			Brilliant	BS 2-5,8	2296	551	120.2	130.3
			Waneta	WS 2-5,7-8	2603	1024	134.5	136.1
3	23 Jun – 26 Jun	2.8	HLK	-	-	1001	106.4	-
			Brilliant	BS 2-5,8	2320	548	119.8	130.0
			Waneta	WS 2-5,7-8	2496	1062	133.4	135.8
4	02 Jul – 04 Jul	1.7	HLK	-	-	1014	107.8	-
			Brilliant	BS 2-4,8	1606	1014	119.3	130.0
			Waneta	WS 2-5	2361	1019	133.0	133.8

Table 5.4: Estimated α and A coefficients of Eq. (5.3) for the Brilliant and Waneta dams

Coefficient	Brilliant Dam							
	Bay 1	Bay 2	Bay 3	Bay 4	Bay 5	Bay 6	Bay 7	Bay 8
α	0.0058	0.0039	0.0025	0.0024	0.0040	0.0051	0.0058	-
A	9.58	8.78	7.81	10.76	12.55	10.27	13.14	-
	Waneta Dam							
	Single bay		Two bays		Four bays		Six bays	
α	0.0017		0.0021		0.0027		0.0052	
A	12.56		21.84		12.22		25.59	

Table 5.5: Hydraulic properties at different reaches of the Columbia River system

Reach	Condition	Q (m^3/s)	H (m)	U (m/s)	D (m^5/s^2)	k (hr^{-1})
Columbia River – reach 1	1	870	10.09	0.26	-	0.002
	2	1019	11.10	0.28	-	0.002
	3	1001	10.98	0.28	-	0.002
	4	1014	11.07	0.28	-	0.002
Kootenay River	1	2407	7.20	1.53	157.5	0.021
	2	2847	7.96	1.63	220.4	0.019
	3	2868	8.00	1.64	223.6	0.019
	4	2621	7.58	1.58	186.7	0.020
Columbia River – reach 2	1	3277	6.49	1.91	192.5	0.030
	2	3866	7.05	2.02	260.6	0.028
	3	3869	7.05	2.02	261.0	0.028
	4	3635	6.84	1.98	232.8	0.029
Pend d'Oreille River	1	3125	13.50	2.31	462.1	0.012
	2	3627	14.77	2.46	622.4	0.011
	3	3557	14.59	2.44	598.6	0.011
	4	3380	14.15	2.39	540.5	0.012
Columbia River – reach 3	1	6402	9.91	1.73	519.2	0.015
	2	7494	10.77	1.83	698.5	0.014
	3	7427	10.72	1.82	686.9	0.014
	4	7015	10.40	1.79	617.0	0.014

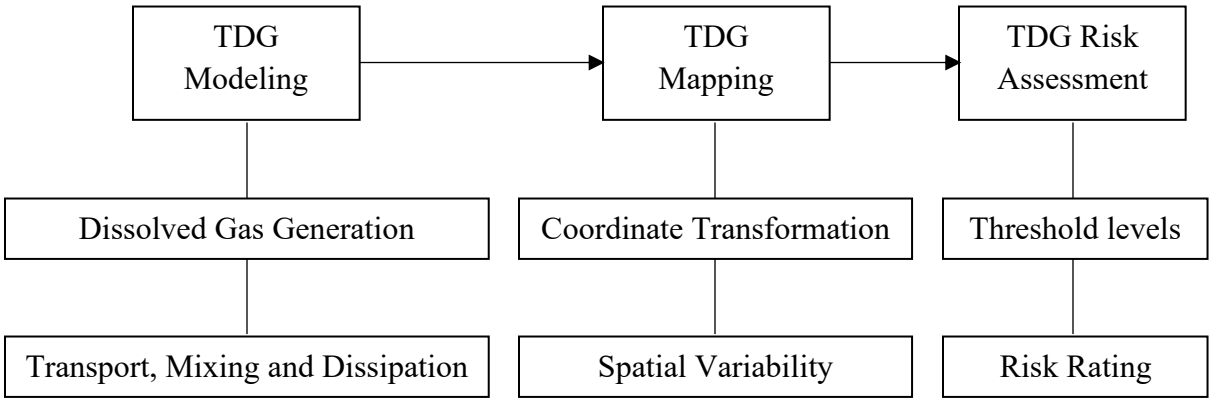

Figure 5.1: Diagram of TDG risk assessment framework

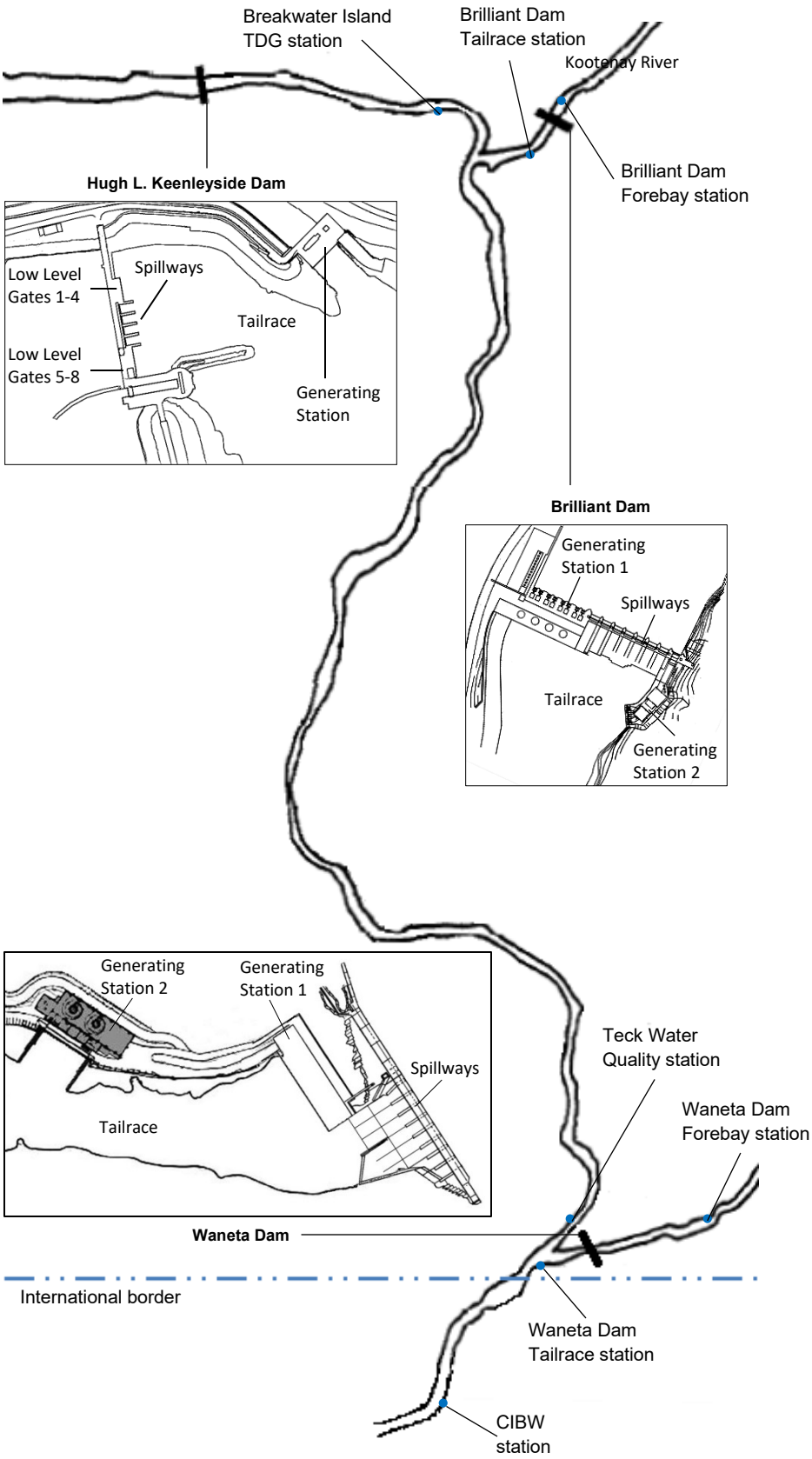

Figure 5.2: Lower Columbia River hydropower system with measurement locations

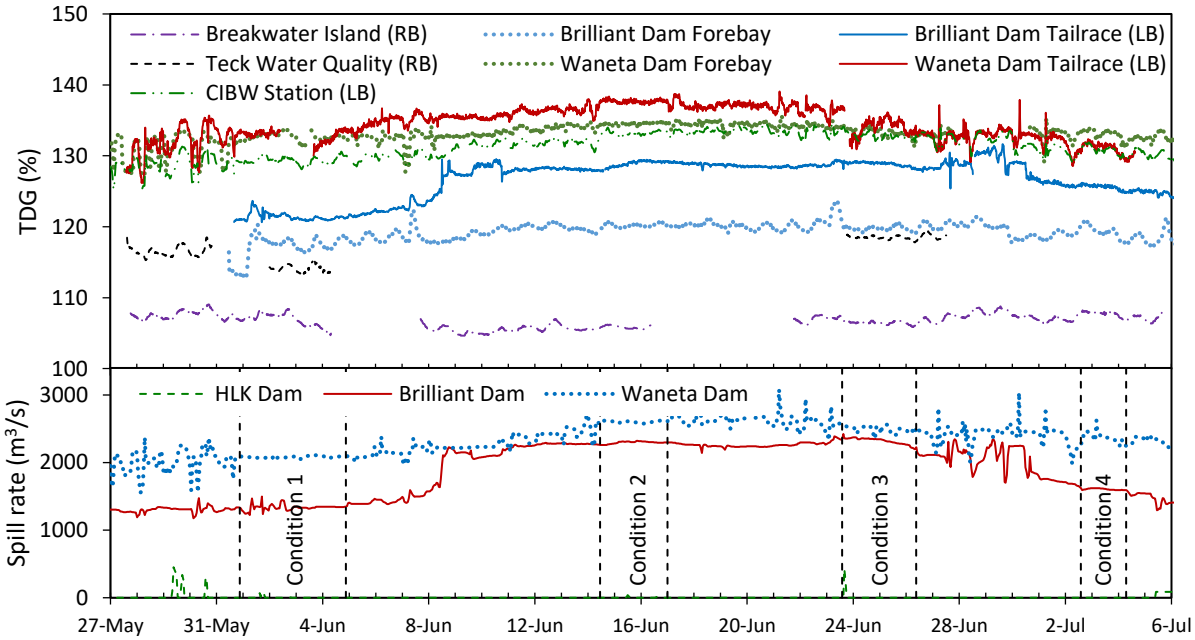

Figure 5.3: Measured TDG at different locations during 2011 spill event

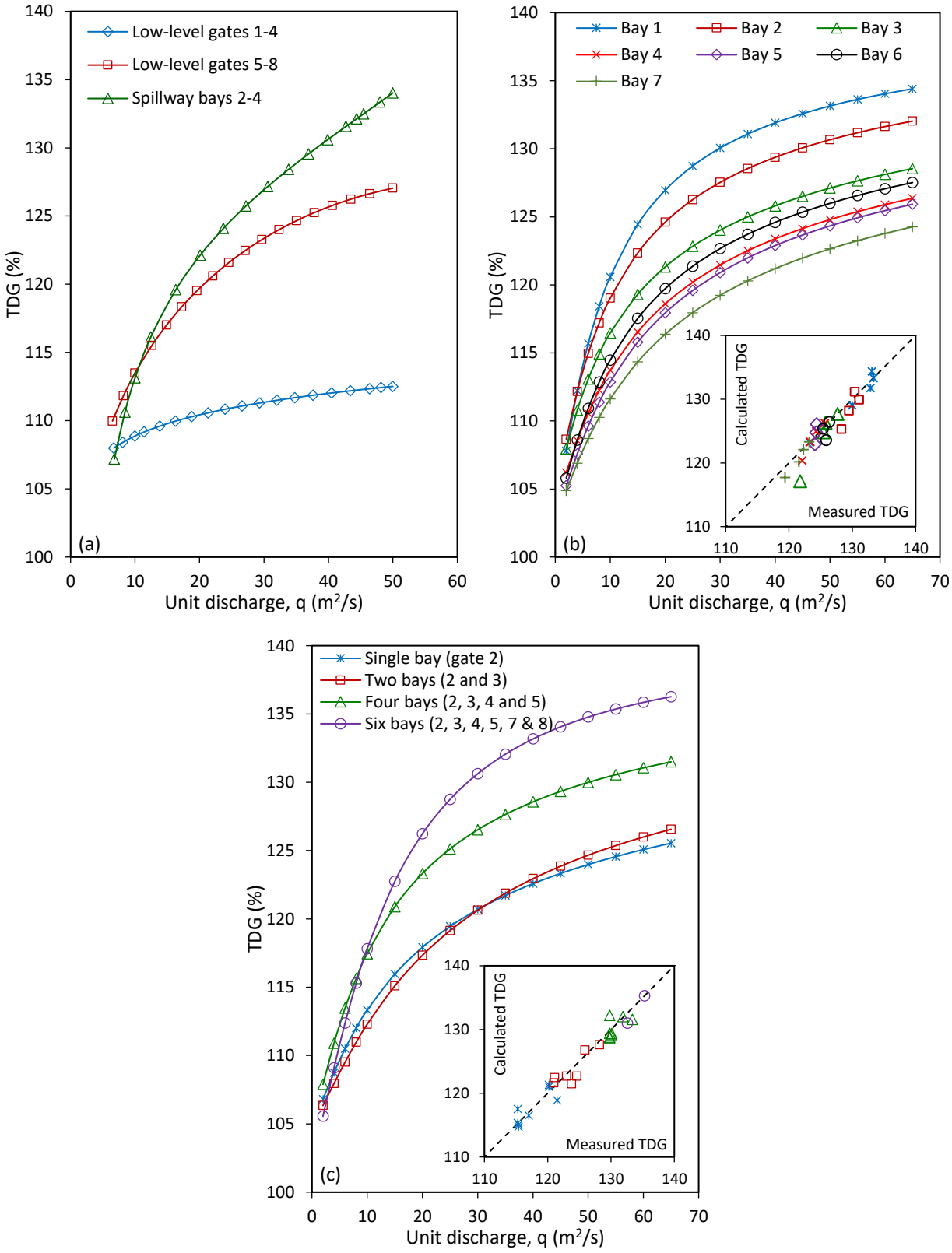

Figure 5.4: TDG generation curves for the (a) HLK dam, (b) Brilliant Dam and (c) Waneta Dam. Inset of (b) and (c) shows the comparison between measured and predicted TDG using Eq. (5.3)

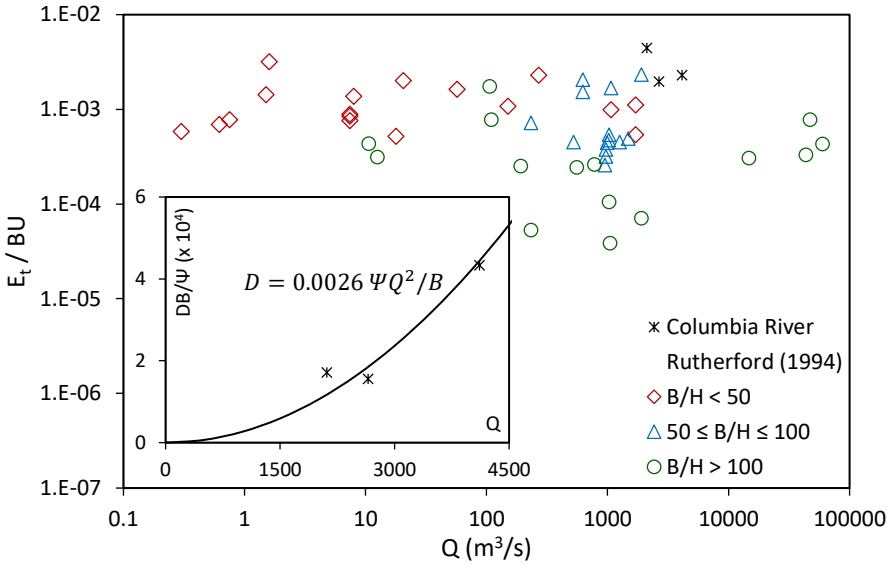

Figure 5.5: Estimation of factor of diffusion

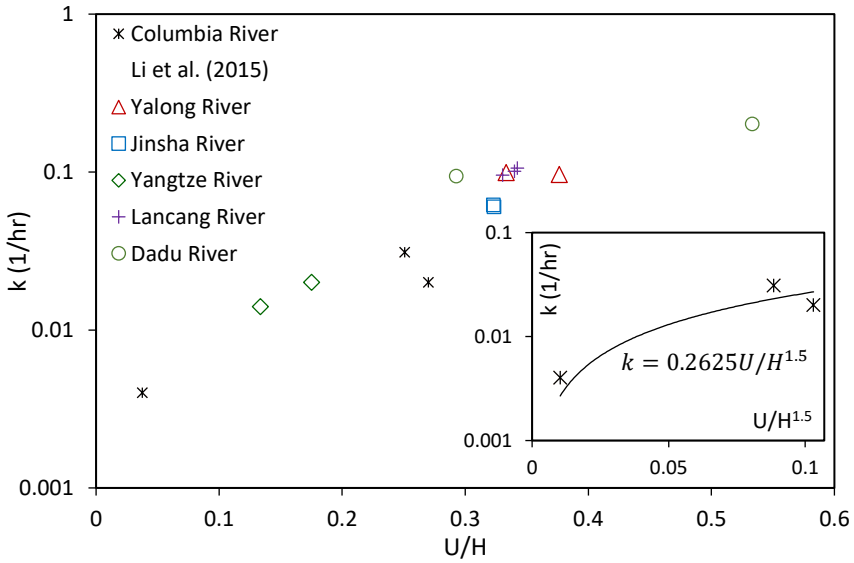

Figure 5.6: Estimation of TDG dissipation rate

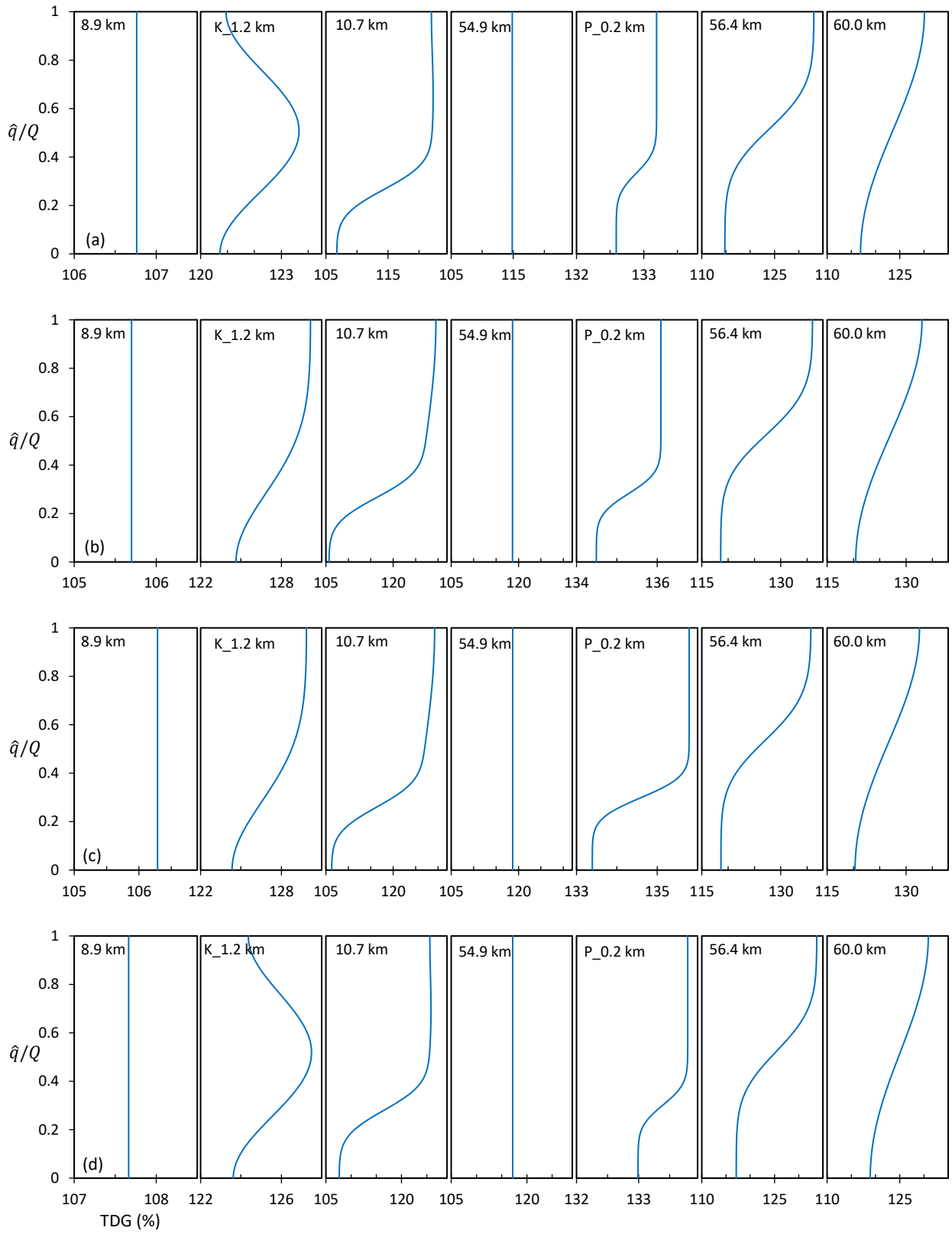

Figure 5.7: Concentration-cumulative discharge (C-$\hat{q}$) distribution of TDG in the Columbia River system for conditions 1-4

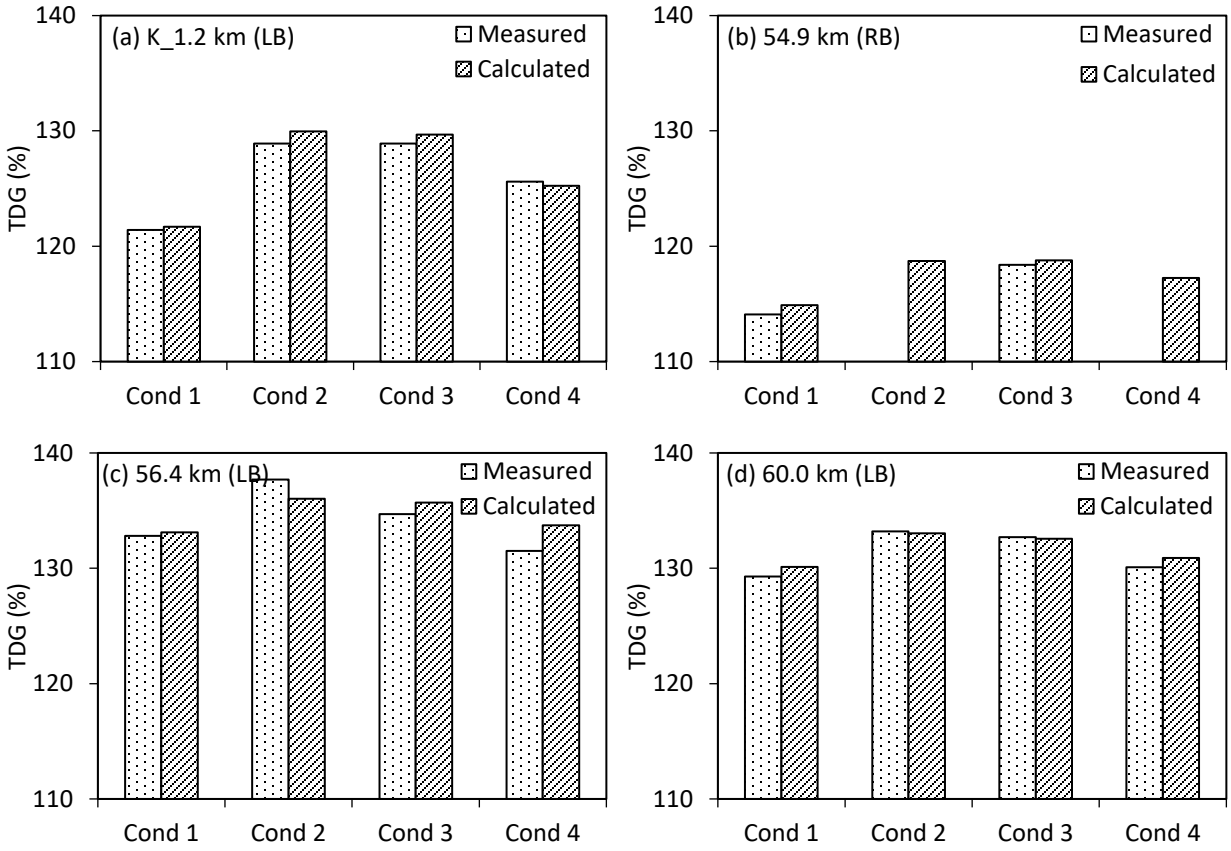

Figure 5.8: Comparison between measured and predicted TDG at different locations

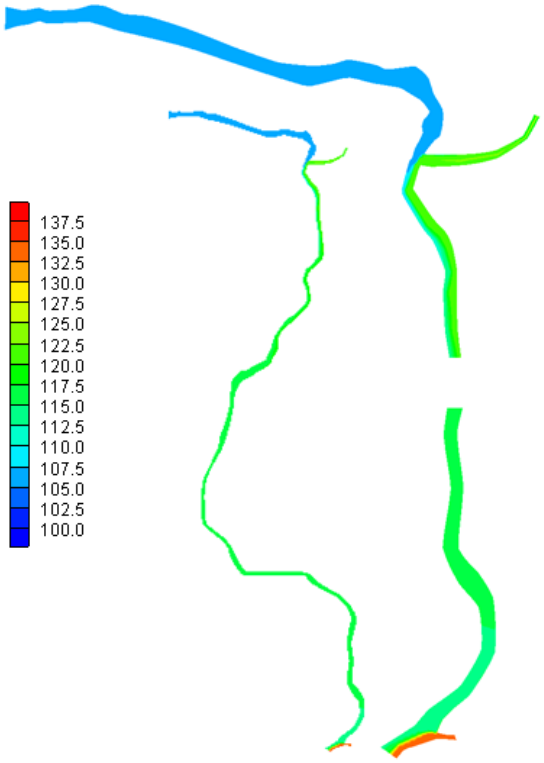

(a) Condition 1

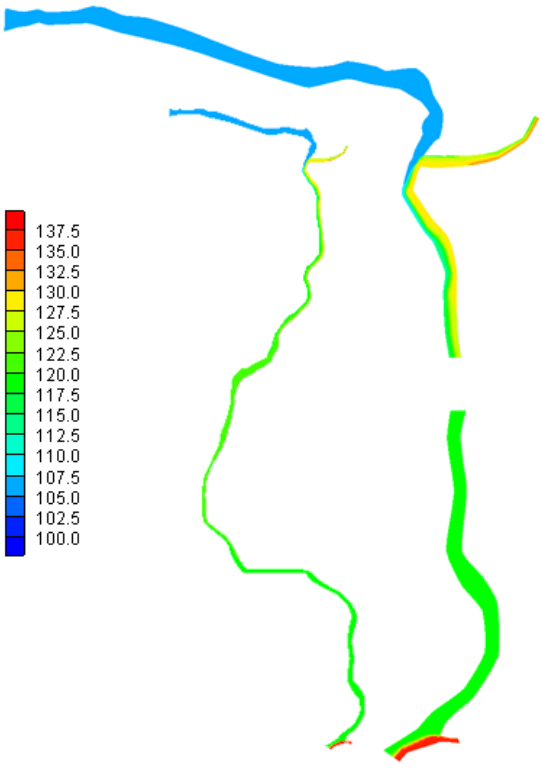

(b) Condition 2

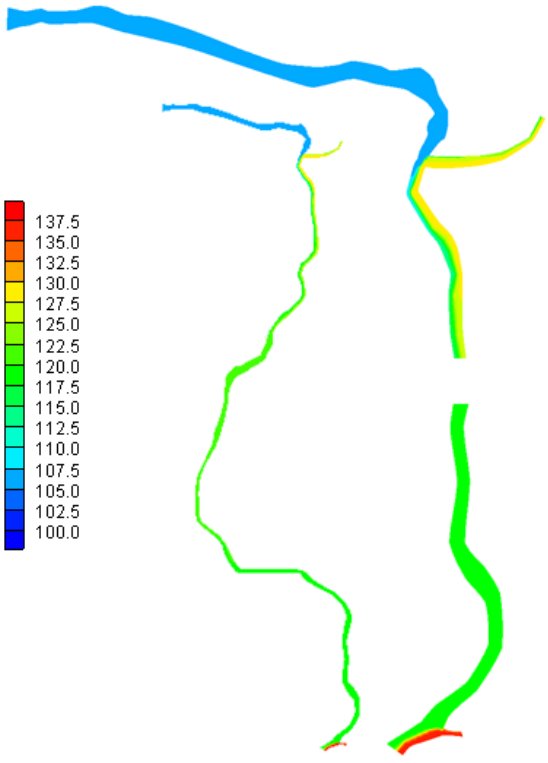

(c) Condition 3

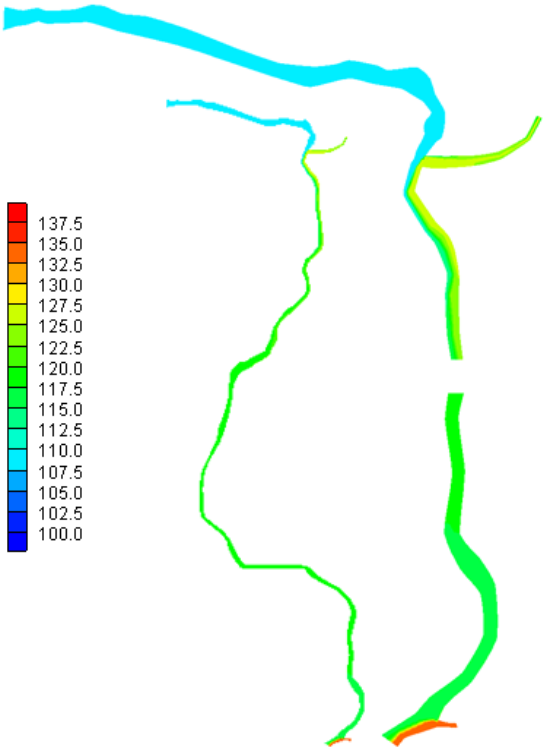

(d) Condition 4

Figure 5.9: TDG concentration maps for conditions 1-4

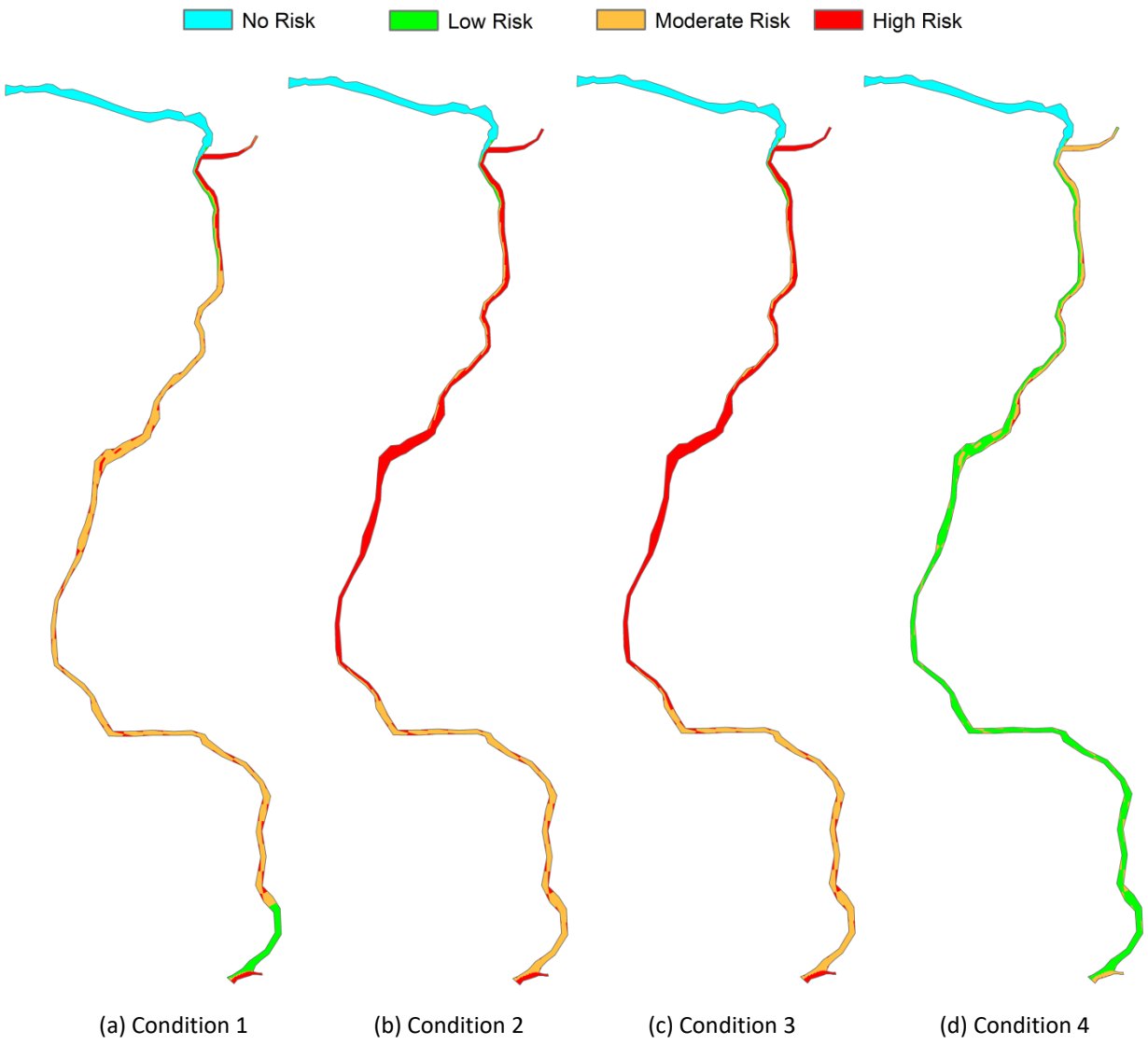

Figure 5.10: TDG risk maps for conditions 1-4

CHAPTER 6

Conclusions and Recommendations

6.1 General Conclusions

Total dissolved gas (TDG) supersaturation in hydropower facilities has been recognized as an environmental issue in different regions of the world and gaining attention over the years by both operators and regulators. This thesis studied three important aspects on supersaturation problem in hydropower system: (1) the transfer of total dissolved gas in different regions of a spillway, (2) its dissipation while transporting and mixing in riverine environment and (3) the cumulative distribution and risk on fish due to combined operation of multiple facilities in a complex river system. Following are the general conclusions for the study:

1. The dissipation rate of total dissolved gases in regulated river was estimated from field measurements and analytical modeling of transverse mixing between spill and generation flows as well as tributary inflow. This modeling technique can be advantageous in cases with limited measurements, particularly in hydropower facilities. Investigation at several hydraulically different reaches provided ranges of dissipation rate, which is rarely available in the literature and hard to obtain in the field. These rates were higher compared to the prediction of some well-known reaeration models. In addition to direct transfer across the free surface, bubble-mediated transfer caused by liquid phase supersaturation can potentially enhance the dissipation rate. To estimate the mixing and dissipation rates, simplified formulations were presented based on field observations.

2. The gas transfer and corresponding generation and degassing of total dissolved gases was investigated in a prototype ski-jump spillway. A physical process based mechanistic approach was utilized to partition gas transfer in spillway face, free jet and plunge pool and evaluate the contribution of each regions supported by extensive field measurements. This involved modeling exercise in discretized control volumes of different regions, calibration and justification of model parameters and modification of theoretical equations for prototype application. Moreover, a method to estimate bubble-penetration depth in the plunge pool was introduced for pre-aerated impinging jet. The modeling effort indicated that gas exchange was

dominated by bubble-mediated transfer and the corresponding concentration change was much higher than the free-surface transfer. Due to flip buckets designed to aerate water with large interfacial area, substantial degassing was observed during spill operations with gas transfer in free jet being considerably higher compared to spillway face and plunge pool. Practical relationships were proposed to estimate degassing in the free jet and assess overall gas transfer efficiency which can be adaptable to prototype spillways. Similar analogy was applied to predict dissolved gas levels in other facilities. Results from this study can be utilized to develop operational alternatives for the management of dissolved gas supersaturation.

3. A system-wide investigation of total dissolved gas supersaturation was carried out to address cumulative risks from the combined operation of multiple facilities in complex river system. Facility specific predictive models, physical relationships describing mixing and dissipation and analytical transport model were integrated into a single platform to develop a two-dimensional TDG distribution model for the system, which is not only physically meaningful but provides rapid and accurate estimations for impact assessment. A risk ranking process was developed considering the severity of supersaturation level, depth compensation and exposure duration for a given spill event, which represented the TDG management thresholds reasonably well. This resulted in a risk assessment framework that identifies the potential risk zones and its degree and extent on fish habitat. It can be utilized to revise facility operating order and spill management scenarios by incorporating TDG-related constraints to avoid or minimize negative ecological consequences. The modeling framework can be generalized for application to other river systems following adjustment of model parameters, and can be expanded to account different water quality variables that can harm the receiving environment.

6.2 Recommendations for Future Research

The supersaturation of total dissolved gases in hydropower facilities covers a wide range of hydraulic engineering topics including air entrainment, air-bubble features and mass transfer across bubble-liquid and free surface in dam spillways, as well as the transport, mixing and surface transfer or dissipation in riverine environment. Although this study covered the major aspects by means of mechanistic and whole-system approaches, opportunities exist to broaden our

understanding on the transfer and transport of total dissolved gases. Some recommendations for future research are described below.

While discussing the variation of dissipation rates, a conceptual argument based on gas transfer theories was presented in this study that indicated that the rate can be enhanced by bubble-mediated transfer. Bubbles can form at pre-existing nucleation sites due to liquid phase supersaturation. Because of limited data availability, the role of this mechanism is not conclusive and requires further investigation particularly in laboratory-controlled settings. Also more generalized relation to estimate dissipation rate can be developed by conducting systematic experiments in rivers under different hydraulic conditions.

Based on the investigation of gas transfer in different regions of spillway, simplified relationships were presented to estimate transfer efficiency and subsequent degassing. These are expected to have more generality since a mechanistic approach was utilized. However, direct measurement in the individual regions is not possible and field measurements for similar ski-jump spillways are needed to verify its application for the assessment of dissolved gas levels. Further research is needed to quantify gas-void ratio in free jet and evaluate how different modes of jet break-up affects the gas transfer process. Detailed investigation on the gas transfer in spillway face for prototype condition is also required, specifically for both aerated and non-aerated conditions. Numerical modeling can be an important supplement in this aspect.

The system model developed for total dissolved gas distribution and risk assessment can be generalized, which can be tested for application to other hydropower systems. The relationship between various impacting factors and the assessment of overall risk require further study for different cases. The severity ranks and weightage of different impacting factors should be explored further to evaluate the most representative combination comparable with general management thresholds. Habitat use requirements for different life stages for each species can be incorporated in this framework to obtain more detailed risk assessment.

Bibliography

Abernethy, R. B., Benedict, R. P., and Dowdell, R. B. (1985). ASME measurement uncertainty. J. Fluids Engrg., 107(2), 161-164.

Anderson D, Moggridge H, Warren P, Shucksmith J (2015). The impacts of 'run-of-river' hydropower on the physical and ecological condition of rivers. Water Environ J, 29(2):268–276.

Anderson, J., Beer, N., Frever, T., Hayes, J., Iltis, S. et al. (2000). Columbia River Salmon Passage Model. Columbia Basin Research, University of Washington, Seattle, WA

Anderson, M.L. and Johnson, B.D. (1992). Gas transfer: A gas tension method for studying equilibration across a gas-water interface. J. Geophys. Res., 97, 17899-17904.

Antcliffe, B.L., L.E. Fidler and I.K. Birtwell (2002). Effect of dissolved gas super saturation on the survival and condition of juvenile rainbow trout (Oncorhynchus mykiss) under static and dynamic exposure scenarios. Canadian Technical Report of Fisheries and Aquatuc Sciences 2370. 70p.

APHA, AWWA, and WEF (1998). Standard Methods for the Examination of Waste and Wastewater. 20th Edition. American Public Health Association, American Water Works Association and Water Environment Federation. Washington, D.C.

Asher, W.E., Karle, L.M., Higgins, B.J. (1997). On the differences between bubble-mediated air-water transfer in freshwater and seawater. Journal of Marine Research 55, 813-845.

Aspen Applied Science Ltd. (1998). Analysis of Brilliant Dam 1997 dissolved gas data and recommendations for the 1998 TGP monitoring program. Report prepared for West Kootenay Power, South Slocan, BC.

Azbel, D. (1981). Two phase flows in chemical engineering, Cambridge University Press, Cambridge, U.K.

BC Hydro. (2014). Total Dissolved Gas Management Strategy: Implementation Plan. Prepared by BC Hydro, Environmental Risk Management, Burnaby, BC.

BC Ministry of Environment, Lands and Parks (1997). Water quality criteria for total gas pressure – Overview. Water Management Branch, Victoria. 10 p.

Bennett, J. P., and Rathbun, R. E. (1972). Reaeration in open-channel flow. USGS Prof. Pap. 737, U.S. Government Printing Office, Washington, DC.

Bin, A.K. (1993). Gas entrainment by plunging liquid jets. Chem. Eng. Sci., 48 , 3585-3630.

Bowie, G. L., Mills, W.B., Porcella, D.B., Campbell, C.L., Pagenkopf, J.R., Rupp, G.L., Johnson, K.M., Chan, P.W.H., Gherini, S.A., Tetra Tech Inc., and Chamberlin, C.E. (1985). Rates, constants, and kinetics formulations in surface water quality modeling. Rep. EPA/600/3-85/040, EPA, Athens, GA.

Brattberg, T. and Chanson, H. (1998). Air Entrapment and Air Bubble Dispersion at Two-Dimensional Plunging Water Jet. Chem. Eng. Sci. 53(24), 4113–4127.

Broecker, W. S. and Peng, T. H. (1974). Gas exchange rates between air and sea. Tellus, 26:1-2, 21–35.

Bruce, J. A. (2016). Fate modeling of air supersaturated waters in the Columbia River: Phase 1 – Model development and information gap analysis. Report No. CAQ-017, Creekside Aquatic Sciences and LGL Ltd., Burnaby, BC.

Bruce, J., Abell, J. & Hatfield, T. (2018). Seven Mile Hydroelectric Project Total Dissolved Gas Risk Assessment. Draft V1. Report prepared for BC Hydro by Ecofish Research Ltd. and Creekside Aquatic Sciences Ltd., April 2018.

Buscaglia, G. C., Bombardelli, F. A., and García, M. H. (2002). Numerical modeling of large-scale bubble plumes accounting for mass transfer effects. Int. J. Multiphase Flow, 28(11), 1763-1785.

Canadian Council of Ministers of the Environment (CCME). (1999). Canadian water quality guidelines for the protection of aquatic life: Dissolved gas supersaturation. In: Canadian environmental quality guidelines, CCME, Winnipeg.

Castillo, L.G., Carrillo, J.M. and Blázquez, A. (2015). Plunge pool dynamic pressures: a temporal analysis in the nappe flow case. J. Hydraul. Res. 53 (1), 101–118.

Castillo, L. G., Carrillo, J. M., and Bombardelli, F. A. (2017). Distribution of mean flow and turbulence statistics in a plunge pool. J. Hydroinformatics, 19(2), 173-190.

Cirpka, 0., Reichert, P., Wanner, 0., MUller, S. R., and Schwarzenbach, R. P. (1993). Gas exchange at river cascades: Field experiments and model calculations. Envir. Sci. and Technol., 27(10), 2086-2097.

Chanson, H. (1995). Predicting oxygen content downstream of weirs, spillways and waterways. Proc. of the Institution of Civil Engineers, Water and Maritime Engineering 112, 20-30.

Chanson, H. (1996). Air bubble entrainment in free-surface turbulent shear flows. Academic Press, London.

Chen, S., Chen, B. and Fath, B.D. (2015). Assessing the cumulative environmental impact of hydropower construction on river systems based on energy network model. Renewable and Sustainable Energy Reviews, 42, 78–92.

Chen, X., Zhu, D.Z. and Steffler, P.M. (2017). Secondary currents induced mixing at channel confluences. Can. J. Civ. Eng., 44, 1071-1083.

Chu, C. and Jirka, G. (2003). Wind and Stream Flow Induced Reaeration. J. Environ. Eng., 129:12, 1129-1136.

Churchill, M. A., Elmore, H. L., and Buckingham, R. A. (1962). The prediction of stream reaeration rates. J. Sanit. Eng. Div., 88(4), 1–46.

Colt, J. (1984). Computation of dissolved gas concentrations in water as functions of temperature, salinity and pressure. American Fisheries Society Special Publication No. 14, Bethesda Maryland.

D'Aoust, B.G. (2007). Technical note: total dissolved gas pressure (TDGP) sensing in the laboratory. Dissolut. technol., 14, 38-41.

D'Aoust, B.G. and Clark, M.J.R. (1980). Analysis of supersaturated air in natural waters and reservoirs. Trans. Am. Fisheries Soc., 109, 708-724.

Davies, J. T. and Ting, S.T. (1967). Mass Transfer into Turbulent Jets. Chem. Eng. Sci., 22, 1539-1548.

DeMoyer, C. D., Schierholz, E. L., Gulliver, J. S., and Wilhelms, S. C. (2003). Impact of bubble and free surface oxygen transfer on aeration systems. Water Res., 37(8), 1890–1904.

Dow, K. E., Steffler, P. M. and Zhu, D. Z. (2009). Case study: Intermediate field mixing for a bank discharge in a natural river. J. Hydr. Eng., 135(1), 1-12.

Ebel, W. J. (1969). Supersaturation of nitrogen in the Columbia River and its effect on salmon and steelhead trout. U.S. Fish Wildlife. Serv., Fish. Bull. 68, I-II.

Elhadi, N., Harrington, A., Hill, I., Lau, Y. L. and Krishnappan, B. G. (1984). River mixing - a state-of-the-art report. Can. J. of Civ. Eng., 11(3), 585-609.

Enriquez, O.R., Hummelink, C., Bruggert, G., Lohse, D., Prosperetti, A., Meer, D. and Sun, C. (2013). Growing bubbles in a slightly supersaturated liquid solution. Rev. Sci. Instrum. 84, 065111.

Ervine, D.A., Falvey, H.T. (1987). Behavior of turbulent water jets in the atmosphere and in plunge pools. Proc. Inst. Civil Eng. 83(2), 295–314.

Feng, J.J, Li, R., Ma Q. and Wang L.L. (2014). Experimental and field study on dissipation coefficient of supersaturated total dissolved gas. J. Cent. South Univ., 21, 1995−2003.

Fidler, L.E. (1988). Gas bubble trauma in fish. Ph.D. Thesis, Department of Zoology, University of British Columbia, Vancouver, British Columbia.

Fidler, L.E. and Miller, S.B. (1997). British Columbia water quality criteria for dissolved gas saturation – technical report. Contract report to the BC Ministry of Environment, Department of Fisheries and Oceans, and Environment Canada. Aspen Applied Sciences Ltd., Cranbrook, B.C.

Fischer, H. B., List, E. G., Koh, R. C. Y., Imberger, J. & Brooks, N. H. (1979). Mixing in Inland and Coastal Waters, Academic Press, New York, NY.

Fortescue, G.E. and Pearson, J.R.A. (1967). On gas absorption into a turbulent liquid. Chem. Eng. Sci. 22, 1163–1176.

Geldert, D.A., Gulliver, J.S., and Wilhelms, S.C. (1998). Modeling dissolved gas supersaturation below spillway plunge pools. J. Hydraul. Eng. 124(5): 513-521.

Golder Associates Ltd. (2011). Total Dissolved Gas Monitoring: Columbia River Basin, 2011 Data Report. Report prepared for BC Hydro, Columbia Power Corporation and Teck Metal Limited. Golder Report No. 11-1492-0095.

Gowda, T. P. H. (1984). Water quality prediction in mixing zones of rivers. J. Environ. Eng., 110(4), 751–769.

Gualtieri, C., Gualtieri, P., and Doria, G.P. (2002). Dimensional analysis of reaeration rate in streams. J. Environ. Eng., 128(1), 12-18.

Gulliver J. S., Groeneveld, J., and Paul, Guy E. (2009). Prediction of Total Dissolved Gas below the Cabinet Gorge Spillway. 33rd IAHR Congress: Water Engineering for a Sustainable Environment, Vancouver, British Columbia, August 9-14, 2009.

Gulliver, J. S. and Halverson, M. J. (1989). Air-water gas transfer in open channels. Water Resour. Res., 25(8), 1783–1793.

Gulliver, J.S., Thene, J.R., Rindels, A.J. (1990). Indexing gas transfer in self-aerated flows. J. Environ. Eng., 116(3), 503-523.

Gulliver, J.S., Wilhelms, S.C. and Parkhill, K.L. (1998). Predictive Capabilities in Oxygen Transfer at Hydraulic Structures. J. Hydraul. Eng., 124:664-671.

HACH (2013). User Manual - Luminescent Dissolved Oxygen Probe: LDO101 Series. Document 022.53.80021, HACH, Loveland, CO.

Heller, V., Hager, W.H., Minor, H.E. (2005). Ski jump hydraulics. J. Hydraul. Eng. 131(5), 347–355.

Hibbs, D.E., and Gulliver, J.S. (1997). Prediction of Effective Saturation Concentration at Spillway Plunge Pools. J. Hydraul. Eng., 123(11), 940–949.

Hikita, H. and Konishi, Y. (1984). Desorption of carbon dioxide from supersaturated water in an agitated vessel. AIChE J., 30, 945–951.

Hinze, J.O. (1955). Fundamental of the Hydrodynamic Mechanism of Splitting in Dispersion Processes. J. Amer. Inst. Chem. Eng. 1(3), 289-295.

Holley, E. R., Siemons, J. and Abraham, G. (1972). Some aspects of analyzing transverse dispersion in rivers. J. Hydraul. Res., 10(1), 27–57.

Jensen, J.O.T., Schnute, J. and D.F. Alderdice (1986). Assessing juvenile salmonid response to gas supersaturation using a general multivariate dose-response model. Can. J. Fish. Aquat. Sci. 43: 1694-1709.

Johnson, E. L., Clabough, T. S., Peery, C. A., Bennett, D. H., Bjornn, T. C., Caudill, C. C. and Richmond, M. C. (2007). Estimating adult Chinook salmon exposure to dissolved gas supersaturation downstream of hydroelectric dams using telemetry and hydrodynamic models. River Research and Applications, 23, 963– 978.

Johnson, P.L. and King, D.L. (1975). Prediction of Dissolved Gas Transfer at Hydraulic Structures". Symp. Reaeration Res. ASCE, NY.

Jones, S.F., Evans, G.M. and Galvin, K.P. (1999). Bubble nucleation from gas cavities - a review. Adv. Colloid Interface Sci. 80(1), 27-50

Kamal, R., Zhu, D.Z., Leake, A. and Crossman, J. (2019). Dissipation of Supersaturated Total Dissolved Gases in the Intermediate Mixing Zone of a Regulated River. J. Environ. Eng., 145(2): 04018135.

Kawakami, K. (1973). A study on the computation of horizontal distance of jet issued from ski-jump spillway. Trans. Jpn. Soc. Civ. Eng., 5, 37–44 (in Japanese).

Keller, R.J. and Rastogi, A.K. (1975). Prediction of flow development on spillways. J. Hydr. Div. ASCE 101(HY9), 1171–1184; 102(HY9), 1401–1404; 103(HY6), 664.

Khatsuria, R.M. (2005). Hydraulics of spillways and energy dissipators. Dekker, New York.

Kierzkowska-Pawlak, H. and Chacuk, A. (2010). Carbon dioxide desorption from saturated organic solvents. Chem. Eng. Technol., 33, 74–81.

Killen, J. M. (1982). Maximum stable bubble size and associated noise spectra in a turbulent boundary layer. Proc. Cavitation and Polyphase Flow Forum, American Society of Mechanical Engineers, 1-3.

Lamont, J.C. and Scott, D.S. (1970). An eddy cell model of mass transfer into the surface of a turbulent liquid. AIChe J., 16, 513–519.

Lau L. Y. (1972). Prediction equation for reaeration in open-channel flow. J. Sanit. Engng. Div. Am. Soc. Civ. Engrs., 98, SA6, 1063-1068.

Lee, P. G., Hanneman, M. and Cheng, R. (2012). Hydropower Developments in Canada: Number, Size and Jurisdictional and Ecological Distribution. Global Forest Watch, Edmonton, AB.

Li, R., Gualtieri, P., Feng, J., and Gualtieri, C. (2015). A dimensional analysis of supersaturated total dissolved gas dissipation. E-Proc., 36th IAHR World Congress, The Hague, Netherlands.

Li, R., Hodges, B., Feng, J., and Yong, X. (2013). Comparison of supersaturated total dissolved gas dissipation with dissolved oxygen dissipation and reaeration. J. Environ. Eng., 139(3), 385-390.

Liang RF, Yun D, You-Cai T et al (2012). Analysis on characteristics of water Temperature's cumulative effects of river Cascade hydropower stations. J Sichuan Univ, 44:221–227.

Lu, J., Li, R., Ma, Q. et al. (2019). Model for Total Dissolved Gas Supersaturation from Plunging Jets in High Dams. J. Hydraul. Eng., 145(1): 04018082.

Ma, Q., Li, R., Feng, J. and Zhou, Q. (2018). Cumulative effects of cascade hydropower stations on total dissolved gas supersaturation. Environmental Science and Pollution Research, 25:13536–13547.

Ma, Q., Li, R., Hodges, B., Feng, J. and Yang, H. (2016). Two phase flow simulation of supersaturated total dissolved gas in the plunge pool of a high dam. Environmental Progress & Sustainable Energy, 35(4), 1139–1148.

Manning, A.H., Solomon, D.K. and Sheldon, A.L. (2003). Applications of a total dissolved gas pressure probe in ground water studies. Ground Water, 41(4), 440–448.

Meireles, I., Renna, F., Matos, J., and Bombardelli, F. A. (2012). Skimming, non-aerated flow on stepped spillways over roller compacted concrete dams. J. Hyd Engrg., 138(10), 870-877.

Melching, C. S. and Flores, H. E. (1999). Reaeration equations derived from U. S. Geological Survey Database. J. Environ. Eng., 1999, 125(5): 407-414.

Moog, D. B. and Jirka, G. H. (1999). Air-water gas transfer in uniform channel flow. J. Hydraul. Eng., 125:1(3), 3-10.

Mortensen, J.D., Barfuss, S.L., Johnson, M.C. (2011). Scale effects of air entrained by hydraulic jumps within closed conduits. J. Hydraulic Res., 49(1), 90–95.

Nezu, I. and Nakagawa, H. (1993). Turbulence in open-channel flows. International Association for Hyd. Research Monograph, Balkema, Rotterdam, The Netherlands.

O'Connor, D. J., and Dobbins, W. E. (1958). Mechanism of reaeration in natural streams. Trans. Am. Soc. Civ. Eng., 123, 641–684.

Ohkawa, A., Kawai, Y., Kusabiraki, D., Sakai, N. and Endoh. K., 1987a. Bubble size, interfacial area and volumetric liquid-phase mass transfer coefficient in downflow bubble columns with gas entrainment by a liquid jet. J. Chem. Engng Japan, 20, 99-101.

Orlins, J.J. and Gulliver, J.S. (2000). Dissolved gas supersaturation downstream of a spillway II: computational model. J. Hydraul. Res., 38(2), 151–159.

Owens, M., Edwards, R. W. and Gibbs, J. W. (1964). Some reaeration studies in streams. Int. J. Air Water Pollut., 8, 469–486.

Palumbo, J.E. and Brown, L.C. (2014). Assessing the Performance of Reaeration Prediction Equations. J. Environ. Eng., 140(3): 04013013

Pentair Aquatic Eco-Systems. (2014). PT4 TGP Probe Technical Manual. Apopka, FL.

Pfister, M. and Hager, W.H. (2012). Deflector-jets affected by preaerated approach flow. J. Hydraul. Res. 50(2), 181–191.

Pfister, M., Hager, W.H. and Boes, R.M. (2014) Trajectories and air flow features of ski jump-generated jets. J. Hydraul. Res., 52:3, 336-346.

Pickett, P. (2006). Standard Operating Procedure for Monitoring Total Dissolved Gas in Freshwater. EAP Report, Washington State Department of Ecology, Environmental Assessment Program, Olympia, WA.

Pilechi, A., Mohammadian, A., Rennie, C., and Zhu, D. (2016). Efficient Method for Coupling Field Data and Numerical Modeling for the Estimation of Transverse Mixing Coefficients in Meandering Rivers. J. Hydraul. Eng., 04016009.

Politano, M. S., Carrica, P. M., Turan, C., and Weber, L. (2007). A multidimensional two-phase flow model for the total dissolved gas downstream of spillways." J. Hydraul. Res., 45(2), 165–177.

Politano, M. S., Carrica, P. M. and Weber, L. (2009). A multiphase model for the hydrodynamics and total dissolved gas in tailraces. Int. J. Multiphase Flow, 35(11), 1036–1050.

Politano, M., Castro, A. and Hadjerioua, B. (2017). Modeling Total Dissolved Gas for Optimal Operation of Multireservoir Systems. J. Hydraul. Eng., 2017, 143(6): 04017007.

Rajaratnam, N. (1976). Turbulent jets. Elsevier, New York.

Raymond, P. A., and J. J. Cole (2001). Gas exchange in rivers and estuaries: Choosing a gas transfer velocity. Estuaries Coasts, 24(2), 312–317.

Richter, B. D. and G. A. Thomas. (2007). Restoring environmental flows by modifying dam operations. Ecology and Society, 12(1): 12.

RL&L Environmental Services. (1997). Total Gas Pressure Monitoring at Waneta Dam; 1997 Investigations. Report prepared for Cominco Ltd, Trail, B.C.

RL&L Environmental Services Ltd. (2002). Fisheries resource information and TGP risk assessment for the Canadian portion of the lower Columbia River basin. Prepared for Columbia River Integrated Environmental Monitoring Program, RL&L Report No. 856F, Castlegar, B.C.

Roesner, L.A. and Norton,W.R. (1971). A Nitrogen Gas Model for the Lower Columbia River. Rep. No. 1–350. Water Resources Engineers, Inc.,Walnut Creek, CA.

Rutherford, J.C. (1994). River mixing. John Wiley & Sons, West Sussex, England.

Sandford, R. W., Harford, D. and O'Riordan, J. (2014). The Columbia River Treaty: A Primer. RMB Rocky Mountain Books, Canada.

Schmocker, L., Pfister, M., Hager, W.H., Minor, H.-E. (2008). Aeration characteristics of ski jump jets. J. Hydraul. Eng. 134(1), 90–97.

Schneider, M. L. and Wilhelms, S. C. (2005). Rocky Reach Dam: Operational and Structural Total Dissolved Gas Management. Report prepared for Chelan County Public Utility District No. 1, U.S. Army Engineer Research and Development Center, Vicksburg, MS, June 2005.

Sene, K. J. (1988). Air entrainment by plunging jets. Chemical Engineering Science, 43(10), 2615-2623.

Sevik, M. and Park, S.H. (1973). The Splitting of Drops and Bubbles by Turbulent Fluid Flow. J. Fluids Eng., ASME 95(1), 53-60.

Shen, X., Liu, S.Y., Li, R. and Ou, Y.M. (2014). Experimental study on the impact of temperature on the dissipation process of supersaturated total dissolved gas. J. Environ. Sci., 26(9), 1874-1878.

Shrimpton, J.M., Randall, D.J. and Fidler, L.E. (1990). Factors affecting swim bladder volume in rainbow trout (Oncorhynchus mykiss) held in gas supersaturated water. Can. J. Zool., 68: 962-968.

Smoot, J. L. (1988). An examination of stream reaeration coefficients and hydraulic conditions in a pool-and-riffle stream. Ph.D. thesis, Virginia Poly. Inst. and State Univ., Blacksburg, VA.

Tavoularis, S. (2005). Measurement in Fluid Mechanics. Cambridge University Press, USA.

Teledyne RD Instruments. (2015). RiverRay ADCP guide, TRDI, San Diego, 156.

Thackston, E. L., and Krenkel, P. A. (1969). Reaeration prediction in natural streams. J. Sanit. Eng. Div., 95(1), 65–94.

Todorova, Y., Lincheva, S., Yotinov, I. and Topalova, Y. (2016). Contamination and Ecological Risk Assessment of Long-Term Polluted Sediments with Heavy Metals in Small Hydropower Cascade. Water Resour Manage, 30, 4171–4184.

Toombes, L. and Chanson, H. (2005). Air-water mass transfer on a stepped waterway. J. Environ. Eng., 131(10), 1377-1386.

Tsivoglou, E. C. and Wallace, R. J. (1972). Characterization of stream reaeration capacity. Research Reporting Series. U.S. Environmental Protection Agency, 317.

Urban, A.L., Gulliver, J.S. and Johnson, D.W. (2008). Modelling total dissolved gas concentration downstream of spillways. J. Hydraul. Eng., 134(5), 550–561.

U.S. Army Corps of Engineers (1996). Dissolved Gas Abatement Study: Phase I. Technical Report, US Army Corps of Engineers, North Pacific Division, Portland District and Walla Walla District.

U.S. Army Corps of Engineers. (2001). Dissolved gas abatement study: Phase II. Technical Report, USACE, North Pacific Division, Portland District and Walla Walla District.

U.S. Environmental Protection Agency. (1986). Quality criteria for water. EPA rep. 440/5-86-001, EPA, Washington, D.C.

Van de Sande, E., and Smith, J. M. (1975). Mass transfer from plunging water jets. Chem. Engrg. J., 10, 225–233.

Vischer, D.L., Hager, W.H. (1998). Dam hydraulics. Wiley, Chichester.

Volkart, P. (1980). The mechanism of air bubble entrainment in self-aerated flow. Int. J. Multiphase Flow, 6, 411-423.

Wahl, T.L., Frizell, K.H. and Cohen, E.A. (2008). Computing the trajectory of free jets. J. Hydraul. Eng., 134(2), 256–260.

Wang, Y., Politano M. and Weber, L. (2018). Spillway jet regime and total dissolved gas prediction with a multiphase flow model. J. Hydraul. Res., 57(1), 26–38.

Weber, L. J., Huang, H., Lai, Y., & McCoy, A. (2004). Modeling total dissolved gas production and transport downstream of spillways: Three-dimensional development and applications. Int. J. River Basin Manage., 2(3), 157–167.

Weitkamp, D.E. (2008). Total dissolved gas literature 1980-2007. An Annotated Bibliography Parametrix, Bellevue, WA.

Weitkamp, D. E., and Katz, M. (1980). A review of dissolved gas supersaturation literature. Trans. of the Am. Fisheries Soc., 109(6), 659-702.

Wen, X., Liu, Z., Lei, X., Lin, R., Fang, G., Tan, Q., Wang, C., Tian, Y., Quan, J. (2018). Future changes in Yuan River ecohydrology: individual and cumulative impacts of climates change and cascade hydropower development on runoff and aquatic habitat quality. Sci. Total Environ., 633, 1403-1417.

Wilhelms, S.C. and Gulliver, J.S. (2005) Gas transfer, cavitation, and bulking in self-aerated spillway flow. J. Hydraul. Res., 43:5, 532-539.

Witt, A., Magee, T., Stewart, K., Hadjerioua, B., Neumann, D., Zagona, E. and Politano, M. (2017). Development and implementation of an optimization model for hydropower and total dissolved gas in the Mid-Columbia River System. J. Water Resour. Plann. Manage., 143(10): 04017063.

Wood, I.R. (1991). Free surface air entrainment on spillways. In IAHR hydraulic structures design manual no. 4 (Air entrainment in free-surface flows), 55–84, I.R. Wood, ed. A.A. Balkema, Rotterdam.

Woolf, D. K. and Thorpe, S. A. (1991). Bubbles and the air-sea exchange of gases in near-saturation conditions. J. Mar. Res., 49(3), 435-466.

Xue, H., Ma, Q., Li, R. et al. (2019). Experimental study of the dissipation of supersaturated TDG during the jet breakup process. Journal of Hydrodynamics, 31(4), 760-766.

Yotsukura, N. and Sayre, W. W. (1976). Transverse mixing in natural channels. Water Resour. Res., 12(4), 695–704.

Zhang, W. and Zhu, D.Z. (2011). Transverse mixing in an unregulated northern river. J. Hydraul. Eng., 137(11), 1426-1440.